Electronic Supplementary Material (ESI) for Dalton Transactions.

Group 1 and 2 cyclic(alkyl)(amino)carbene complexes.

Zoë R. Turner and Jean-Charles Buffet*

Chemistry Research Laboratory, Department of Chemistry, University of Oxford, Mansfield Road, Oxford OX1 3TA, United Kingdom. Tel: +44(0) 1865 285157; E-mail: zoe.turner@chem.ox.ac.uk

Table of Contents

I. General Considerations

All manipulations were carried out using standard Schlenk line or drybox techniques under an atmosphere of dinitrogen. Protio solvents were degassed by sparging with dinitrogen, dried by passing through a column of activated sieves (pentane, hexane, toluene, benzene) and stored over potassium mirrors or distilled from sodium metal (thf) and stored activated 4 Å molecular sieves or distilled from sodium-potassium alloy (diethyl ether) and stored over a potassium mirror. Deuterated solvents were dried over potassium (C_7H_8, C_6D_6) or CaH_2 ($CDCl_3$), distilled under reduced pressure and freeze-pump-thaw degassed three times prior to use.

^{1}H NMR spectra were recorded at 298 K, unless otherwise stated, on Bruker AVIII 400 nanobay or Bruker AVIII 500 spectrometers and ^{13}C{^{1}H} or ^{13}C spectra on the same spectrometers at operating frequencies of 100 and 125 MHz respectively. Two dimensional ^{1}H-^{1}H and ^{13}C-^{1}H correlation experiments were used, when necessary, to confirm ^{1}H and ^{13}C assignments. All NMR spectra were referenced internally to residual protio solvent (^{1}H) or solvent (^{13}C) resonances and are reported relative to tetramethylsilane (δ = 0 ppm). Chemical shifts are quoted in δ (ppm) and coupling constants in Hertz. Elemental analyses were carried out at London Metropolitan University. MALDI-ToF-MS were collected using a Voyager DE-STR from Applied Biosystems equipped with a 337 nm nitrogen laser. Polymer molecular weights were determined by GPC using a Polymer Laboratories Plgel Mixed-D column (300 mm length, 7.5 mm diameter) and a Polymer Laboratories PL-GPC50 Plus instrument equipped with a refractive index detector.

KN",[1] $(MgN"_2)_2$,[2] $(SrN"_2)_2$,[3] $BaN"_2(thf)_{1.6}$,[3] [^{Cy}CAACH]Cl,[4] [^{Me2}CAACH]Cl[4] were prepared accorded to reported literature procedures.

II. Synthesis and characterisation of group 1 and 2 complexes

(^{Me2}CAAC)Mg(N{SiMe$_3$}$_2$)$_2$ (1)

To a mixture of [^{Me2}CAACH]Cl (0.205 g, 0.638 mmol) and KN" (0.128 g, 0.638 mmol) was added benzene (5 mL) and the reaction mixture was stirred for 1 h at 23 °C to afford a yellow solution and colorless precipitate of KCl. The reaction mixture was added to a slurry of [MgN"$_2$]$_2$ (0.220 g, 0.319 mmol) in benzene (1 mL) to afford a yellow solution and was then stirred for 1 h. Removal of the volatiles *in vacuo* and extraction into pentane afforded a pale yellow residue. Recrystallization from pentane at -30 °C afforded (^{Me2}CAAC)Mg(N{SiMe$_3$}$_2$)$_2$ (**1**)as crystals suitable for an x-ray diffraction study. Yield = 0.15 g (37%). ^{1}H NMR (C_6D_6, 298 K): δ 7.08 (t, 1H, $^3J_{HH}$ = 7.8 Hz, 4-C$_6$*H*$_3$), 6.97 (d, 2H, $^3J_{HH}$ = 7.7 Hz, 3,5-C$_6$*H*$_3$), 2.61 (sept., 2H, $^3J_{HH}$ = 6.6 Hz, C*H*(CH$_3$)$_2$), 1.58 (s, 6H, C(C*H*$_3$)$_2$), 1.41 (d, 6H, $^3J_{HH}$ = 6.6 Hz, CH(C*H*$_3$)$_2$), 1.27 (s, 2H, C*H*$_2$), 1.01 (d, 6H, $^3J_{HH}$ = 6.6 Hz, CH(C*H*$_3$)$_2$), 0.91 (s, 6H, C(C*H*$_3$)$_2$), 0.34 (s, 36H, Si(C*H*$_3$)$_3$). ^{13}C{^{1}H} NMR (C_6D_6, 298 K): δ 266.6 (*C*$_{carbene}$), 145.4 (2,6-C$_6$*H*$_3$), 136.6 (1-C$_6$*H*$_3$), 129.9 (4-C$_6$*H*$_3$), 126.0 (3,5-*C*$_6$H$_3$), 83.1 57.8 (*C*(CH$_3$)$_2$), 51.9 (*C*H$_2$), 29.5 (C(*C*H$_3$)$_2$), 29.0 (*C*H(CH$_3$)$_2$), 28.4 (C(*C*H$_3$)$_2$), 27.7 26.1 (CH(*C*H$_3$)$_2$),7.1 (Si(*C*H$_3$)$_3$). Anal. Calcd for $C_{32}H_{67}Mg_1N_3Si_4$: C, 60.95; H, 10.71; N, 6.66. Found: C, 60.77; H, 10.57; N, 6.52.

(^{Cy}CAAC)Mg(N{SiMe$_3$}$_2$)$_2$ (2)

To a mixture of [^{Cy}CAACH]Cl (0.245 g, 0.676 mmol) and KN" (0.135 g, 0.676 mmol) was added benzene (5 mL) and the reaction mixture was stirred for 1 h at 23 °C to afford a yellow solution and colorless precipitate of KCl. The reaction mixture was added to a slurry of [MgN"$_2$]$_2$ (0.233 g, 0.338 mmol) in benzene (1 mL) to afford a yellow solution and was then stirred for 1 h. Removal of the volatiles *in vacuo* and extraction into pentane afforded a pale yellow residue. Recrystallization from pentane at -30 °C afforded (^{Cy}CAAC)Mg(N{SiMe$_3$}$_2$)$_2$ (**2**) as crystals suitable for an x-ray diffraction study. Yield = 0.070 g (15%). ^{1}H NMR (C_6D_6, 298 K): δ 7.25 – 6.83 (overlapping m, 3H, 3,5-C$_6$H$_3$ and 4-C$_6$H$_3$), 3.15 (sept., 2H, $^3J_{HH}$ = 6.8 Hz, C*H*(CH$_3$)$_2$, 2.32 – 1.35 (overlapping m, 10H, *Cy*), 1.53 (2, 2H, C*H*$_2$), 1.25 1.21 (d, 6H each, $^3J_{HH}$ = 6.8 Hz, CH(C*H*$_3$)$_2$), 1.09 (s, 6H, C(C*H*$_3$)$_2$), 0.30 (s, 36H, Si(C*H*$_3$)$_3$). Anal. Calcd for $C_{35}H_{71}MgN_3Si_4$: C, 62.69; H, 10.67; N, 6.27. Found: C, 62.42; H, 10.65; N, 6.19.

(^{Me2}CAAC)Sr(N{SiMe$_3$}$_2$)$_2$ (3)

To a mixture of [^{Me2}CAACH]Cl (0.228 g, 0.708 mmol) and KN" (0.141 g, 0.708 mmol) was added benzene (5 mL) and the reaction mixture was stirred for 1 h at 23 °C to afford a yellow solution and colorless precipitate of KCl. The reaction mixture was added to a slurry of [SrN"$_2$]$_2$ (0.289 g, 0.354 mmol) in benzene (1 mL) to afford a yellow solution and was then stirred for 1 h. Removal of the volatiles *in vacuo* and extraction into pentane afforded a pale yellow residue. Recrystallization from pentane at -30 °C afforded (^{Me2}CAAC)Sr(N{SiMe$_3$}$_2$)$_2$ (**3**) as a pale yellow microcrystalline solid. Yield = 0.25 g (50%). ^{1}H NMR (C_6D_6, 298 K): δ 7.08 (t, 1H, $^3J_{HH}$ = 7.8 Hz, 4-*C*$_6$H$_3$), 6.96 (d, 2H, $^3J_{HH}$ = 7.8 Hz, 3,5-*C*$_6$H$_3$), 2.62 (sept., 2H, $^3J_{HH}$ = 6.9 Hz, C*H*(CH$_3$)$_2$), 1.32 (s, 6H, C(C*H*$_3$)$_2$), 1.24 (s, 2H, C*H*$_2$), 1.19 1.05 (d, 6H each, $^3J_{HH}$ = 6.9 Hz, CH(C*H*$_3$)$_2$), 0.81 (s, 6H, C(C*H*$_3$)$_2$), 0.30 (s, 36H, Si(C*H*$_3$)$_3$). ^{13}C{^{1}H} NMR (C_6D_6, 298 K): δ 283.8 (*C*$_{carbene}$), 145.0 (2,6-*C*$_6$H$_3$), 135.7 (1-*C*$_6$H$_3$), 129.7 (4-*C*$_6$H$_3$), 125.4 (3,5-*C*$_6$H$_3$), 83.2 56.8 (*C*(CH$_3$)$_2$, 50.1 (*C*H$_2$), 29.0 (C(*C*H$_3$)$_2$), 28.8 *C*H(CH$_3$)$_2$, 28.3 (CH(*C*H$_3$)$_2$), 28.2 (C(*C*H$_3$)$_2$), 23.3 (CH(*C*H$_3$)$_2$), 6.5 (Si(*C*H$_3$)$_3$). Anal. Calcd for $C_{32}H_{67}Sr_1N_3Si_4$: C, 55.39; H, 9.73; N, 6.06. Found: C, 55.50; H, 9.75; N, 5.93.

(^{Me2}CAAC)Ba(N{SiMe$_3$}$_2$)$_2$ (4)

To a mixture of [^{Me2}CAACH]Cl (0.211 g, 0.654 mmol) and KN" (0.131 g, 0.654 mmol) was added benzene (5 mL) and the reaction mixture was stirred for 1 h at 23 °C to afford a yellow solution and colorless precipitate of KCl. The reaction mixture was added to a solution of BaN"$_2$(thf)$_{1.6}$ (0.375 g, 0.654 mmol) in benzene (5 mL) to afford a yellow solution and was then stirred for 1 h. Removal of the volatiles *in vacuo* and extraction into benzene (2 x 5 mL) afforded a pale yellow residue. Recrystallization from pentane at -30 °C afforded (^{Me2}CAAC)Ba(N{SiMe$_3$}$_2$)$_2$ (**4**) as a pale yellow solid. Single crystals of (^{Me2}CAAC)Ba(N{SiMe$_3$}$_2$)$_2$(thf) suitable for an x-ray diffraction study were grown from a pentane/thf mixture (1/10) at -30 °C. Yield = 0.24 g (49%). ^{1}H NMR (C$_6$D$_6$, 400 MHz, 298 K): δ 7.14 (m, 1H, 4-C$_6$*H*$_3$), 7.05 (m, 2H, 3,5-C$_6$*H*$_3$), 2.91 (sept., $^3J_{HH}$ = 6.9 Hz, C*H*(CH$_3$)$_2$), 1.41 (s, 2H, C*H*$_2$), 1.39 (s, 6H, C(C*H*$_3$)$_2$), 1.17 1.14 (d, 6H each, $^3J_{HH}$ = 6.9 Hz, CH(C*H*$_3$)$_2$), 0.96 (s, 6H, C(C*H*$_3$)$_2$), 0.33 (s, 36H, Si(C*H*$_3$)$_3$). ^{13}C{^{1}H} NMR (C$_6$D$_6$, 100 MHz, 298 K): δ 303.0 ($C_{carbene}$), 145.7 (2,6-*C*$_6$H$_3$), 137.1 (1-*C*$_6$H$_3$), 129.2 (4-*C*$_6$H$_3$), 124.9 (3,5-*C*$_6$H$_3$), 82.6 *C*(CH$_3$), 57.6 (*C*(CH$_3$)$_2$), 50.6 (*C*H$_2$), 29.1 (C(C*H*$_3$)$_2$), 29.0 (*C*H(CH$_3$)$_2$), 28.1 (C(C*H*$_3$)$_2$), 26.9 (CH(*C*H$_3$)$_2$), 22.7 (CH(*C*H$_3$)$_2$), 6.1 (Si(*C*H$_3$)$_3$). Anal. Calcd for C$_{32}$H$_{67}$BaN$_3$Si$_{41}$: C, 51.69; H, 9.08; N, 5.65. Found: C, 51.51; H, 9.17; N, 5.55.

(^{Cy}CAAC)(Ba(N{SiMe$_3$}$_2$)$_2$ (5)

To a mixture of [^{Cy}CAACH]Cl (0.226 g, 0.624 mmol) and KN" (0.124 g, 0.624 mmol) was added benzene (5 mL) and the reaction mixture was stirred for 1 h at 23 °C to afford a yellow solution and colorless precipitate of KCl. The reaction mixture was added to a solution of BaN"$_2$(thf)$_{1.6}$ (0.358 g, 0.0.624 mmol) in benzene (5 mL) to afford a yellow solution and was then stirred for 1 h. Removal of the volatiles *in vacuo* and extraction into benzene (2 x 5 mL) afforded a pale yellow residue. Recrystallization from pentane at -30 °C afforded (^{Cy}CAAC)Ba(N{SiMe$_3$}$_2$)$_2$ (**4**) as a pale yellow solid. Single crystals of (^{Cy}CAAC)Ba(N{SiMe$_3$}$_2$)$_2$(thf) suitable for an x-ray diffraction study were grown from a pentane/thf mixture (1/10) at -30 °C. Yield = 0.080 g (16%). ^{1}H NMR (C$_6$D$_6$, 298 K): δ 7.13 (m, 1H, 4-C$_6$*H*$_3$), 7.04 (m, 2H, 3,5-C$_6$*H*$_3$), 2.96 (sept., $^3J_{HH}$ = 6.8 Hz, C*H*(CH$_3$)$_2$), 2.26 (m, 2H, *Cy*), 1.96-1.49 (overlapping m, 3 x 2H, *Cy*), 1.46 (s, 2H, C*H*$_2$), 1.35 (m, 2H, *Cy*), 1.16 (overlapping d, 12H, CH(C*H*$_3$)$_2$), 0.98 (s, 6H, C(C*H*$_3$)$_2$), 0.35 (s, 36H, Si(C*H*$_3$)$_3$). ^{13}C{^{1}H} NMR (C$_6$D$_6$, 298 K): δ . 145.6 (2,6-*C*$_6$H$_3$), 137.5 (1-*C*$_6$H$_3$), 124.3 (3,5-*C*$_6$H$_3$), 123.2 (4-*C*$_6$H$_3$), 81.5 63.6 (*C*(CH$_3$)$_2$ and *C*Cy), 47.3 (*C*H$_2$), 36.2 (*Cy*), 29.6 (C(*C*H$_3$)$_2$), 29.2 (*C*H(CH$_3$)$_2$), 27.0 (CH(*C*H$_3$)$_2$), 26.1 22.9 22.4 (*Cy*), 22.0 (CH(*C*H$_3$)$_2$), 5.80 (Si(*C*H$_3$)$_3$). Anal. Calcd for C$_{39}$H$_{79}$BaN$_3$OSi$_4$: C, 54.74; H, 9.31; N, 4.91. Found: C, 51.57; H, 8.72; N, 4.65.

[(^{Cy}CAAC)$_3$K][Sr(N{SiMe$_3$}$_2$)$_3$] (6)

To a mixture of [^{Cy}CAACH]Cl (0.250 g, 0.690 mmol) and KN" (0.138 g, 0.690 mmol) was added benzene (5 mL) and the reaction mixture was stirred for 1 h at 23 °C to afford a yellow solution and colorless precipitate of KCl. The reaction mixture was added to a solution of [SrN"$_2$]$_2$ (0.282 g, 0.345 mmol) in benzene (5 mL) to afford a yellow solution and was then stirred for 1 h. Removal of the volatiles *in vacuo* and extraction into benzene (2 x 5 mL) afforded a pale yellow residue. Recrystallization from pentane at -30 °C afforded [(^{Cy}CAAC)$_3$K][Sr(N{SiMe$_3$}$_2$)$_3$] (**6**) as a pale yellow solid. Single crystals suitable for an x-ray diffraction study were grown from a toluene/pentane mixture (1/10) at -30 °C. Yield = 0.10 g (28%) based on pro-ligand. ^{1}H NMR (C$_6$D$_6$, 298 K): δ 7.22 (m, 3H, 4-C$_6$*H*$_3$), 7.14 (m, 6H, 3,5-C$_6$*H*$_3$), 3.12 (sept., 6H, $^3J_{HH}$ = 6.8 Hz, C*H*(CH$_3$)$_2$), 2.25 2.00 (m, 6H each, *Cy*), 1.71 – 1.35 (overlapping m, 18H, *Cy*), 1.52 (s, 6H, C*H*$_2$), 1.24 1.19 (d, 18H each, $^3J_{HH}$ = 6.8 Hz, CH(C*H*$_3$)$_2$), 1.08 (s, 18H, C(C*H*$_3$)$_2$), 0.26 (s, 54H, Si(C*H*$_3$)$_3$). ^{13}C{^{1}H} NMR (C$_6$D$_6$, 298 K):

270.6 ($C_{carbene}$), 146.1 (2,6-C_6H_3), 137.8 (1-C_6H_3), 123.7 (3,5-C_6H_3), 81.2 63.6 ($C(CH_3)_2$ and *C*Cy), 48.7 (CH_2), 36.5 (*Cy*), 29.6 ($C(CH_3)_2$), 29.4 ($CH(CH_3)_2$), 26.8 ($CH(CH_3)_2$), 26.2 23.4 (*Cy*), 22.0 ($CH(CH_3)_2$), 6.6 ($Si(CH_3)_3$). The carbon resonance for 4-C_6H_3 was obscured by the resonance associated with C_6D_6. Anal. Calcd for $C_{87}H_{159}K_1N_6Si_6Sr_1$: C, 65.95; H, 10.11; N, 5.03. Found: C, 61.58; H, 10.41; N, 4.46.

III. **Representative NMR spectra**

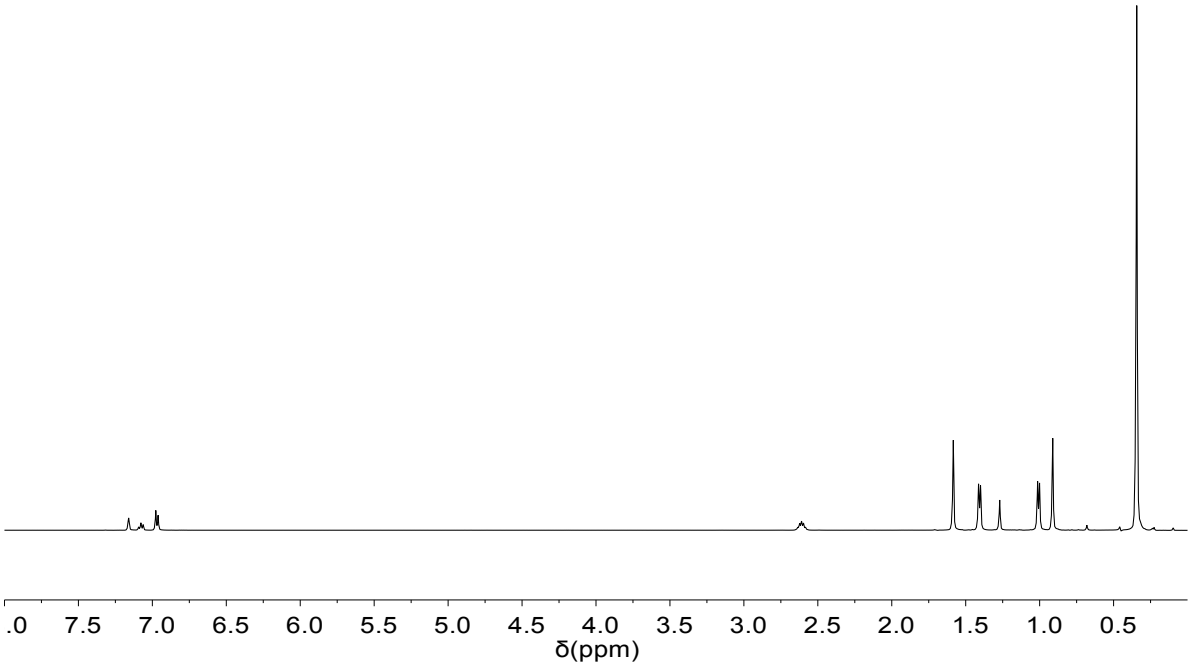

Figure S1: ^{1}H NMR spectrum (C_6D_6, 500 MHz, 298 K) of (^{Me2}CAAC)Mg(N{$SiMe_3$}$_2$)$_2$ (**1**).

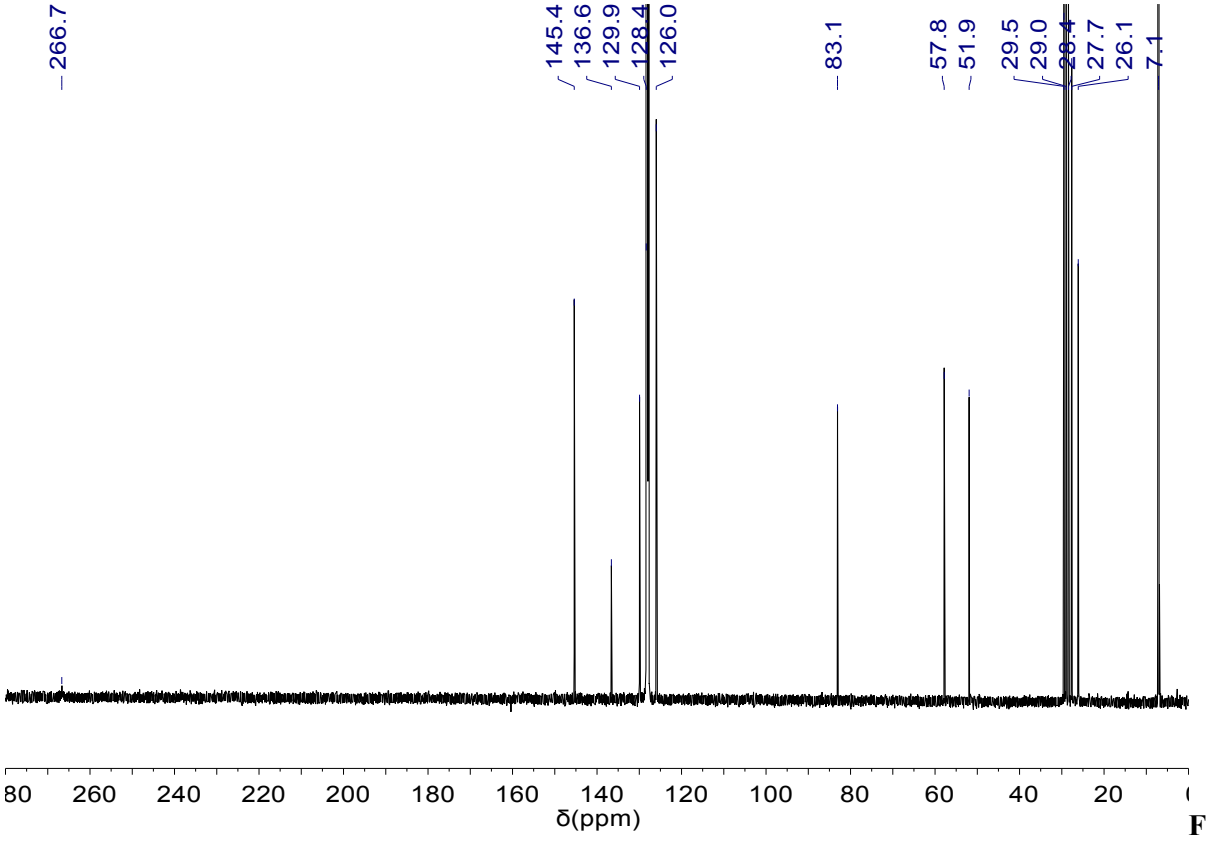

igure S2: $^{13}C\{^{1}H\}$ NMR spectrum (C_6D_6, 125 MHz, 298 K) of (^{Me2}CAAC)Mg(N{$SiMe_3$}$_2$)$_2$ (**1**).

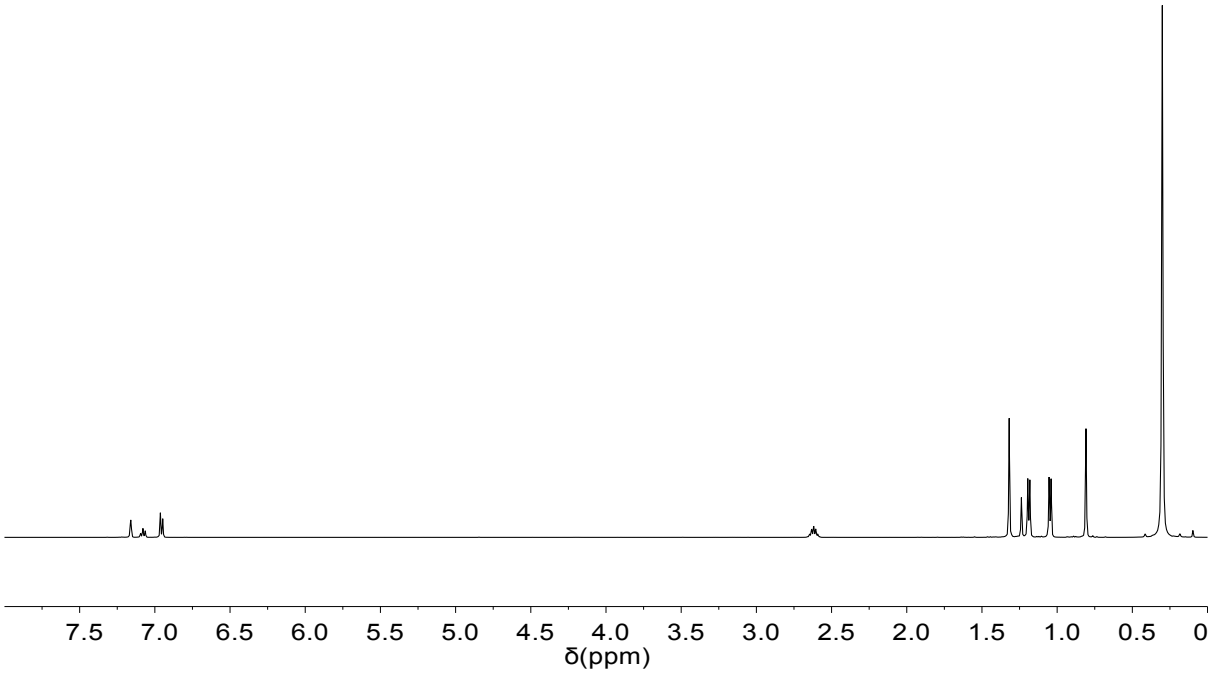

Figure S3: ^{1}H NMR spectrum (C_6D_6, 125 MHz, 298 K) of (^{Me2}CAAC)Sr(N{$SiMe_3$}$_2$)$_2$ (**3**).

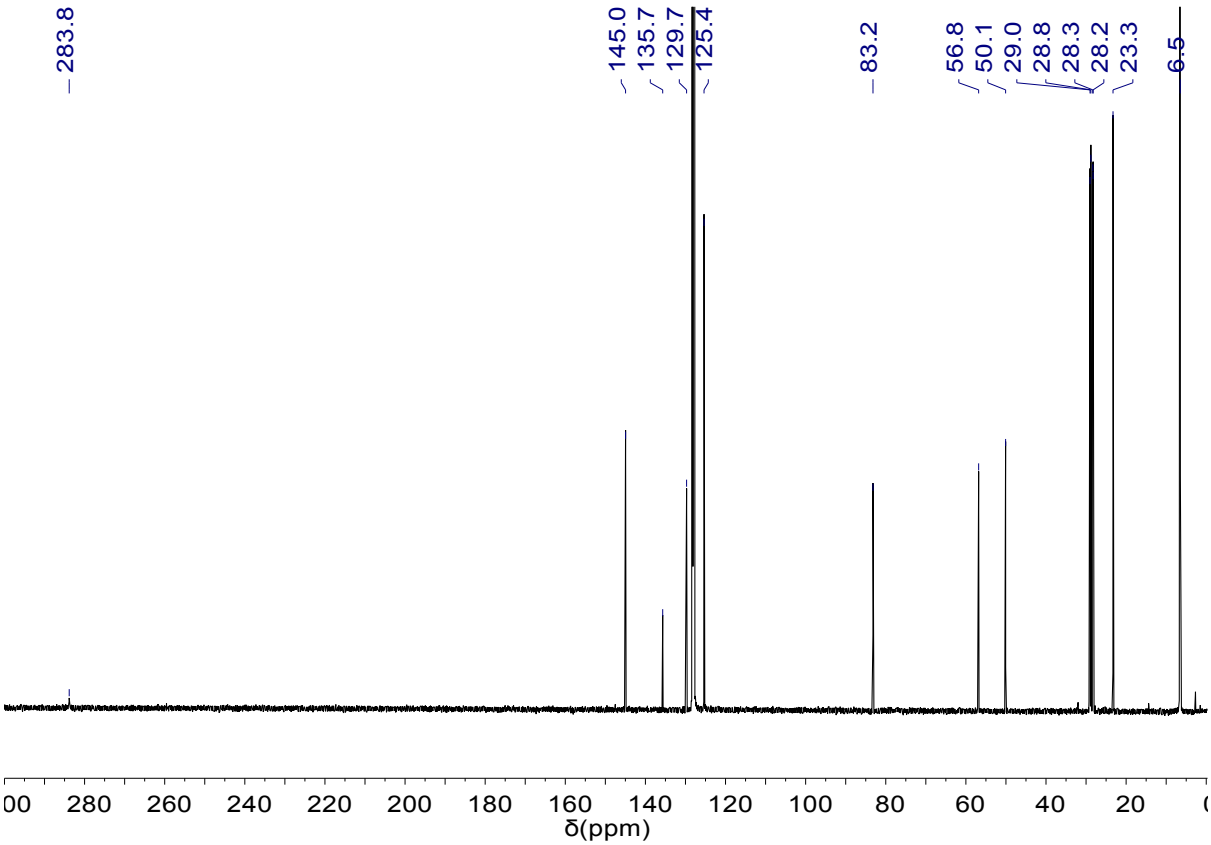

Figure S4: $^{13}C\{^{1}H\}$ NMR spectrum (C_6D_6, 125 MHz, 298 K) of (^{Me2}CAAC)Sr(N{$SiMe_3$}$_2$)$_2$ (**3**).

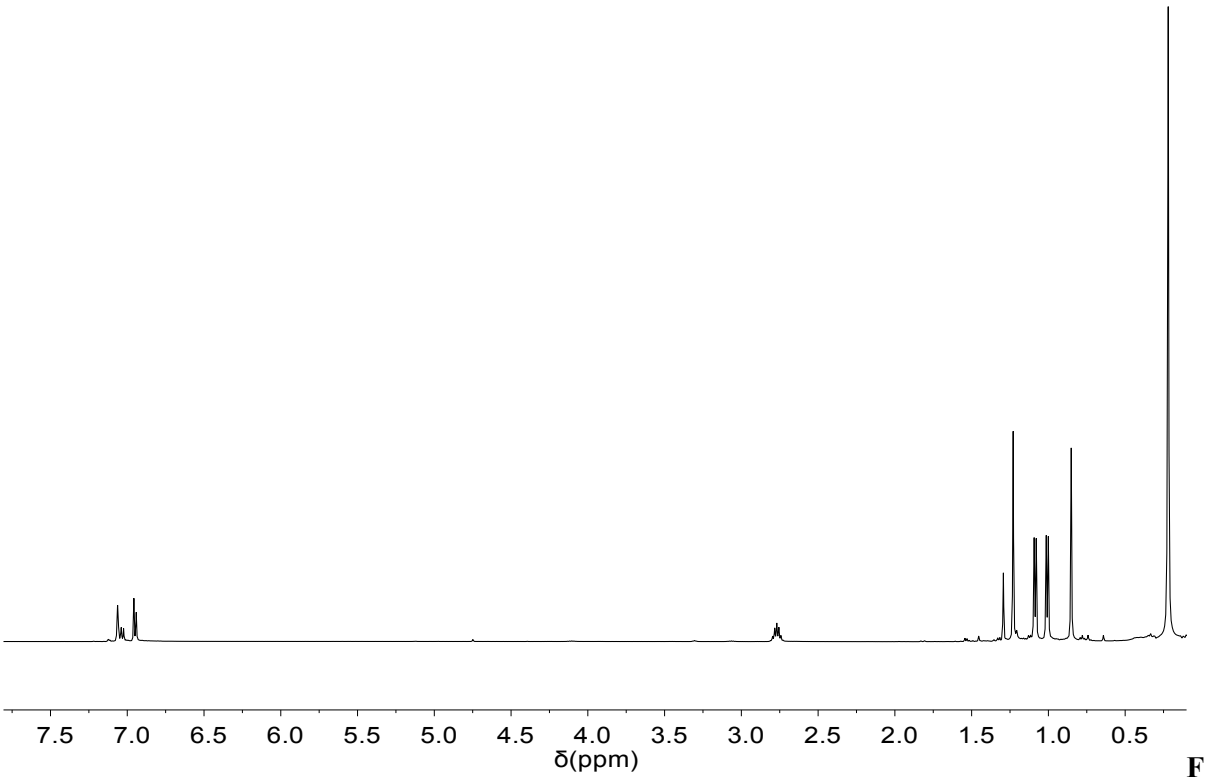

F

igure S5: ^{1}H NMR spectrum (C_6D_6, 500 MHz, 298 K) of (^{Me2}CAAC)Ba(N{$SiMe_3$}$_2$)$_2$ (**4**)

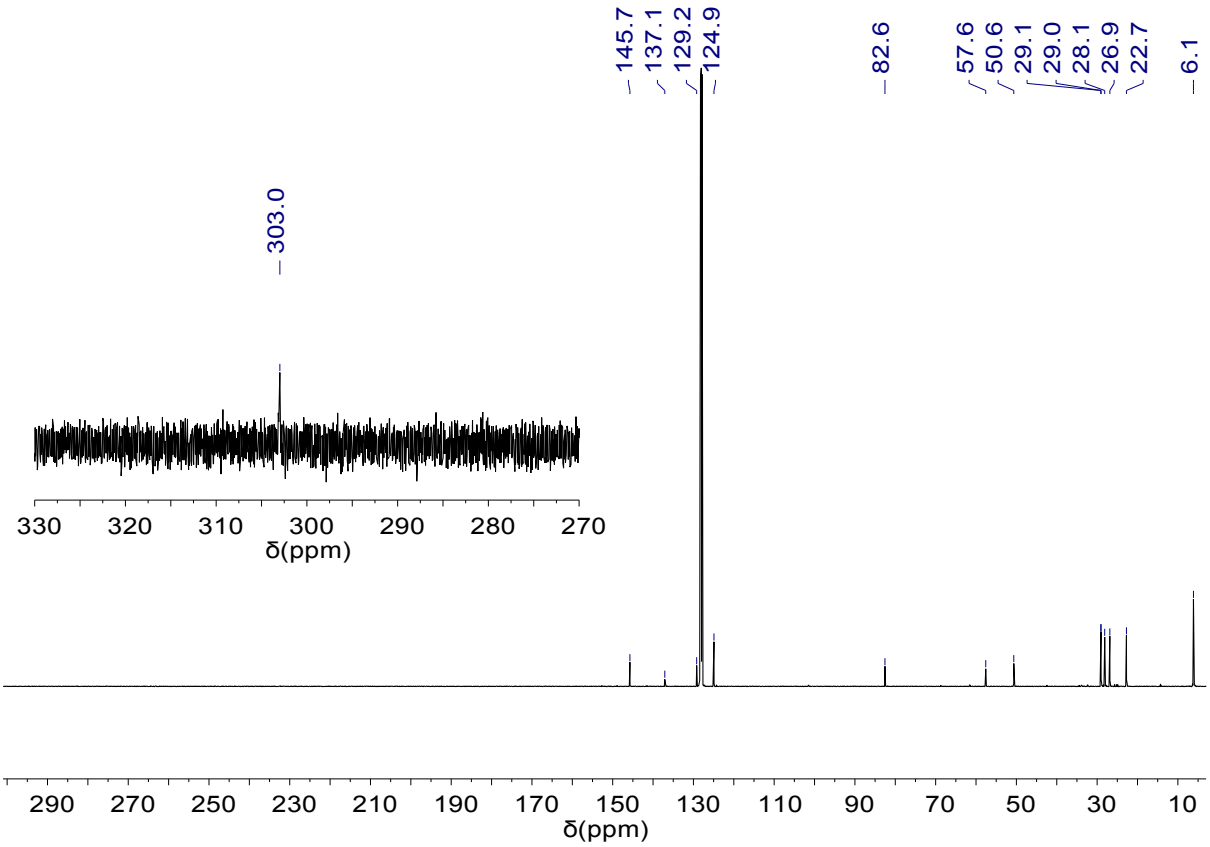

Figure S6: $^{13}C\{^{1}H\}$ NMR spectrum (C_6D_6, 125 MHz, 298 K) of (^{Me2}CAAC)Ba(N{$SiMe_3$}$_2$)$_2$ (**4**)

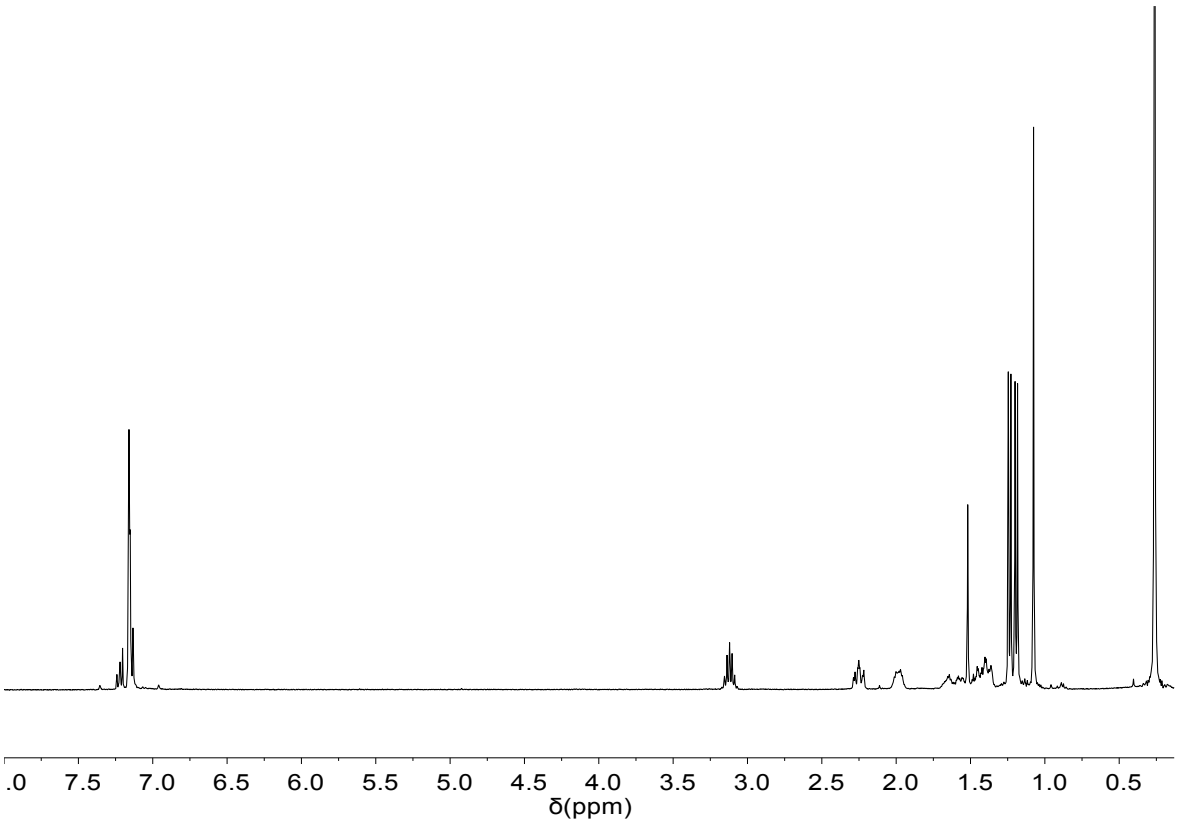

Figure S7: ^{1}H NMR spectrum (C_6D_6, 400 MHz, 298 K) of $[(^{Cy}CAAC)_3K][Sr(N\{SiMe_3\}_2)_3]$ (**6**)

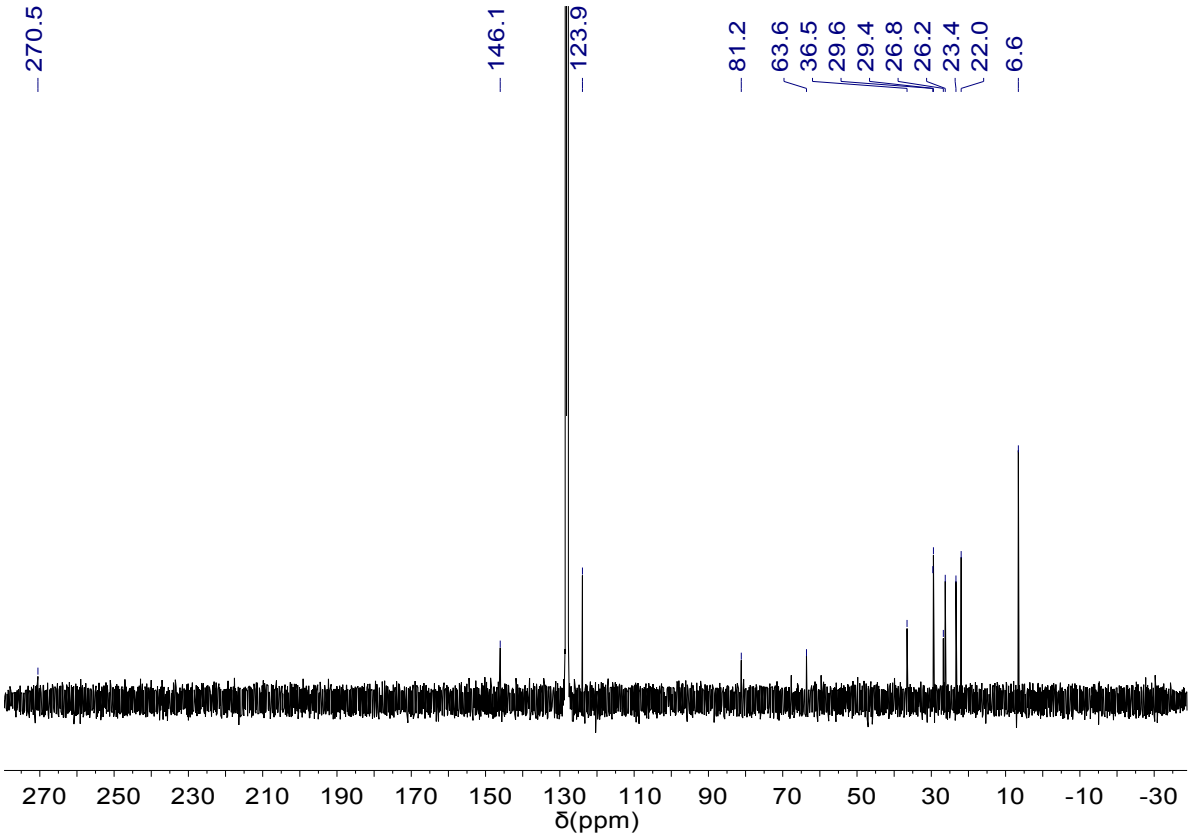

Figure S8: $^{13}C\{^{1}H\}$ NMR spectrum (C_6D_6, 100 MHz, 298 K) of $[(^{Cy}CAAC)_3K][Sr(N\{SiMe_3\}_2)_3]$ (**6**)

IV. **Crystallographic data**

Crystals were mounted on MiTeGen MicroMounts using perfluoropolyether oil and rapidly transferred to a goniometer head on a diffractometer fitted with an Oxford Cryosystems Cryostream open-flow nitrogen cooling device.[5] Data collections were carried out at 150 K using an Oxford Diffraction Supernova diffractometer using mirror-monochromated Cu *Kα* radiation (λ = 1.54178 Å) and data were processed using CrysalisPro [6] The structures were solved using direct methods (SIR-92)[7] or a charge flipping algorithm (SUPERFLIP)[8] and refined by full-matrix least-squares procedures.

Table S1: Selected experimental crystallographic data.

Complex	$(^{Me2}CAAC)Mg(N\{SiMe_3\}_2)_2$ (**1**)	$(^{Cy}CAAC)Mg(N\{SiMe_3\}_2)_2$ (**2**)	$(^{Me2}CAAC)Ba(N\{SiMe_3\}_2)_2(thf)$ (**4**)
Crystal data			
Chemical formula	$C_{32}H_{67}MgN_3Si_4$	$C_{35}H_{71}MgN_3Si_4$	$C_{36}H_{75}BaN_3OSi_4$
M_r	630.55	670.61	815.69
Crystal system, space group	Monoclinic, $P2_1/n$	Monoclinic, $P2_1/n$	Monoclinic, $P2_1/n$
Temperature (K)	150	150	150
a, *b*, *c* (Å)	12.5690 (1), 24.6401 (2), 13.4387 (1)	10.4910 (1), 20.8334 (1), 20.0585 (2)	12.5830 (2), 20.8237 (4), 17.9449 (4)
α, *β*, *γ* (°)	90, 106.479 (1), 90	90, 103.328 (1), 90	90, 93.982 (2), 90
V (Å^3)	3991.02 (6)	4265.97 (6)	4690.65 (16)
Z	4	4	4
Radiation type	Cu *Kα*	Cu *Kα*	Cu *Kα*
μ (mm^{-1})	1.70	1.61	7.76
Crystal size (mm)	0.12 × 0.10 × 0.07	0.14 × 0.08 × 0.08	0.13 × 0.08 × 0.07
Data Collection			
Diffractometer	SuperNova, Dual, Cu at zero, Atlas diffractometer	SuperNova, Dual, Cu at zero, Atlas diffractometer	SuperNova, Dual, Cu at zero, Atlas diffractometer
Absorption correction	Multi-scan. *CrysAlis PRO*, Agilent Technologies, Version 1.171.35.21 (release 20-01-2012 CrysAlis171 .NET) (compiled Jan 23 2012,18:06:46) Empirical absorption correction using spherical harmonics, implemented in SCALE3 ABSPACK	Multi-scan. *CrysAlis PRO*, Agilent Technologies, Version 1.171.35.21 (release 20-01-2012 CrysAlis171 .NET) (compiled Jan 23 2012,18:06:46) Empirical absorption correction using spherical harmonics, implemented in SCALE3 ABSPACK	Multi-scan. *CrysAlis PRO*, Agilent Technologies, Version 1.171.35.21 (release 20-01-2012 CrysAlis171 .NET) (compiled Jan 23 2012,18:06:46) Empirical absorption correction using spherical harmonics, implemented in SCALE3 ABSPACK

	scaling algorithm.	scaling algorithm.	scaling algorithm.
T_{min}, T_{max}	0.814, 1.000	0.815, 1.000	0.762, 1.000
No. of measured, independent and observed [$I > 2\sigma(I)$] reflections	35149, 8275, 7419	50487, 8814, 8315	22748, 9620, 8301
R_{int}	0.024	0.019	0.034
	Refinement		
$R[F^2 > 2\sigma(F^2)]$, $wR(F^2)$, S	0.033, 0.089, 1.05	0.032, 0.089, 1.03	0.041, 0.114, 1.04
No. of reflections	8275	8814	9620
No. of parameters	381	406	426
No. of restraints	-	-	-
$\Delta\rho_{max}$, $\Delta\rho_{min}$ (e Å^{-3})	0.68, -0.71	0.54, −0.33	0.86, -1.86

Complex	(^{Cy}CAAC)Ba(N{SiMe$_3$}$_2$)$_2$(thf) (**5**)	[(^{Cy}CAAC)$_3$K][Sr(N{SiMe$_3$}$_2$)$_3$] (**6**)
	Crystal data	
Chemical formula	$C_{39}H_{79}BaN_3OSi_4$	$C_{69}H_{105}KN_3 \cdot C_{18}H_{54}N_3Si_6Sr$
M_r	855.75	1584.45
Crystal system, space group	Monoclinic, $P2_1/n$	Trigonal, $R3{:}H$
Temperature (K)	150	150
a, b, c (Å)	12.0901 (1), 18.1027 (2), 23.5571 (2)	20.6446 (6), 20.6446 (6), 20.1037 (8)
α, β, γ (°)	90, 98.407 (1), 90	90, 90, 120
V (Å^3)	5100.39 (8)	7420.3 (5)
Z	4	3

Radiation type	Cu *Kα*	Mo *Kα*
μ (mm^{-1})	7.16	0.70
Crystal size (mm)	0.17 × 0.08 × 0.07	0.15 × 0.08 × 0.08
	Data Collection	
Diffractometer	SuperNova, Dual, Cu at zero, Atlas diffractometer	SuperNova, Dual, Cu at zero, Atlas diffractometer
Absorption correction	Multi-scan. *CrysAlis PRO*, Agilent Technologies, Version 1.171.35.21 (release 20-01-2012 CrysAlis171 .NET) (compiled Jan 23 2012,18:06:46) Empirical absorption correction using spherical harmonics, implemented in SCALE3 ABSPACK scaling algorithm.	Multi-scan. *CrysAlis PRO*, Agilent Technologies, Version 1.171.35.21 (release 20-01-2012 CrysAlis171 .NET) (compiled Jan 23 2012,18:06:46) Empirical absorption correction using spherical harmonics, implemented in SCALE3 ABSPACK scaling algorithm.
T_{min}, T_{max}	0.396, 1.000	
No. of measured, independent and observed [$I > 2\sigma(I)$] reflections	60384, 10543, 9928	28852, 8920, 7984
R_{int}	0.033	0.032
	Refinement	
$R[F^2 > 2\sigma(F^2)]$, $wR(F^2)$, S	0.023, 0.060, 1.05	0.034, 0.076, 1.03
No. of reflections	10543	8920
No. of parameters	488	316
No. of restraints	8	1
$\Delta\rho_{max}$, $\Delta\rho_{min}$ (e $Å^{-3}$)	0.57, -0.60	0.35, -0.21
Absolute structure	-	Flack x determined using 3417

		quotients [(I+)-(I-)]/[(I+)+(I-)] (Parsons, Flack and Wagner, Acta Cryst. B69 (2013) 249-259).
Absolute structure parameter	-	-0.0116 (18)

Computer programs: *CrysAlis PRO*, Agilent Technologies, Version 1.171.35.21 (release 20-01-2012 CrysAlis171 .NET) (compiled Jan 23 2012,18:06:46), : SUPERFLIP. Palatinus, L.; Chapuis, G. J. Appl. Cryst. 2007, 40, 786-790, : Sir-92. Altomare, A.; Cascarano, G.; Giacovazzo, C.; Guagliardi, A. J. Appl. Cryst. 1994, 27, 435., *SHELXL2014* (Sheldrick, 2014), *ORTEP-3 for Windows*. Farrugia, L. J. J. Appl. Cryst. 1997, 30, 565.

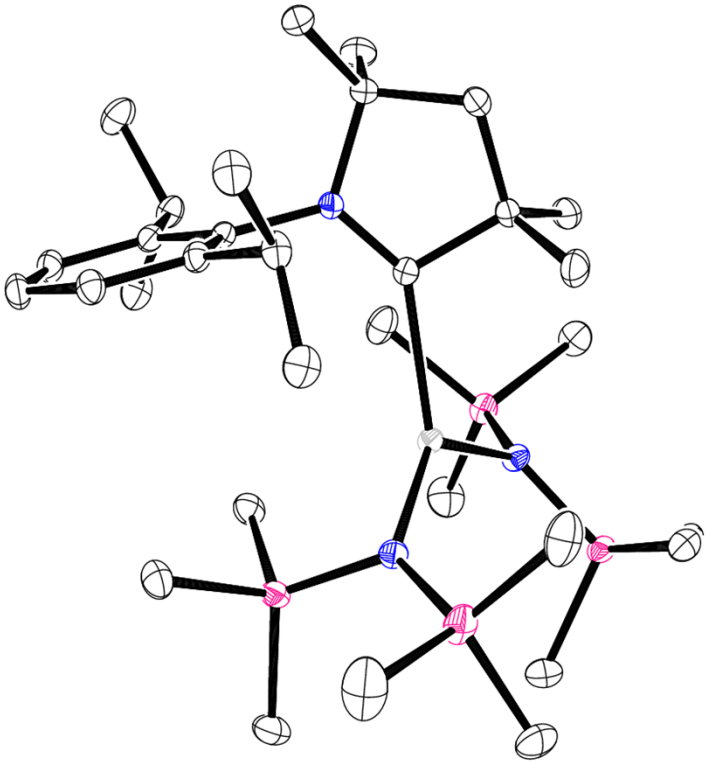

Figure S9: Thermal displacement ellipsoid drawings (30% probability) of (^{Me2}CAAC)Mg(N{SiMe$_3$}$_2$)$_2$ (**1**) All hydrogen atoms have been omitted for clarity.

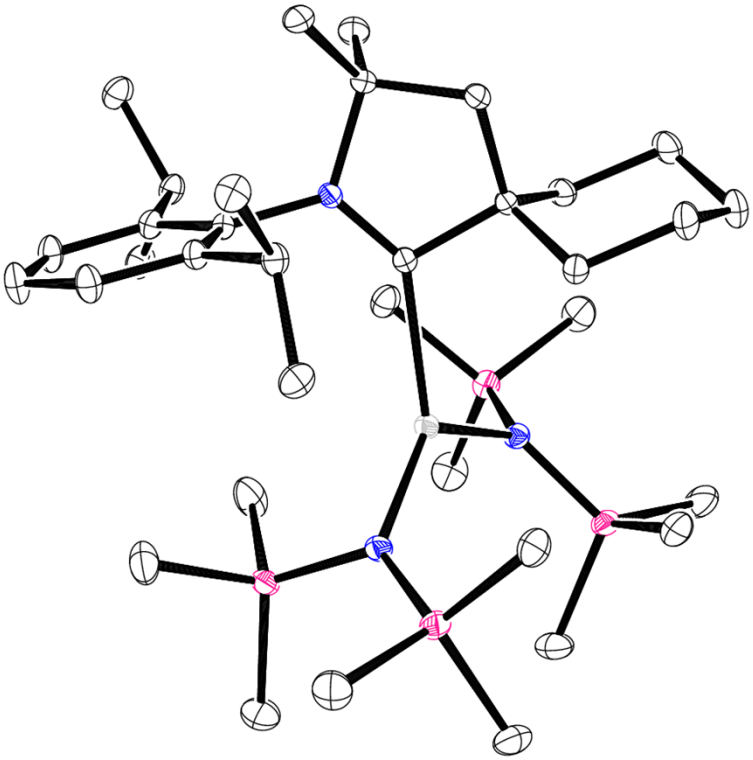

Figure S10: Thermal displacement ellipsoid drawings (30% probability) of (^{Cy}CAAC)Mg(N{SiMe$_3$}$_2$)$_2$.(**2**) All hydrogen atoms have been omitted for clarity.

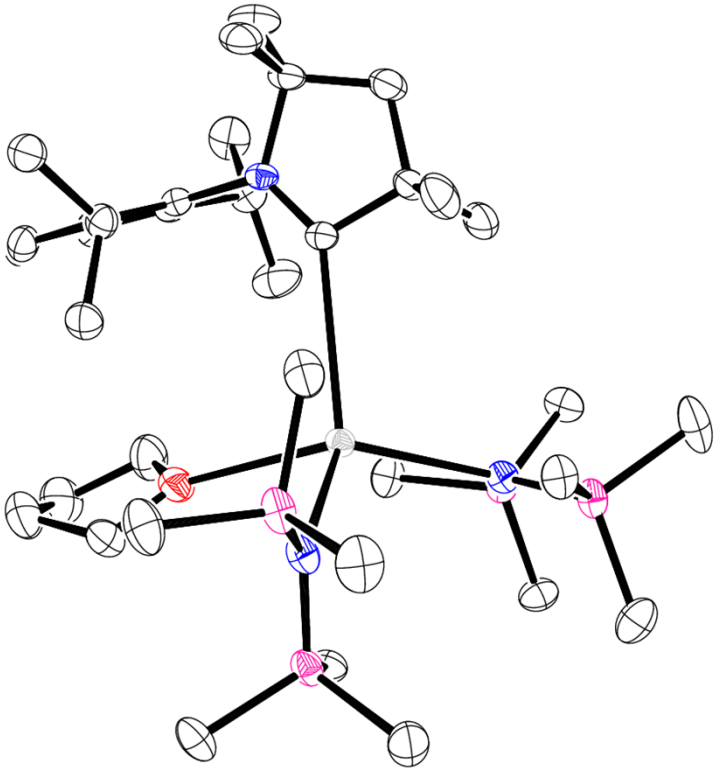

Figure S11: Thermal displacement ellipsoid drawings (30% probability) of (^{Me2}CAAC)Ba(N{SiMe$_3$}$_2$)$_2$(thf) (**4**). All hydrogen atoms have been omitted for clarity.

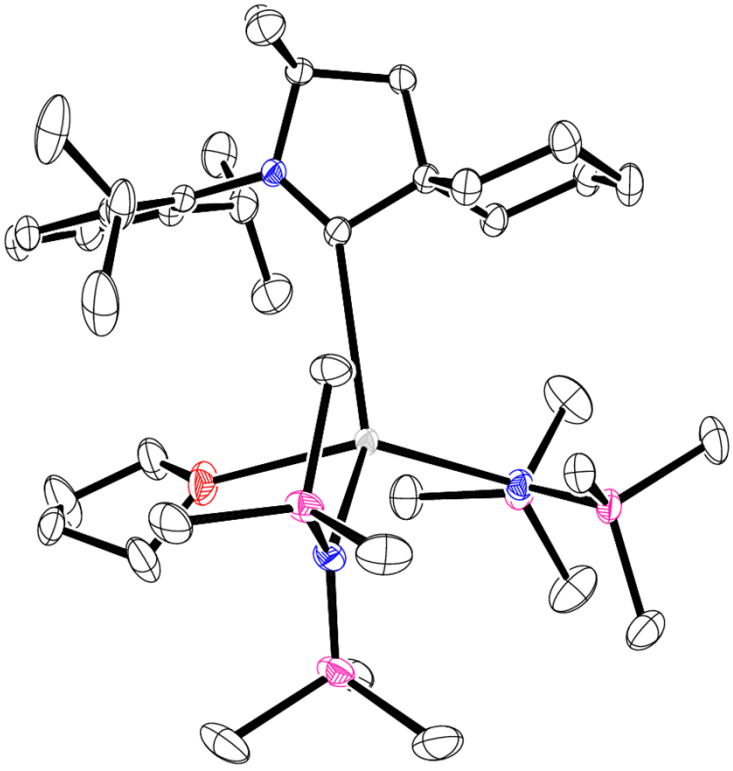

Figure S12: Thermal displacement ellipsoid drawings (30% probability) of (^{Cy}CAAC)Ba(N{SiMe$_3$}$_2$)$_2$(thf) (**5**). All hydrogen atoms have been omitted for clarity.

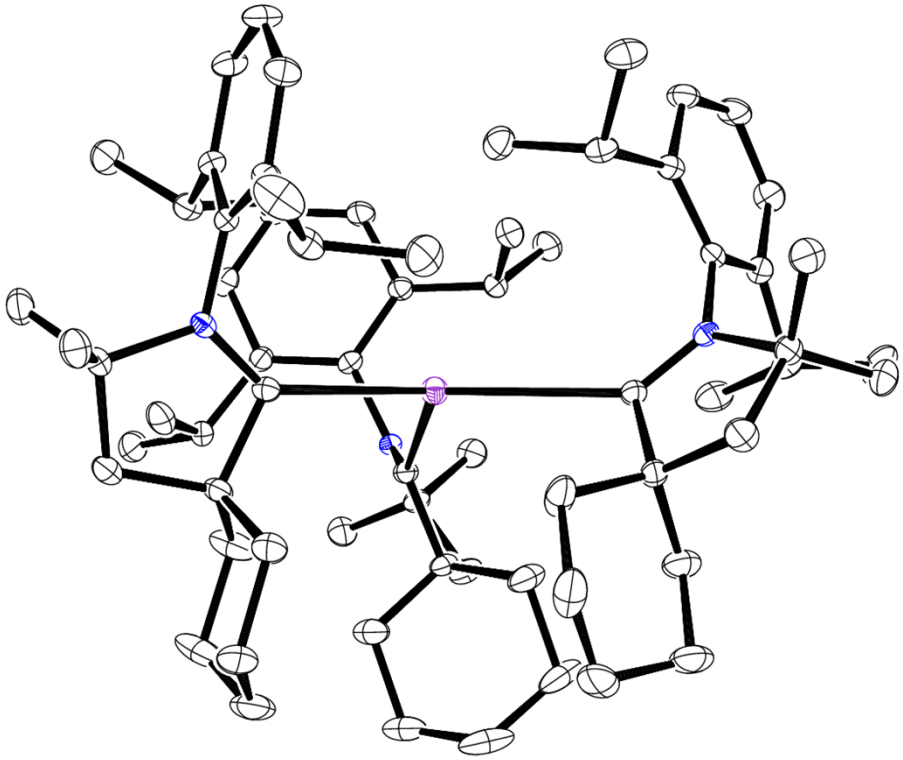

Figure S13: Thermal displacement ellipsoid drawings (30% probability) of $[(^{Cy}CAAC)_3K][Sr(N\{SiMe_3\}_2)_3]$ (**6**). Only the cationic species is depicted; The $[Sr(N\{SiMe_3\}_2)_3]$ and all hydrogen atoms have been omitted for clarity.

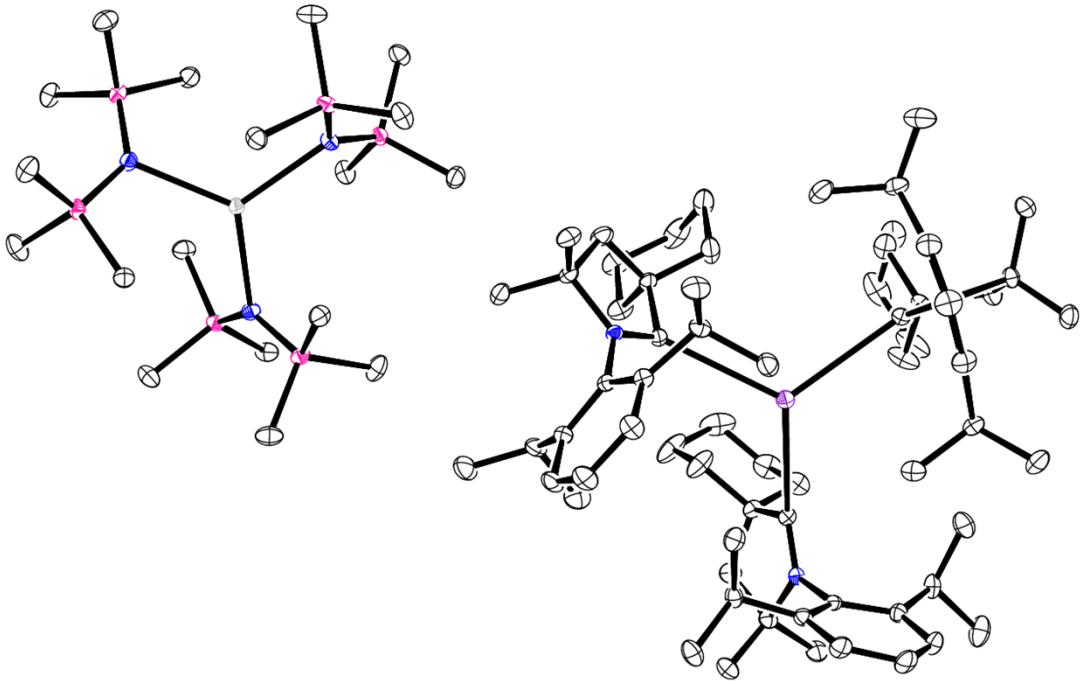

Figure S14: Thermal displacement ellipsoid drawings (30% probability) of $[(^{Cy}CAAC)_3K][Sr(N\{SiMe_3\}_2)_3]$ (**6**). All hydrogen atoms have been omitted for clarity.

Table S2: Comparison of pitch (φ) and yaw (σ) angles (°) in complexes

	1	**2**	**4**	**5**	**6**
Pitch	1	1	8	1	19
Yaw	14	13	15	14	12

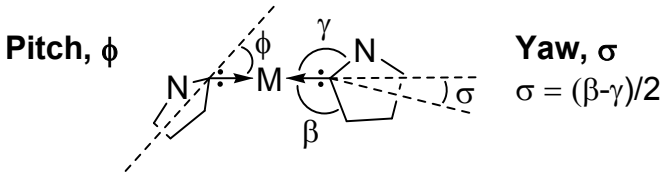

Figure S15: Graphical representation of pitch and yaw to quantify asymmetrical coordination of the CAAC ligand to the metal center.

Table S3: Comparison of pitch (φ) and yaw (σ) angles (°) in complexes

	$(C\{NMeCMe\}_2)BaCp^*_2$[9]	$(C\{N^iPrCMe\}_2)BaCp^{Me_4,tBu}_2$[9]	$(IMes)Ba(N\{SiMe_3\}_2)_2$[10]
Pitch	20	32	1
Yaw	3	4	13

V. DFT computational studies

All DFT calculations were performed with the ORCA program package.[11] The geometry optimizations of the complexes and single-point calculations on the optimized geometries were carried out at the BP86[12-14] or B3LYP[12, 15, 16] level of DFT. Relativistic effects were accounted for by including the zeroth-order regular approximation (ZORA).[17-20] The def2-TZVP(-f) basis set in the scalar relativistic recontraction reported by Neese *et al.* (segmented all-electron relativistic basis sets, SARC) was applied.[21, 22] For all elements up to bromine, the SARC basis sets are simply scalar relativistic recontractions of the basis sets developed by the Karlsruhe group,[23, 24] while for heavier elements, the primitives and contraction patterns were designed in references 21 and 22. The Coulomb fitting basis set of Weigend[25] was used in uncontracted form in all calculations. The RI[26-28] approximation was used to accelerate the calculations. Orbitals were generated with the program Chimera.[29]

Table S4: Comparison of experimental and calculated metrical parameters in (^{Me2}CAAC)Mg(N{SiMe$_3$}$_2$)$_2$ (**1**)

	1 Experimental	**1** Calculated (B3LYP)
C1-Mg1	2.2931(12)	2.390
C1-N1	1.3090(15)	1.314
C1-C2	1.5352(16)	1.543
N2-Mg1	2.0266(11)	2.037
N3-Mg1	2.0101(11)	2.023
C2-C1-N1		
C2-C1-Mg1	112.28(8)	112.31
N1-C1-Mg1	139.74(9)	139.46
C1-Mg1-N2	112.28(8)	110.22
C1-Mg1-N3	120.85(5)	120.82
N2-Mg1-N3	125.47(5)	128.12
C2-C1-Mg1-N2	54.73(9)	54.25

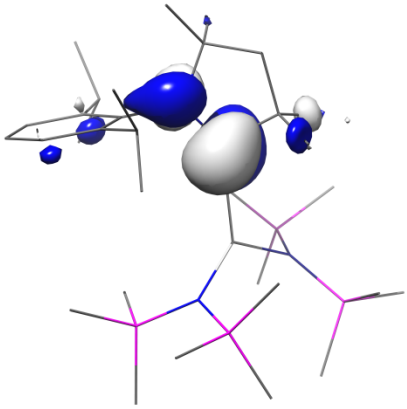

LUMO

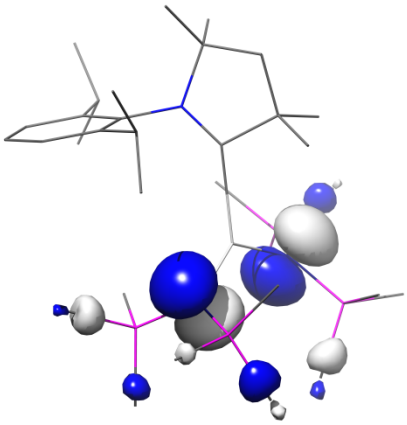

HOMO

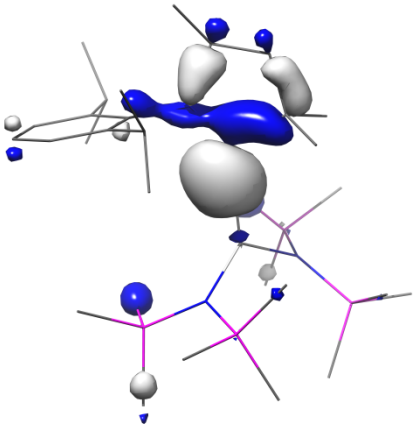

HOMO-10

Figure S16: DFT-computed LUMO (top), HOMO (middle) and HOMO-10 (bottom) of (^{Me2}CAAC)Mg(N{SiMe$_3$}$_2$)$_2$ (**1**).

Table S5: Comparison of experimental and calculated metrical parameters in (^{Cy}CAAC)Mg(N{SiMe$_3$}$_2$)$_2$ (**2**)

	2 Experimental	**2** Calculated (B3LYP)
C1-Mg1	2.2989(12)	2.393
C1-N1	1.3110(15)	1.315
C1-C2	1.5350(15)	1.542
N2-Mg1	2.0149(10)	2.027
N3-Mg1	2.0226(11)	2.045
C2-C1-N1	107.87(9)	108.31
C2-C1-Mg1	112.68(7)	112.49
N1-C1-Mg1	139.42(8)	139.18
C1-Mg1-N2	123.11(4)	119.29
C1-Mg1-N3	111.65(4)	111.66
N2-Mg1-N3	123.30(4)	128.16
C2-C1-Mg1-N2	118.32(8)	114.37

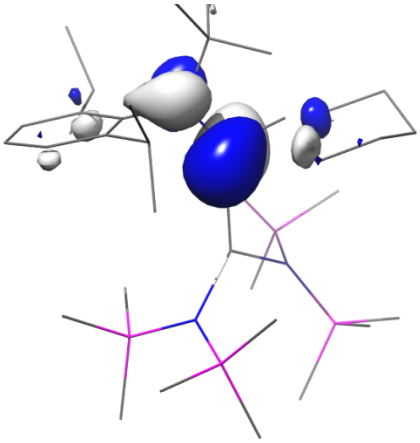

LUMO

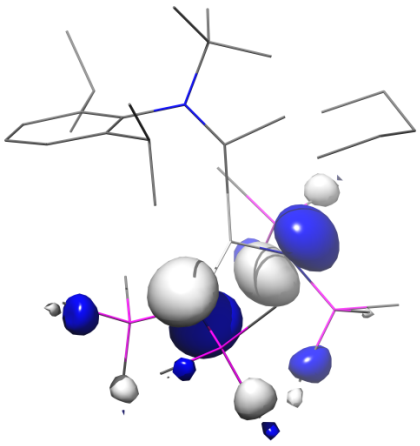

HOMO

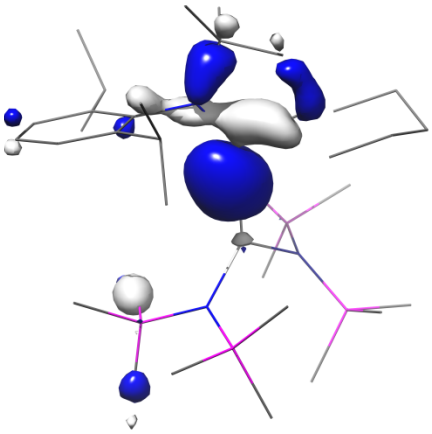

HOMO-10

Figure S17: DFT-computed LUMO (top), HOMO (middle) and HOMO-10 (bottom) of (^{Cy}CAAC)Mg(N{SiMe$_3$}$_2$)$_2$ (**2**).

Table S6: Comparison of experimental and calculated metrical parameters in (^{Me2}CAAC)Ba(N{$SiMe_3$}$_2$)$_2$(thf)(**4**)

	4 Experimental	**4** Calculated (BP86)
C1-Ba1	3.108(3)	3.338
C1-N1	1.298(5)	1.314
C1-C2	1.533(5)	1.529
N2-Ba1	2.600(3)	2.636
N3-Ba1	2.617(3)	2.623
O1-Ba1	2.798(3)	2.864
C2-C1-N1	107.1(3)	107.42
C2-C1-Ba1	111.4(2)	109.79
N1-C1-Ba1	140.8(2)	142.40
C1-Ba1-N2	133.30(10)	130.55
C1-Ba1-N3	103.40(9)	103.56
C2-C1-Ba1-N2	91.89(1)	92.70

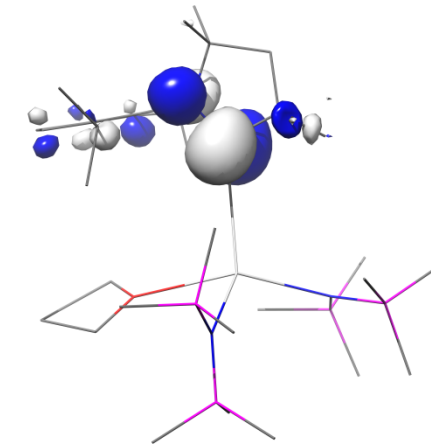

LUMO

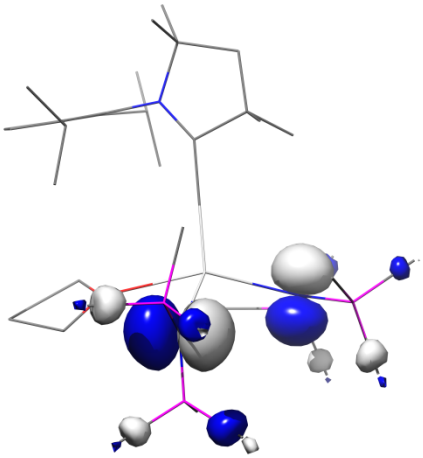

HOMO

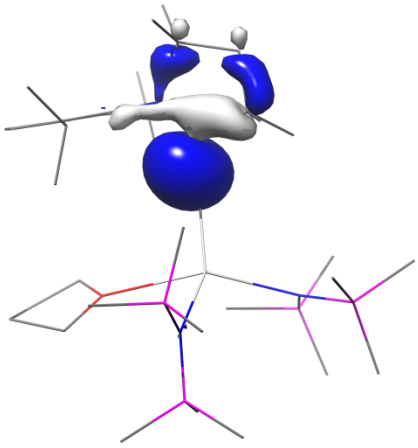

HOMO-4

Figure S18: DFT-computed LUMO (top), HOMO (middle) and HOMO-4 (bottom) of (^{Me2}CAAC)Ba(N{SiMe$_3$}$_2$)$_2$(thf) (**4**).

VI. **Polymerisation data**

General procedure for polymerisation were carried out in Young's tap NMR tubes containing 40 mg of lactide in 0.56 mL of a benzene-d_6 (giving a initial concentration of $[LA]_0 = 0.5$ M) and a catalyst (to ensure $[LA]_0/[M]_0 = 200$). Lactide conversion was subsequently calculated by comparing the integration values of the methine signal of PLA and lactide monomer in the ^{1}H NMR spectrum. The polymerisations were carried out at ambient temperature (23 °C).

The polymerisations were quenched by precipitation in cold pentane, filtered and washed with cold pentane. The polylactide obtained were dried in a vacuum oven over-night before ^{1}H{^{1}H} and ^{13}C{^{1}H} NMR spectroscopy and gel permeation chromatography.

Using (^{Me2}CAAC)Mg(N{SiMe$_3$}$_2$)$_2$ (**1**)

Table S7: L-lactide polymerisation using (^{Me2}CAAC)Mg(N{SiMe$_3$}$_2$)$_2$ (**1**). Polymerisation conditions: benzene-d_6, $[LA]_0/[M]_0 = 200$, [LA]0 = 0.5 M, 23 °C.

Time (h)	Conversion (%)
0.13	21.2
0.68	26.2
1.1	27.3
1.58	27.8
2.13	29.3
2.98	29.5
3.52	29.9
5.65	30.4
9.28	31.7

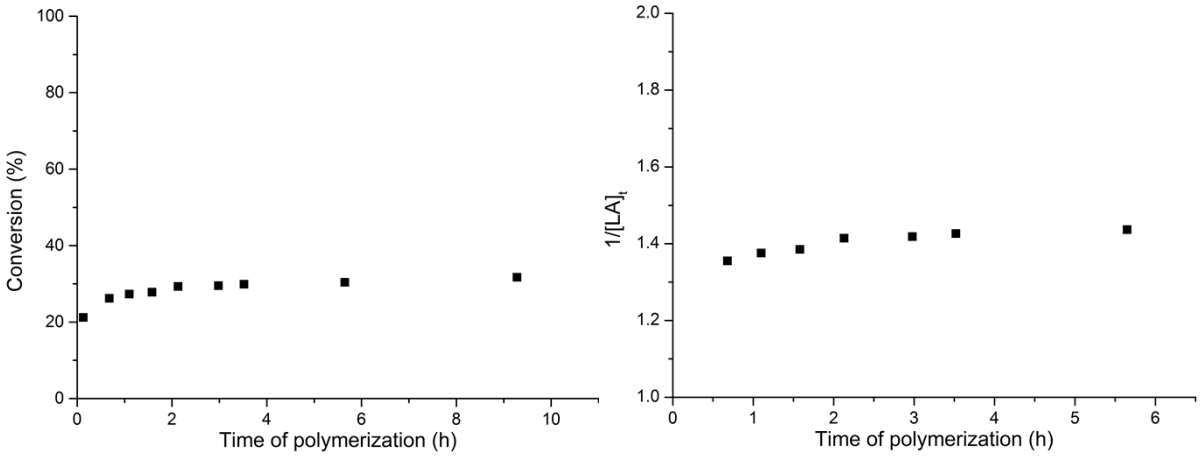

Figure S19: L-lactide polymerisation using complex (^{Me2}CAAC)Mg(N{SiMe$_3$}$_2$)$_2$ (**1**), conversion in function of time profile (left) and second-order rate plot (right). Polymerisation conditions: benzene-d_6 at 23 °C with $[LA]_0/[M]_0 = 200$, $[LA]_0 = 0.5$ M.

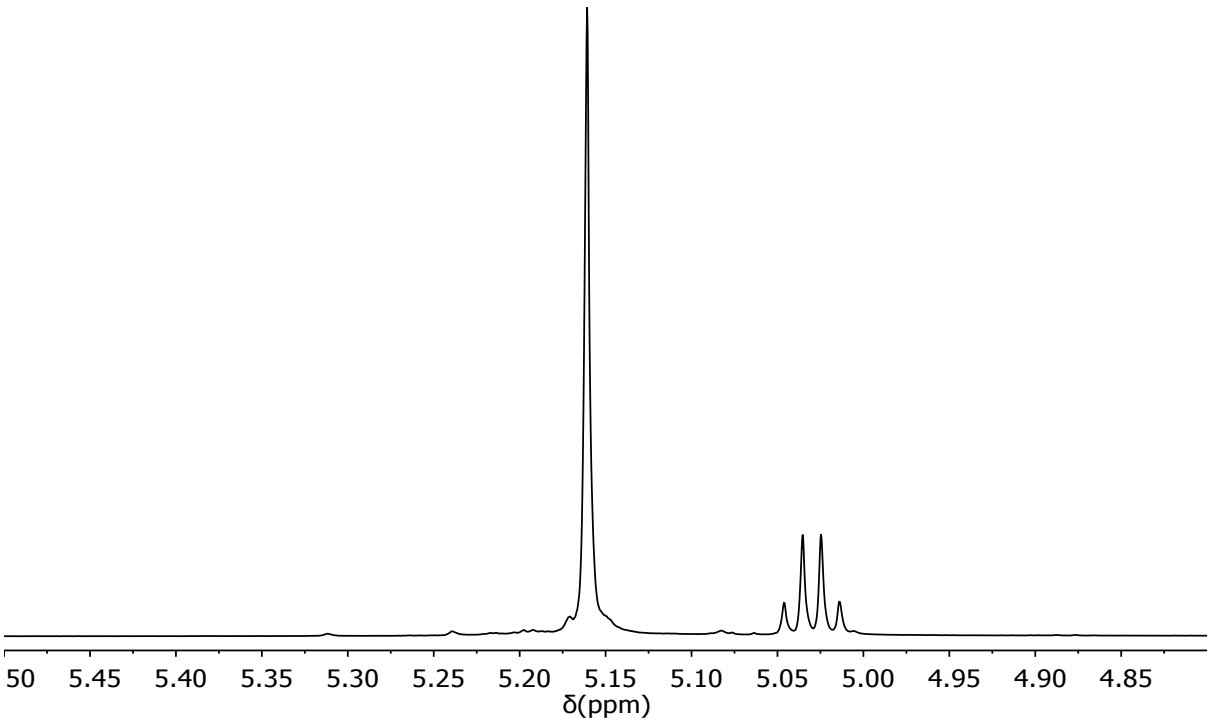

Figure S120: $^{1}H\{^{1}H\}$ NMR spectrum of poly-L-lactide synthesised using complex (^{Me_2}CAAC)Mg(N{SiMe$_3$}$_2$)$_2$ (**1**) in chloroform-d_1 at 23 °C on a 500 MHz. Polymerisation conditions: benzene-d_6 at 23 °C with $[LA]_0/[M]_0 = 200$, $[LA]_0 = 0.5$ M. L-lactide at 5.03 ppm.

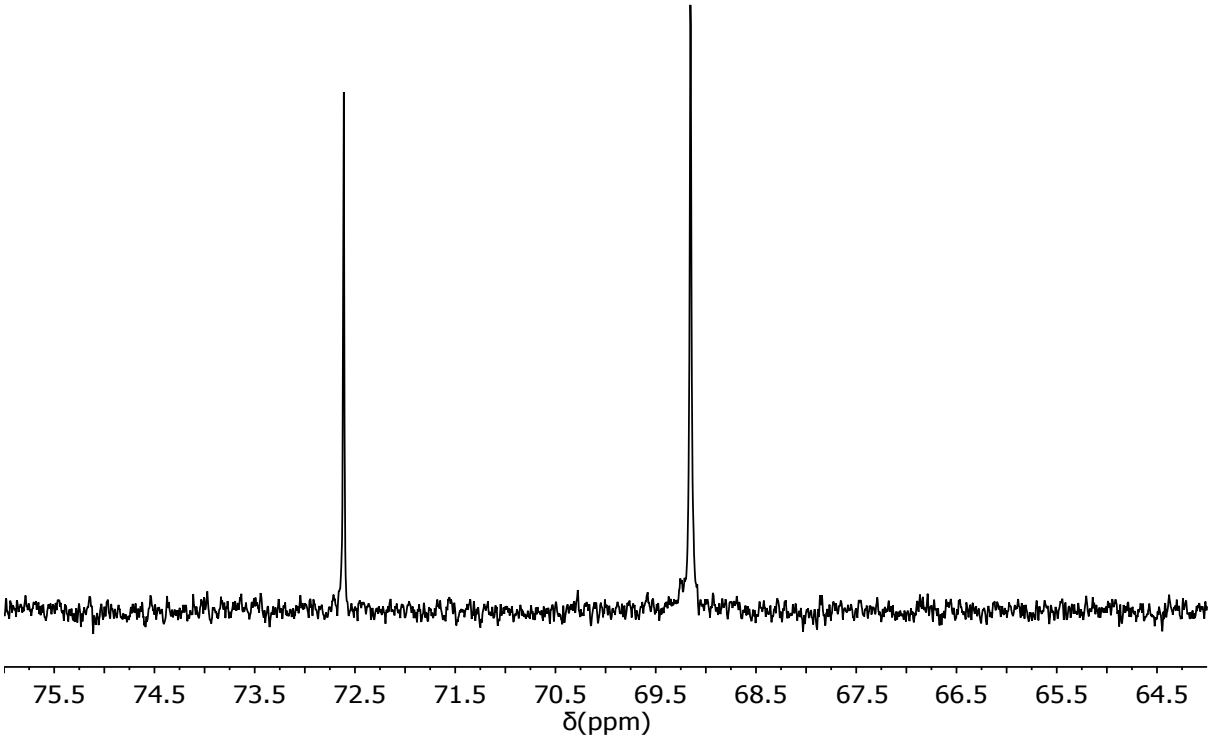

Figure S21: $^{13}C\{^{1}H\}$ NMR spectrum of poly-L-lactide synthesised using complex (^{Me_2}CAAC)Mg(N{SiMe$_3$}$_2$)$_2$ (**1**) in chloroform-d_1 at 23 °C on a 500 MHz. Polymerisation conditions: benzene-d_6 at 23 °C with $[LA]_0/[M]_0 = 200$, $[LA]_0 = 0.5$ M. L-lactide at 72.60 ppm.

Using (^{Me2}CAAC)Sr(N{SiMe$_3$}$_2$)$_2$ (**3**)

Table S8: L-lactide polymerisation using (^{Me2}CAAC)Sr(N{SiMe$_3$}$_2$)$_2$ (**3**). Polymerisation conditions: benzene-d_6, $[LA]_0/[M]_0 = 200$, [LA]0 = 0.5 M, 23 °C.

Time (h)	Conversion (%)
0.15	32.9
0.72	50.9
1.12	56.3
1.62	60.8
2.17	65.0
3	68.9
3.55	71.2
5.67	76.5
9.15	81.3

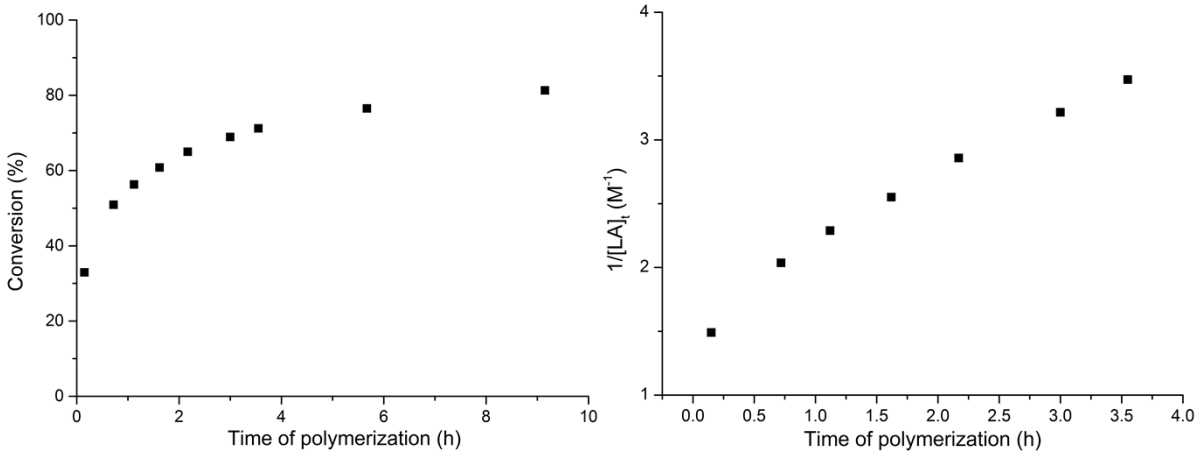

Figure S22: L-lactide polymerisation using complex (^{Me2}CAAC)Sr(N{SiMe$_3$}$_2$)$_2$ (**3**), conversion in function of time profile (left) and second-order rate plot (right). Polymerisation conditions: benzene-d_6 at 23 °C with $[LA]_0/[M]_0 = 200$, $[LA]_0 = 0.5$ M.

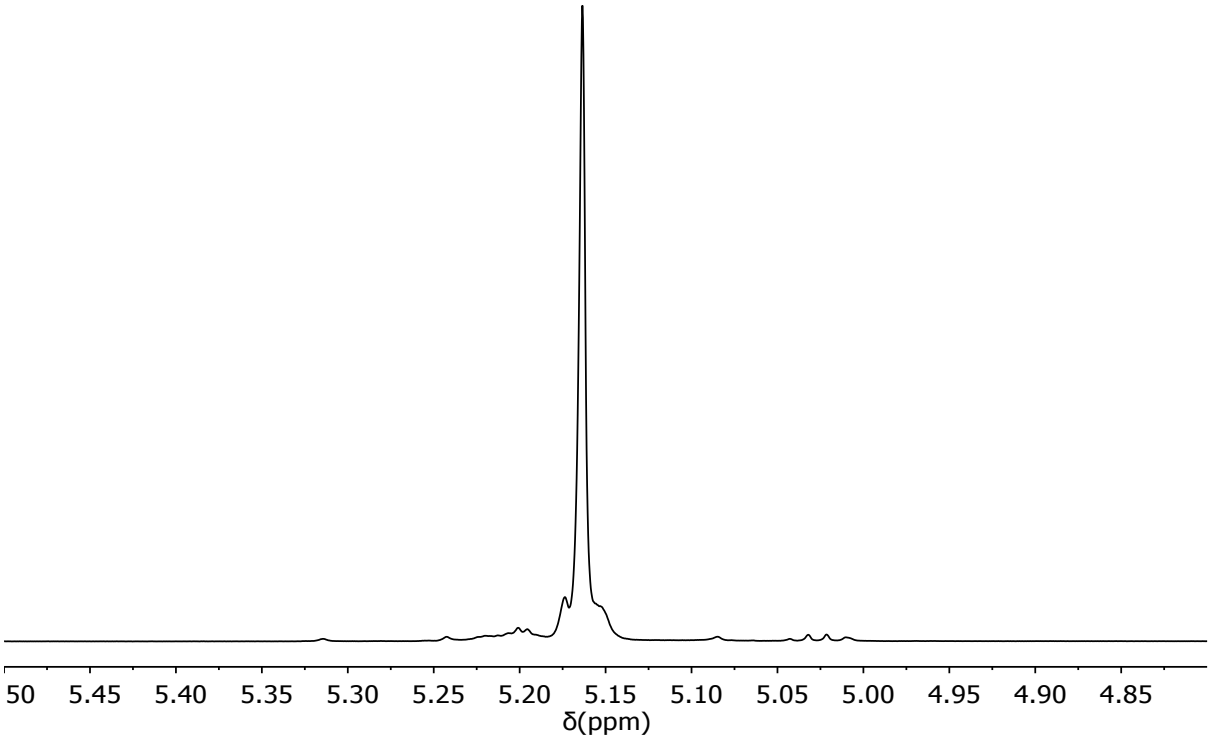

Figure S23: $^{1}H\{^{1}H\}$ NMR spectrum of poly-L-lactide synthesised using complex (^{Me2}CAAC)Sr(N{SiMe$_3$}$_2$)$_2$ (**3**) in chloroform-d_1 at 23 °C on a 500 MHz. Polymerisation conditions: benzene-d_6 at 23 °C with $[LA]_0/[M]_0 = 200$, $[LA]_0 = 0.5$ M. L-lactide at 5.03 ppm.

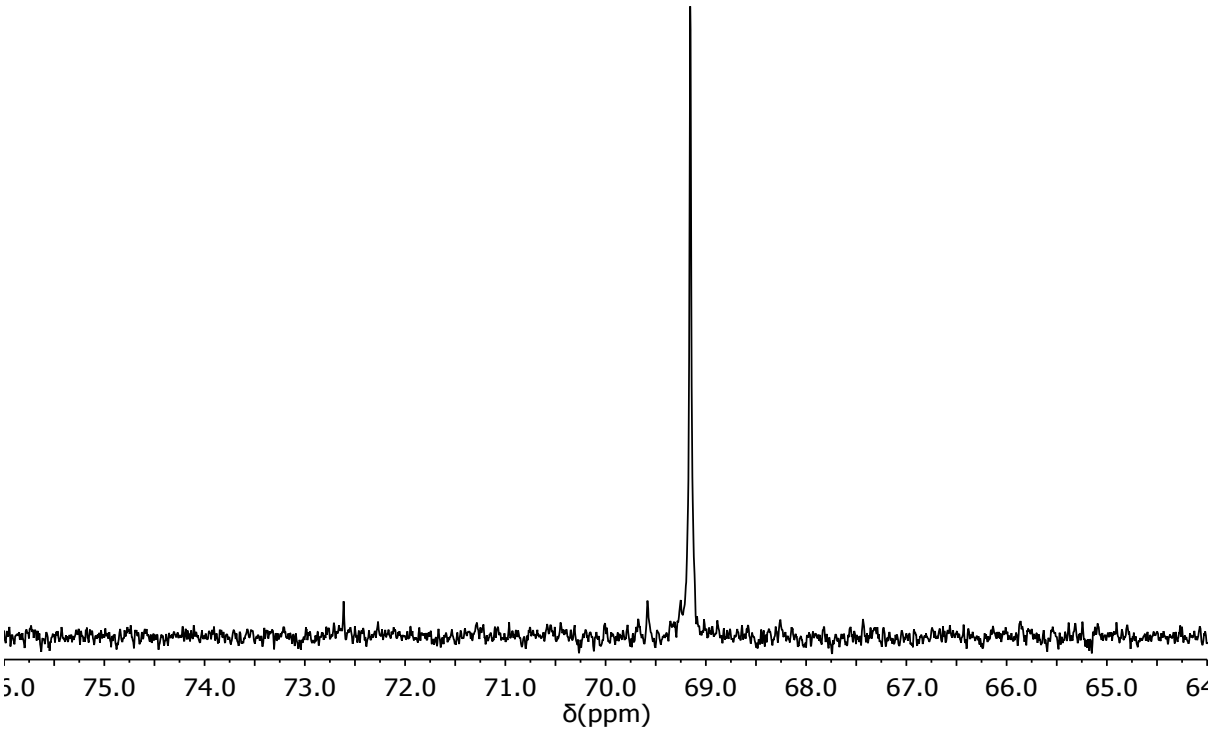

Figure S24: $^{13}C\{^{1}H\}$ NMR spectrum of poly-L-lactide synthesised using complex (^{Me2}CAAC)Sr(N{SiMe$_3$}$_2$)$_2$ (**3**) in chloroform-d_1 at 23 °C on a 500 MHz. Polymerisation conditions: benzene-d_6 at 23 °C with $[LA]_0/[M]_0 = 200$, $[LA]_0 = 0.5$ M. L-lactide at 72.60 ppm.

Table S9: *rac*-lactide polymerisation using (^{Me2}CAAC)Sr(N{SiMe$_3$}$_2$)$_2$ (**3**). Polymerisation conditions: benzene-d_6, $[LA]_0/[M]_0 = 200$, [LA]0 = 0.5 M, 23 °C.

Time (h)	Conversion (%)
0.21	8.2
0.77	17.4
1.18	21.4
1.68	26.0
2.23	30.2
3.08	34.5
3.6	37.0
5.73	46.1
9.22	55.9
20.0	67.4
28.0	72.8

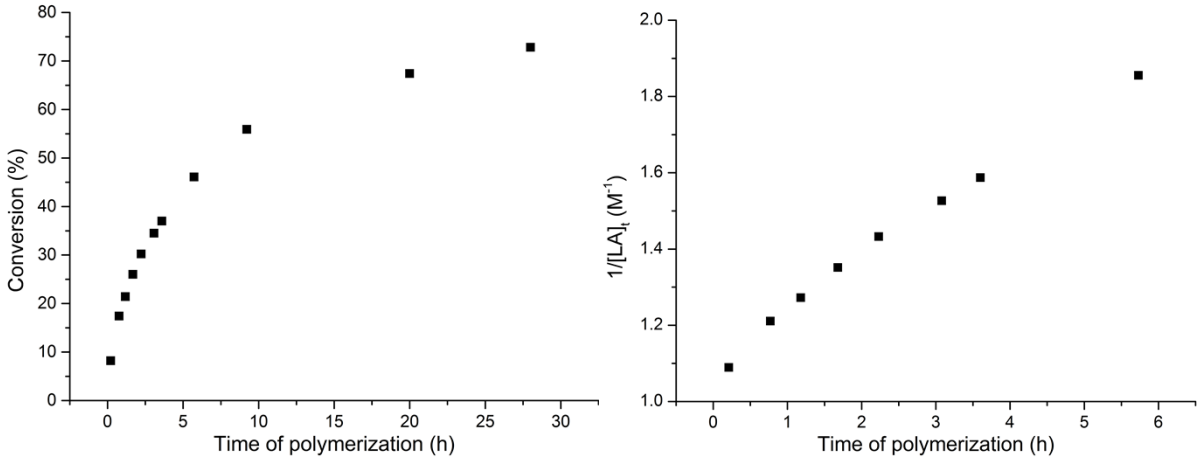

Figure S25: *rac*-lactide polymerisation using complex (^{Me2}CAAC)Sr(N{SiMe$_3$}$_2$)$_2$ (**3**), conversion in function of time profile (left) and second-order rate plot (right). Polymerisation conditions: benzene-d_6 at 23 °C with $[LA]_0/[M]_0 = 200$, $[LA]_0 = 0.5$ M.

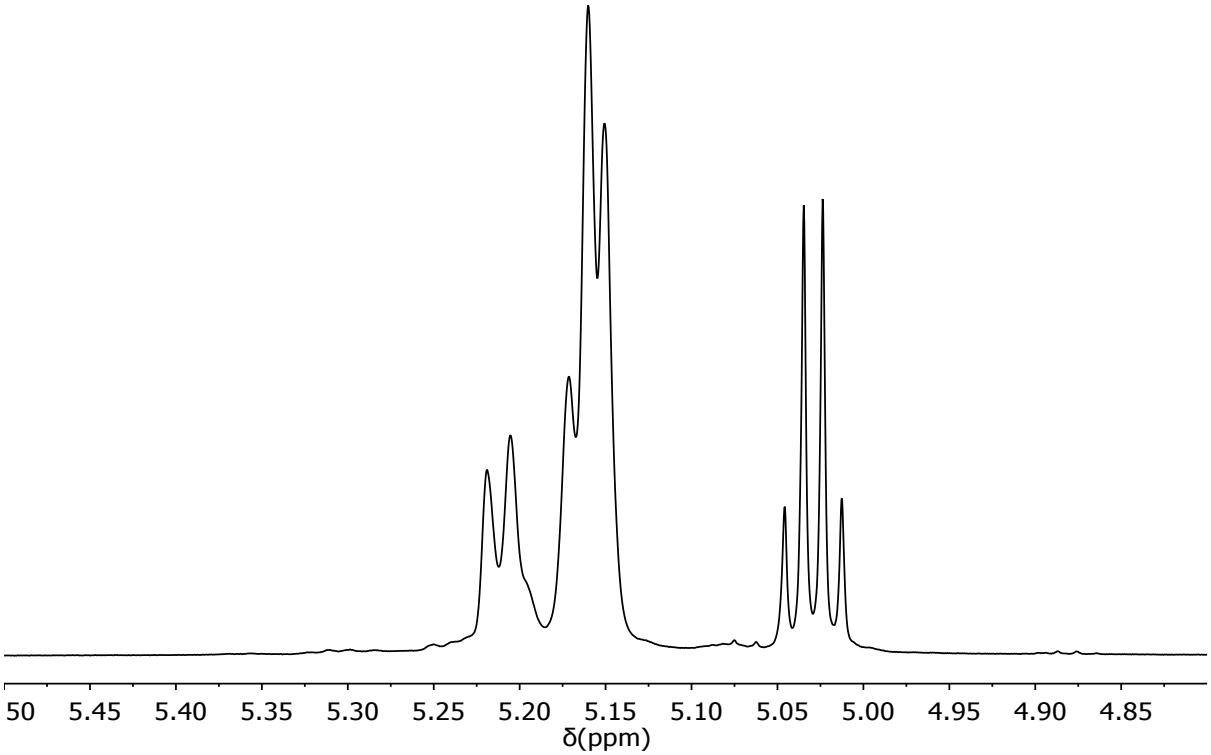

Figure S26: $^{1}H\{^{1}H\}$ NMR spectrum of poly-*rac*-lactide synthesised using complex (^{Me2}CAAC)Sr(N{SiMe$_3$}$_2$)$_2$ (**3**) in chloroform-d_1 at 23 °C on a 500 MHz. Polymerisation conditions: benzene-d_6 at 23 °C with $[LA]_0/[M]_0 = 200$, $[LA]_0 = 0.5$ M. *rac*-lactide at 5.03 ppm.

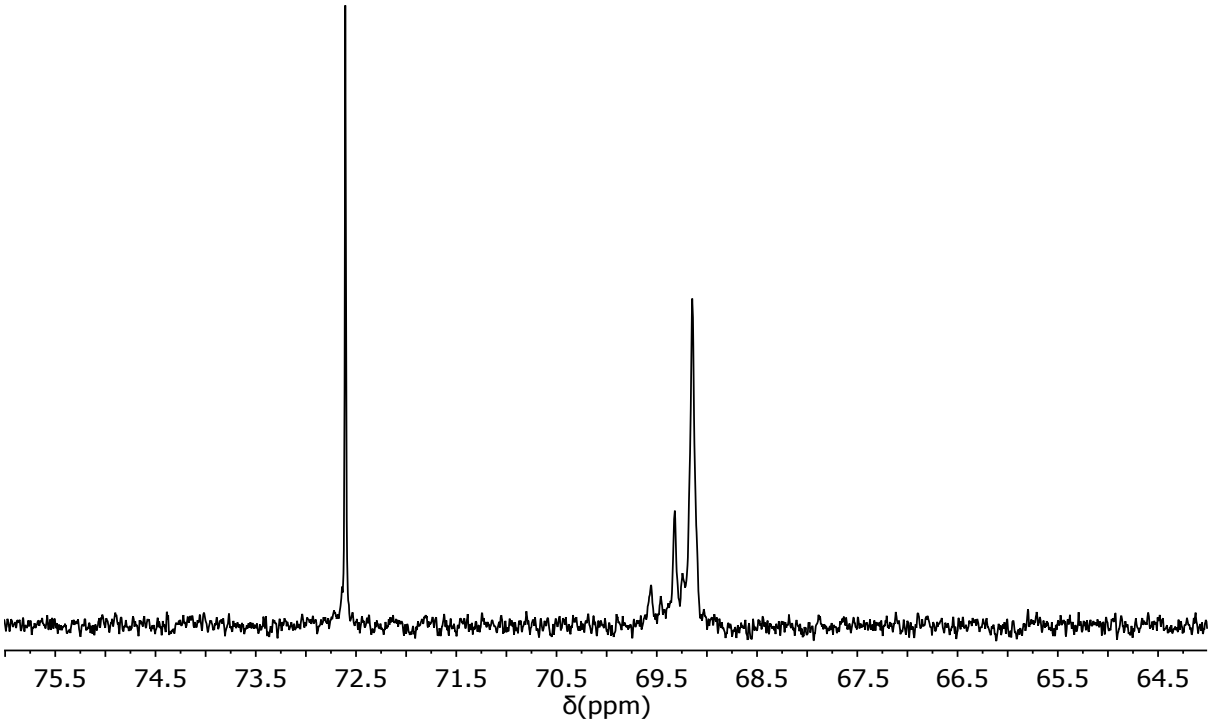

Figure S27: $^{13}C\{^{1}H\}$ NMR spectrum of poly-*rac*-lactide synthesised using complex (^{Me2}CAAC)Sr(N{SiMe$_3$}$_2$)$_2$ (**3**) in chloroform-d_1 at 23 °C on a 500 MHz. Polymerisation conditions: benzene-d_6 at 23 °C with $[LA]_0/[M]_0 = 200$, $[LA]_0 = 0.5$ M. *rac*-lactide at 72.60 ppm.

Using (^{Me2}CAAC)Ba(N{SiMe$_3$}$_2$)$_2$ (**4**)

Table S10: L-lactide polymerisation using (^{Me2}CAAC)Ba(N{SiMe$_3$}$_2$)$_2$ (**4**). Polymerisation conditions: benzene-d_6, $[LA]_0/[M]_0 = 200$, [LA]0 = 0.5 M, 23 °C.

Time (h)	Conversion (%)
0.17	6.0
0.53	23.0
0.97	36.0
2.1	57.5
3.4	70.1
4.78	77.7
6.76	84.4
8.47	87.6

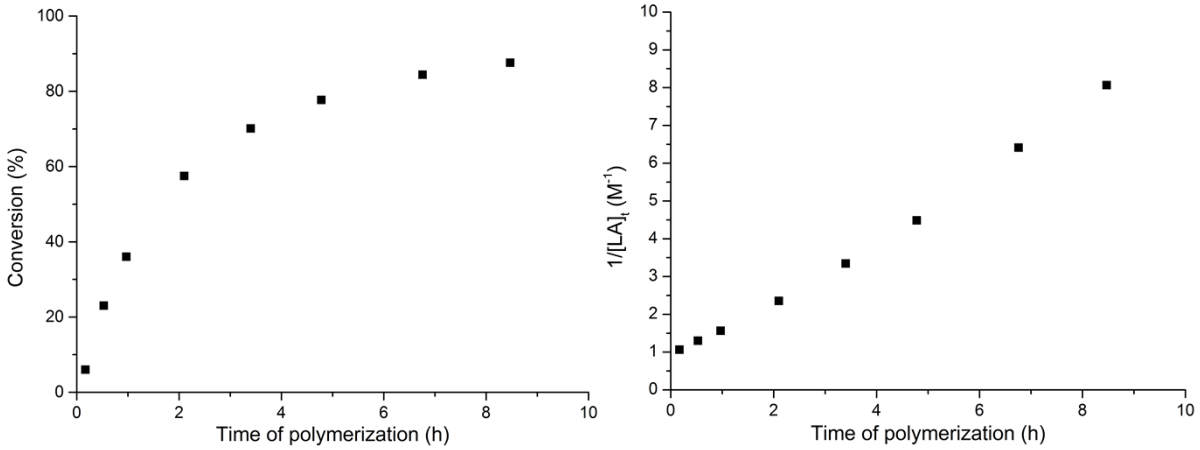

Figure S28: L-lactide polymerisation using complex (^{Me2}CAAC)Ba(N{SiMe$_3$}$_2$)$_2$ (**4**), conversion in function of time profile (left) and second-order rate plot (right). Polymerisation conditions: benzene-d_6 at 23 °C with $[LA]_0/[M]_0 = 200$, $[LA]_0 = 0.5$ M.

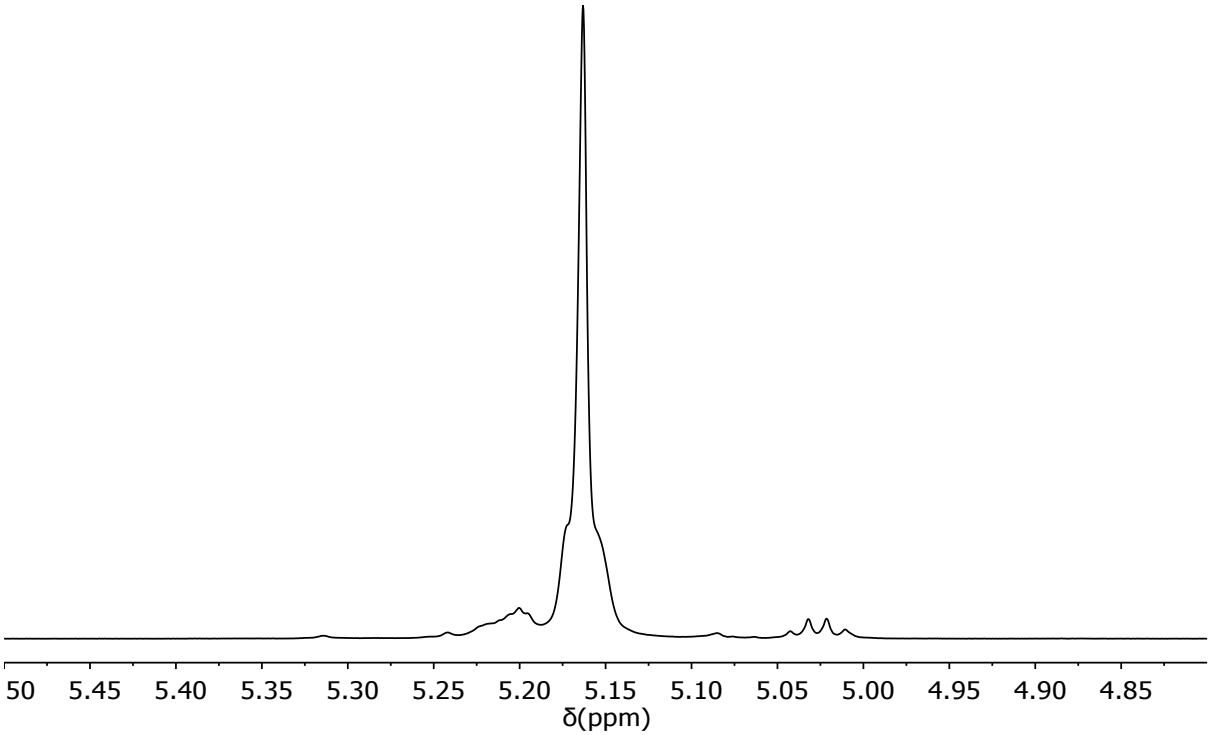

Figure S29: $^{1}H\{^{1}H\}$ NMR spectrum of poly-L-lactide synthesised using complex (^{Me2}CAAC)Ba(N{SiMe$_3$}$_2$)$_2$ (**4**) in chloroform-d_1 at 23 °C on a 500 MHz. Polymerisation conditions: benzene-d_6 at 23 °C with $[LA]_0/[M]_0 = 200$, $[LA]_0 = 0.5$ M. L-lactide at 5.03 ppm.

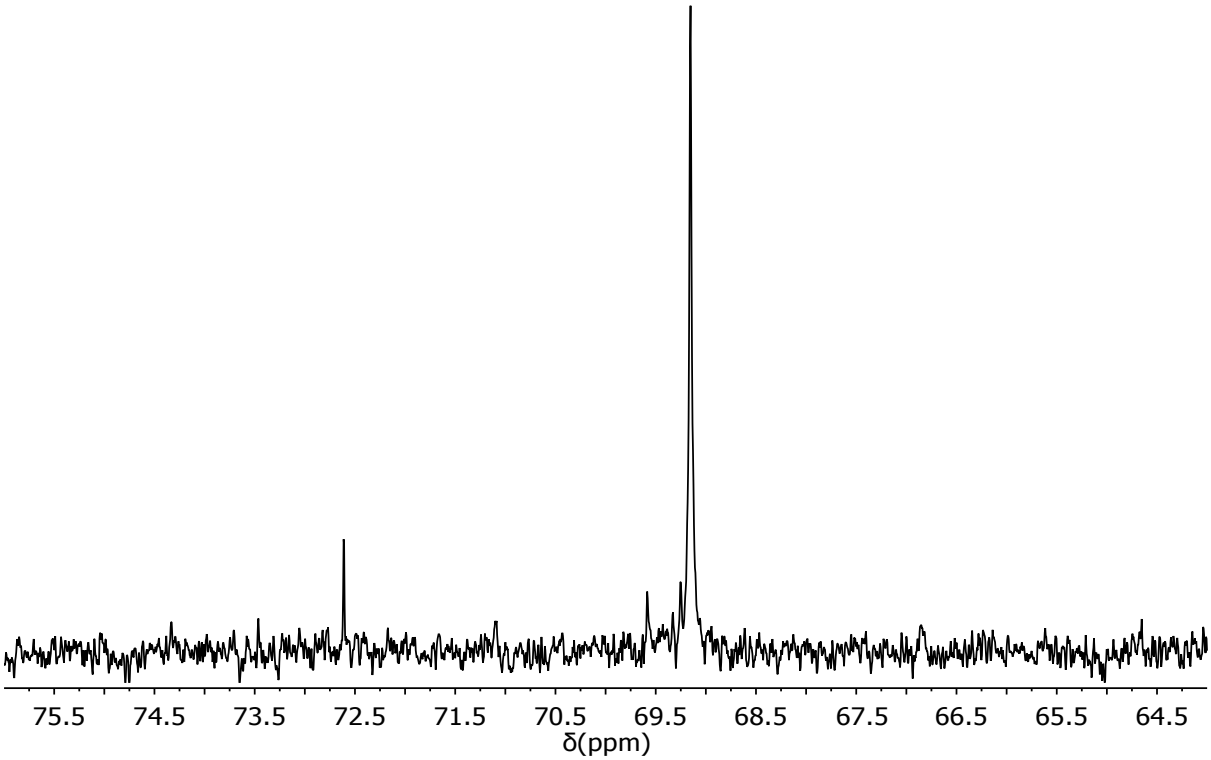

Figure S30: $^{13}C\{^{1}H\}$ NMR spectrum of poly-L-lactide synthesised using complex (^{Me2}CAAC)Ba(N{SiMe$_3$}$_2$)$_2$ (**4**) in chloroform-d_1 at 23 °C on a 500 MHz. Polymerisation conditions: benzene-d_6 at 23 °C with $[LA]_0/[M]_0 = 200$, $[LA]_0 = 0.5$ M. L-lactide at 72.60 ppm.

Table S11: L-lactide polymerisation using (^{Me2}CAAC)Ba(N{SiMe$_3$}$_2$)$_2$ (**4**). Polymerisation conditions: thf-d_8, $[LA]_0/[M]_0 = 200$, [LA]0 = 0.5 M, 23 °C.

Time (h)	Conversion (%)
0.671	92.3

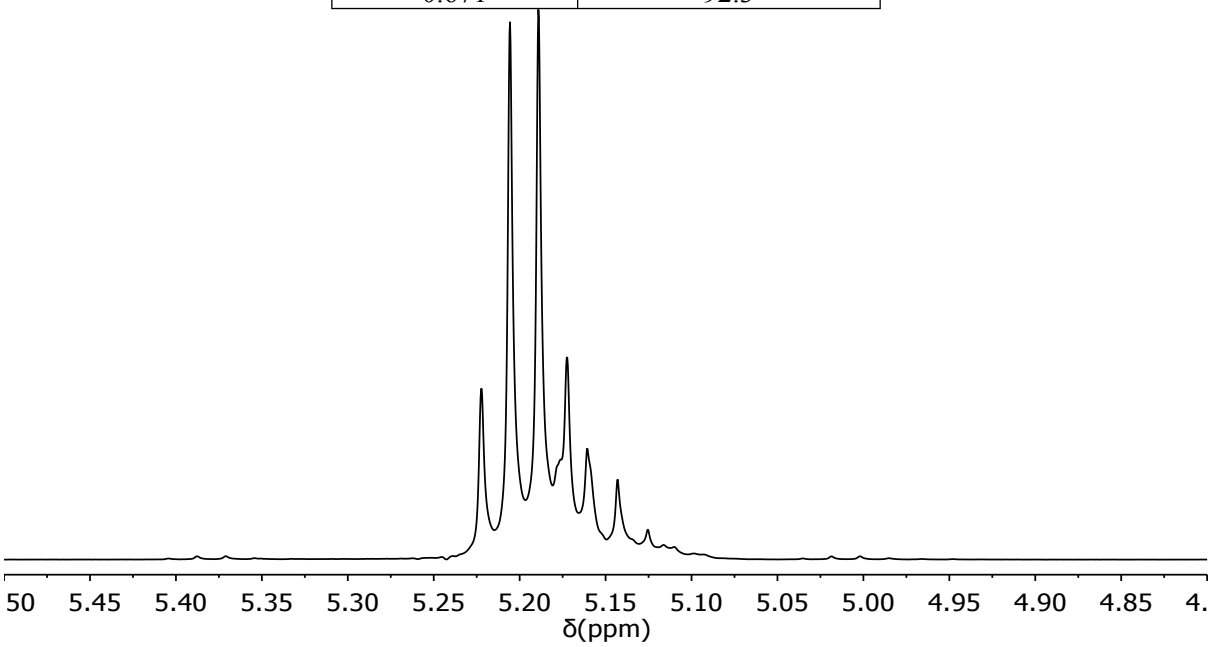

Figure S31: ^{1}H NMR spectrum of poly-L-lactide synthesised using complex (^{Me2}CAAC)Ba(N{SiMe$_3$}$_2$)$_2$ (**4**) in chloroform-d_1 at 23 °C on a 500 MHz. Polymerisation conditions: thf-d_8 at 23 °C with $[LA]_0/[M]_0 = 200$, $[LA]_0 = 0.5$ M.

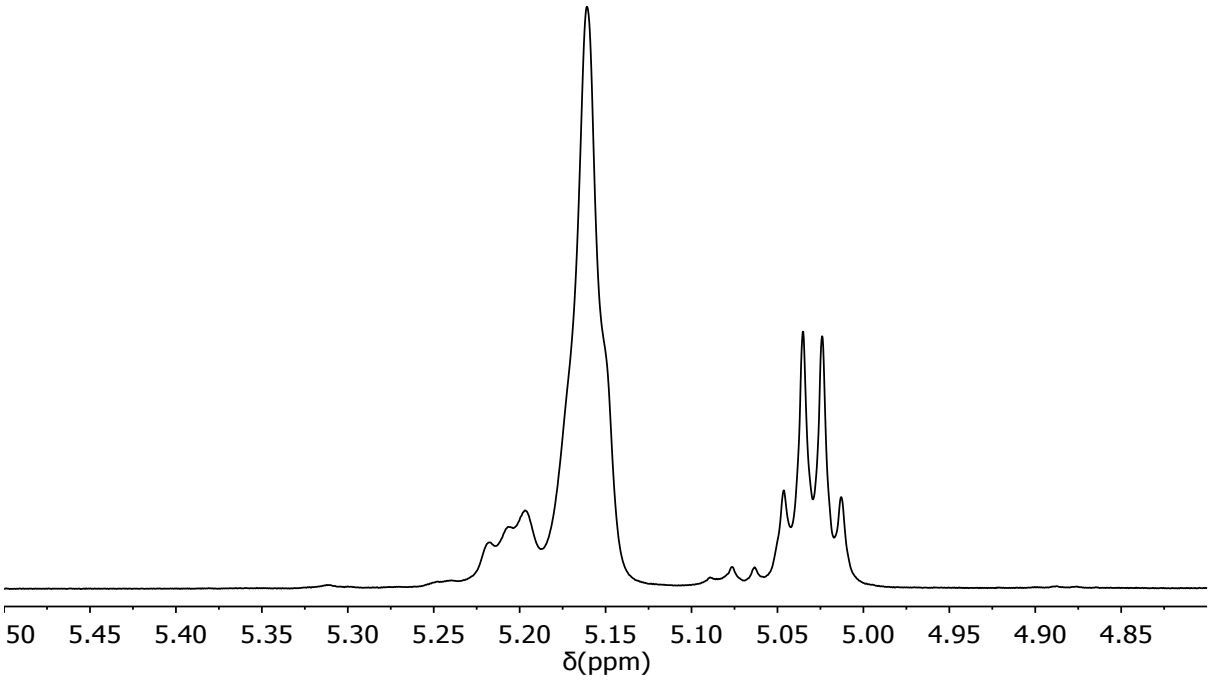

Figure S32: ^{1}H{^{1}H} NMR spectrum of poly-L-lactide synthesised using complex (^{Me2}CAAC)Ba(N{SiMe$_3$}$_2$)$_2$ (**4**) in chloroform-d_1 at 23 °C on a 500 MHz. Polymerisation conditions: tetrahydrofuran-d_8 at 23 °C with $[LA]_0/[M]_0 = 200$, $[LA]_0 = 0.5$ M. L-lactide at 5.03 ppm.

Table S12: *rac*-lactide polymerisation using (^{Me2}CAAC)Ba(N{SiMe$_3$}$_2$)$_2$ (**4**). Polymerisation conditions: benzene-d_6, $[LA]_0/[M]_0 = 200$, [LA]0 = 0.5 M, 23 °C.

Time (h)	Conversion (%)
0.22	1.9
0.6	7.4
1.02	12.5
2.15	25.0
3.43	36.2
4.82	48.9
6.83	55.9
8.53	64.0

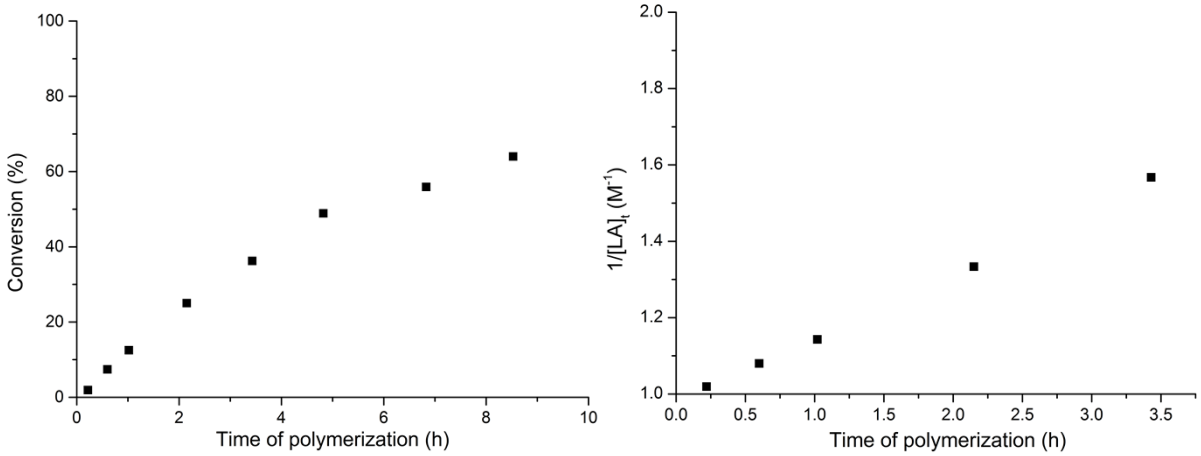

Figure S33: *rac*-lactide polymerisation using complex (^{Me2}CAAC)Ba(N{SiMe$_3$}$_2$)$_2$ (**4**), conversion in function of time profile (left) and second-order rate plot (right). Polymerisation conditions: benzene-d_6 at 23 °C with $[LA]_0/[M]_0 = 200$, $[LA]_0 = 0.5$ M.

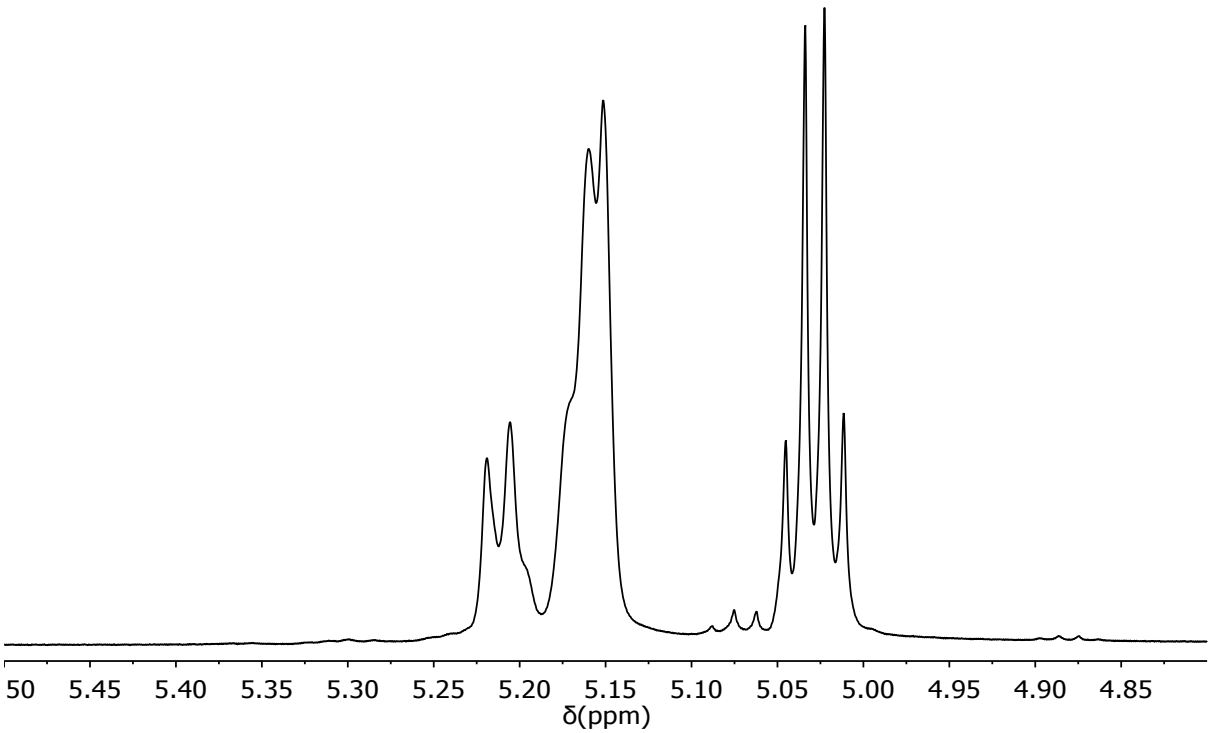

Figure S34: $^{1}H\{^{1}H\}$ NMR spectrum of poly-*rac*-lactide synthesised using complex (^{Me2}CAAC)Ba(N{SiMe$_3$}$_2$)$_2$ (**4**) in chloroform-d_1 at 23 °C on a 500 MHz. Polymerisation conditions: benzene-d_6 at 23 °C with $[LA]_0/[M]_0 = 200$, $[LA]_0 = 0.5$ M. *rac*-lactide at 5.03 ppm.

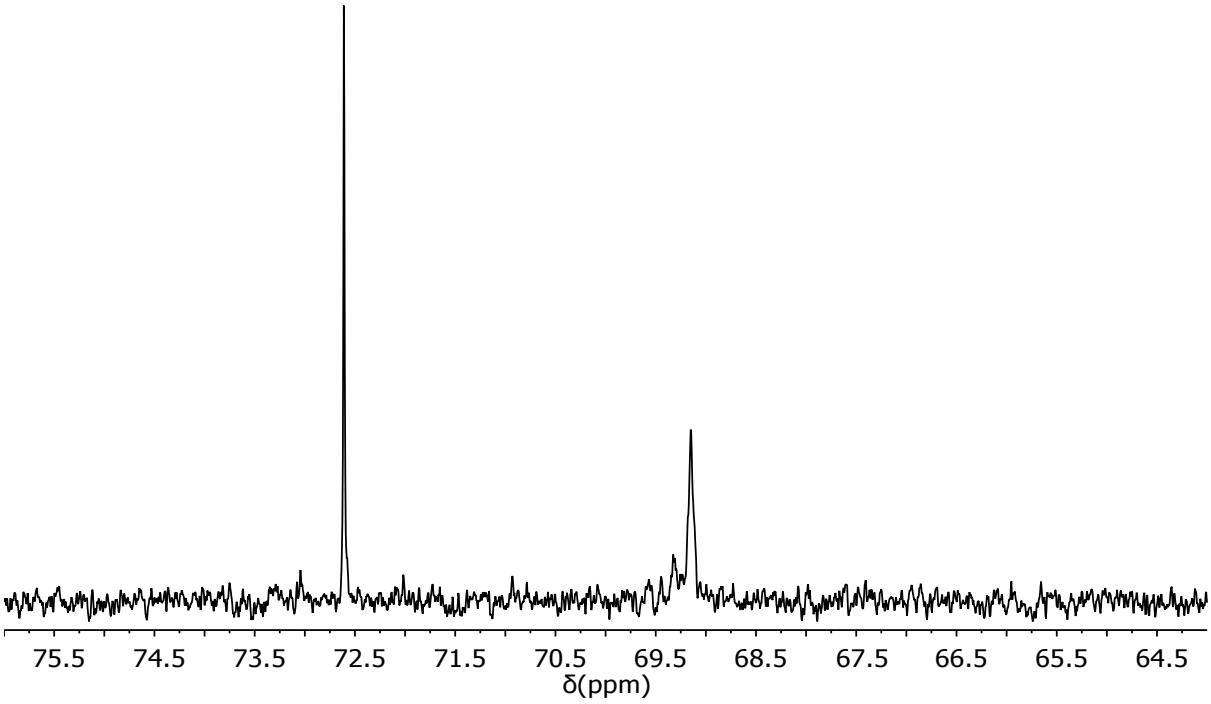

Figure S35: $^{13}C\{^{1}H\}$ NMR spectrum of poly-*rac*-lactide synthesised using complex (^{Me2}CAAC)Ba(N{SiMe$_3$}$_2$)$_2$ (**4**) in chloroform-d_1 at 23 °C on a 500 MHz. Polymerisation conditions: benzene-d_6 at 23 °C with $[LA]_0/[M]_0 = 200$, $[LA]_0 = 0.5$ M. *rac*-lactide at 72.60 ppm.

Table S13: L-lactide polymerisation using (^{Me2}CAAC)Ba(N{SiMe$_3$}$_2$)$_2$ (**4**). Polymerisation conditions: benzene-d_6, $[LA]_0/[M]_0 = 150$, [LA]0 = 0.5 M, 23 °C.

Time (h)	Conversion (%)
0.78	47.1
1.1	57.1
1.48	65.1
2.2	74.9
2.66	79.4

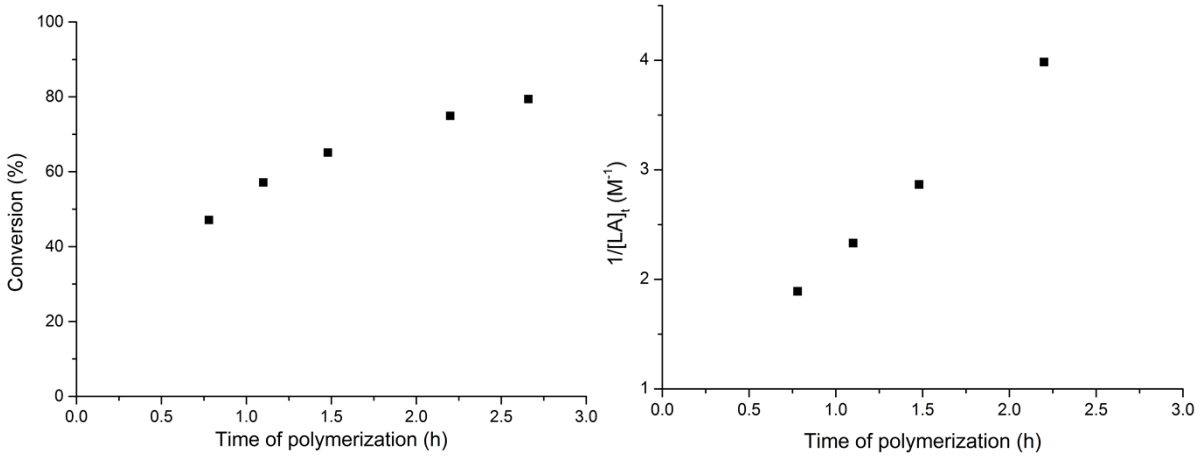

Figure S36: L-lactide polymerisation using complex (^{Me2}CAAC)Ba(N{SiMe$_3$}$_2$)$_2$ (**4**), conversion in function of time profile (left) and second-order rate plot (right). Polymerisation conditions: benzene-d_6 at 23 °C with $[LA]_0/[M]_0 = 150$, $[LA]_0 = 0.5$ M.

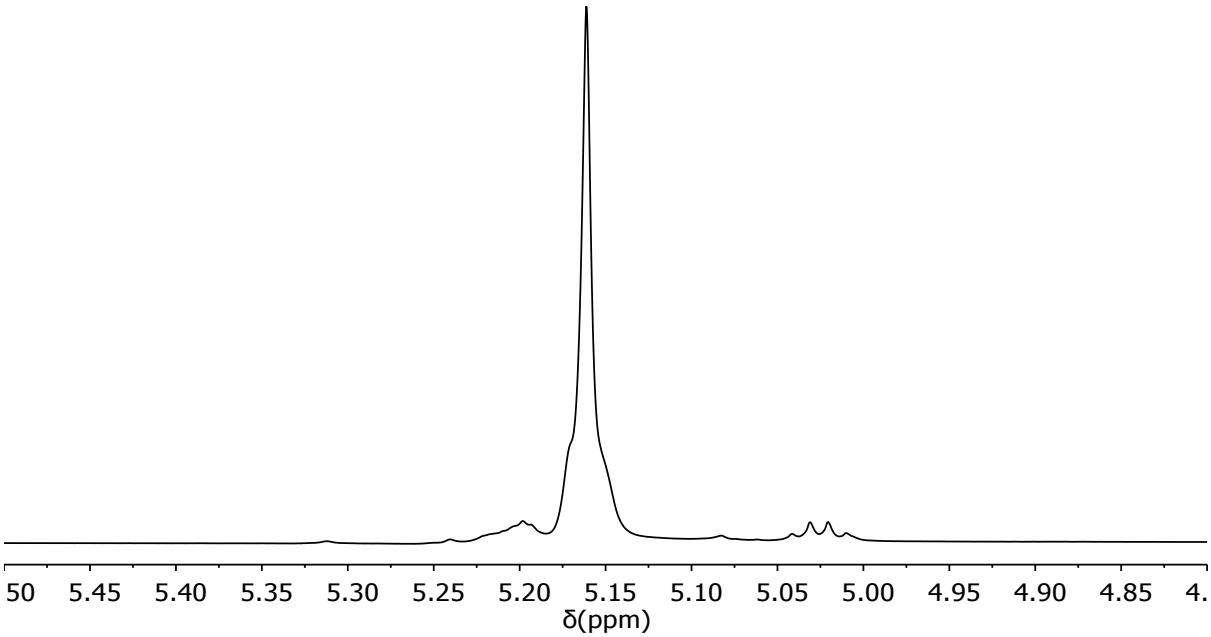

Figure S37: ^{1}H{^{1}H} NMR spectrum of poly-L-lactide synthesised using complex (^{Me2}CAAC)Ba(N{SiMe$_3$}$_2$)$_2$ (**4**) in chloroform-d_1 at 23 °C on a 500 MHz. Polymerisation conditions: benzene-d_6 at 23 °C with $[LA]_0/[M]_0 = 150$, $[LA]_0 = 0.5$ M. L-lactide at 5.03 ppm.

Table S14: L-lactide polymerisation using (^{Me2}CAAC)Ba(N{SiMe$_3$}$_2$)$_2$ (**4**). Polymerisation conditions: benzene-d_6, $[LA]_0/[M]_0 = 100$, [LA]0 = 0.5 M, 23 °C.

Time (h)	Conversion (%)
0.73	68.3
1.05	77.7
1.43	83.8
2.13	90.3
2.6	92.8

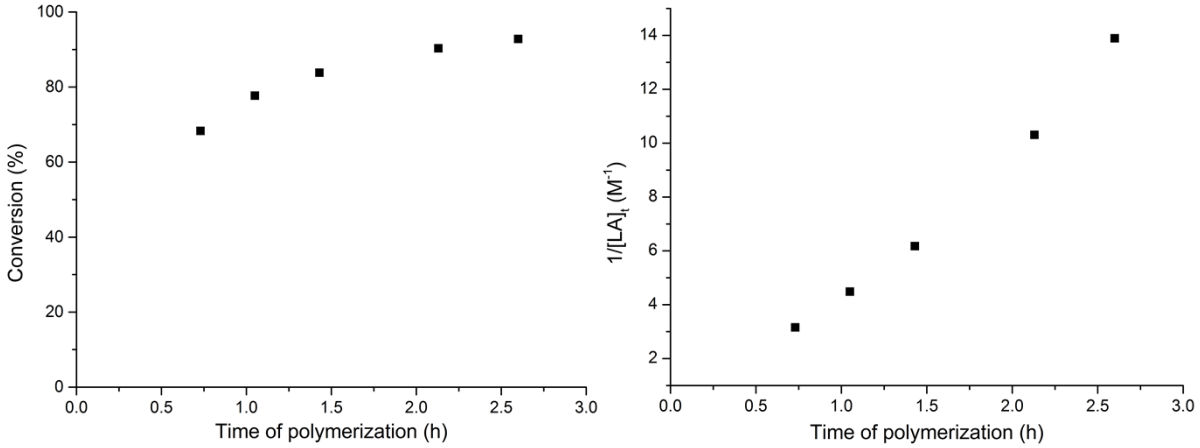

Figure S38: L-lactide polymerisation using complex (^{Me2}CAAC)Ba(N{SiMe$_3$}$_2$)$_2$ (**4**), conversion in function of time profile (left) and second-order rate plot (right). Polymerisation conditions: benzene-d_6 at 23 °C with $[LA]_0/[M]_0 = 100$, $[LA]_0 = 0.5$ M.

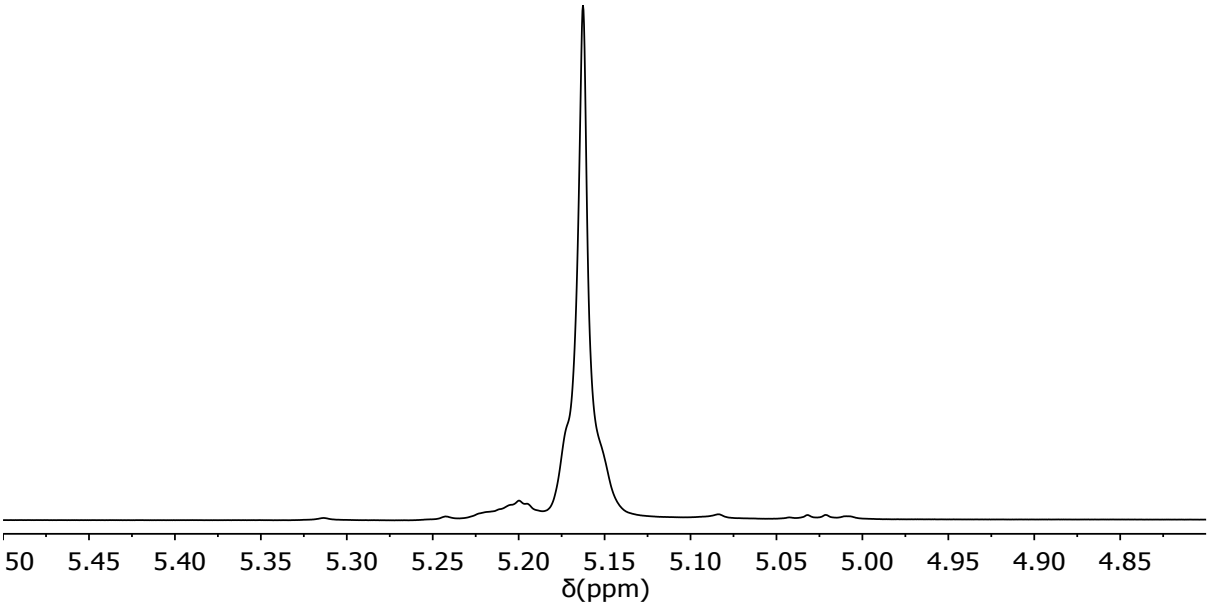

Figure S39: ^{1}H{^{1}H} NMR spectrum of poly-L-lactide synthesised using complex (^{Me2}CAAC)Ba(N{SiMe$_3$}$_2$)$_2$ (**4**) in chloroform-d_1 at 23 °C on a 500 MHz. Polymerisation conditions: benzene-d_6 at 23 °C with $[LA]_0/[M]_0 = 100$, $[LA]_0 = 0.5$ M. L-lactide at 5.03 ppm.

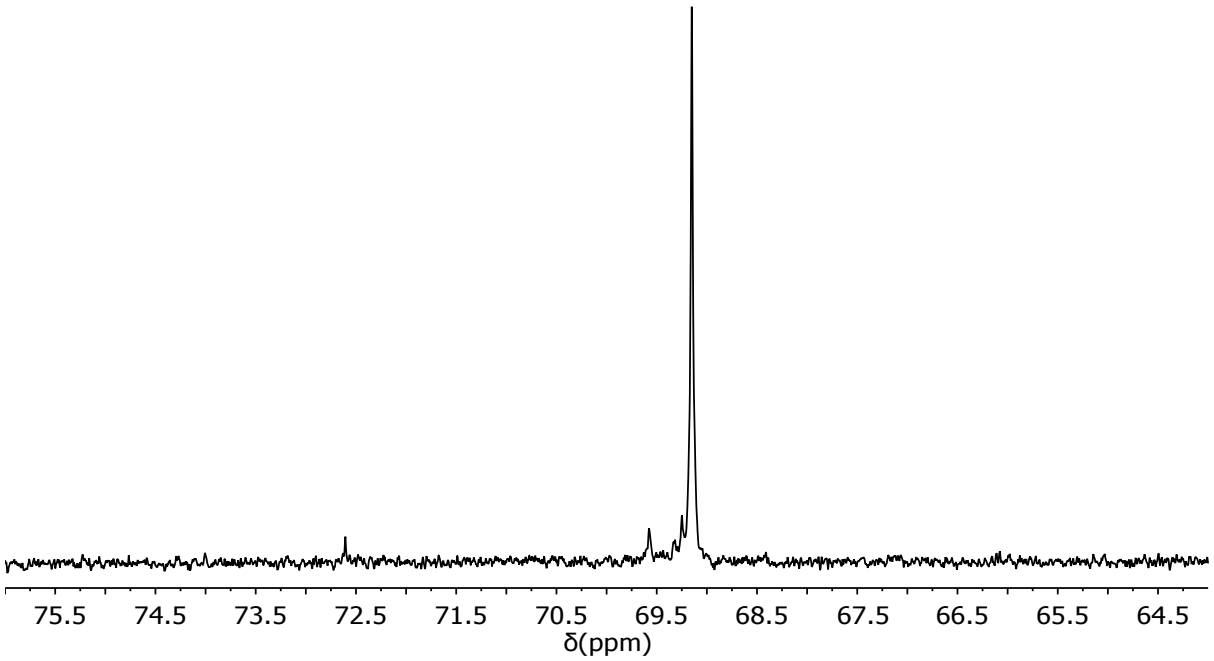

Figure S40: $^{13}C\{^{1}H\}$ NMR spectrum of poly-L-lactide synthesised using complex (^{Me2}CAAC)Ba(N{SiMe$_3$}$_2$)$_2$ (**4**) in chloroform-d_1 at 23 °C on a 500 MHz. Polymerisation conditions: benzene-d_6 at 23 °C with $[LA]_0/[M]_0 = 100$, $[LA]_0 = 0.5$ M. L-lactide at 72.60 ppm.

Using $[(^{Cy}CAAC)_3K][Sr(N\{SiMe_3\}_2)_3]$ (**6**)

Table S15: L-lactide polymerisation using $[(^{Cy}CAAC)_3K][Sr(N\{SiMe_3\}_2)_3]$ (**6**). Polymerisation conditions: benzene-d_6, $[LA]_0/[M]_0 = 200$, $[LA]0 = 0.5$ M, 23 °C.

Time (h)	Conversion (%)
0.3	38.5
0.68	51.1
1.02	57.7
1.35	61.1
1.87	62.4
2.07	64.2
2.3	65.8
3.07	69.3
3.98	72.1
6.12	75.8
8.13	77.5
23.5	83.8
32.5	85.5

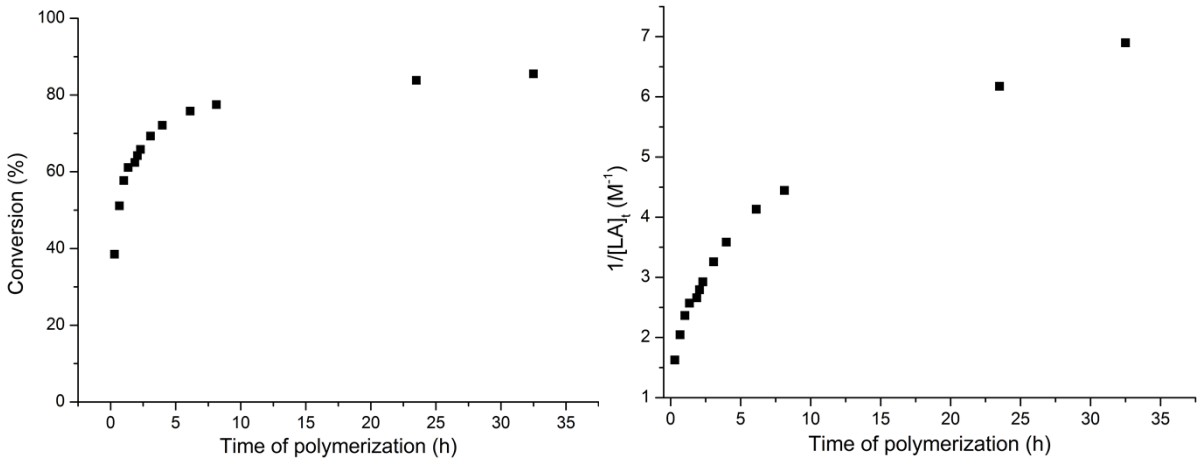

Figure S41: L-lactide polymerisation using complex $[(^{Cy}CAAC)_3K][Sr(N\{SiMe_3\}_2)_3]$ (**6**), conversion in function of time profile (left) and second-order rate plot (right). Polymerisation conditions: benzene-d_6 at 23 °C with $[LA]_0/[M]_0 = 200$, $[LA]_0 = 0.5$ M.

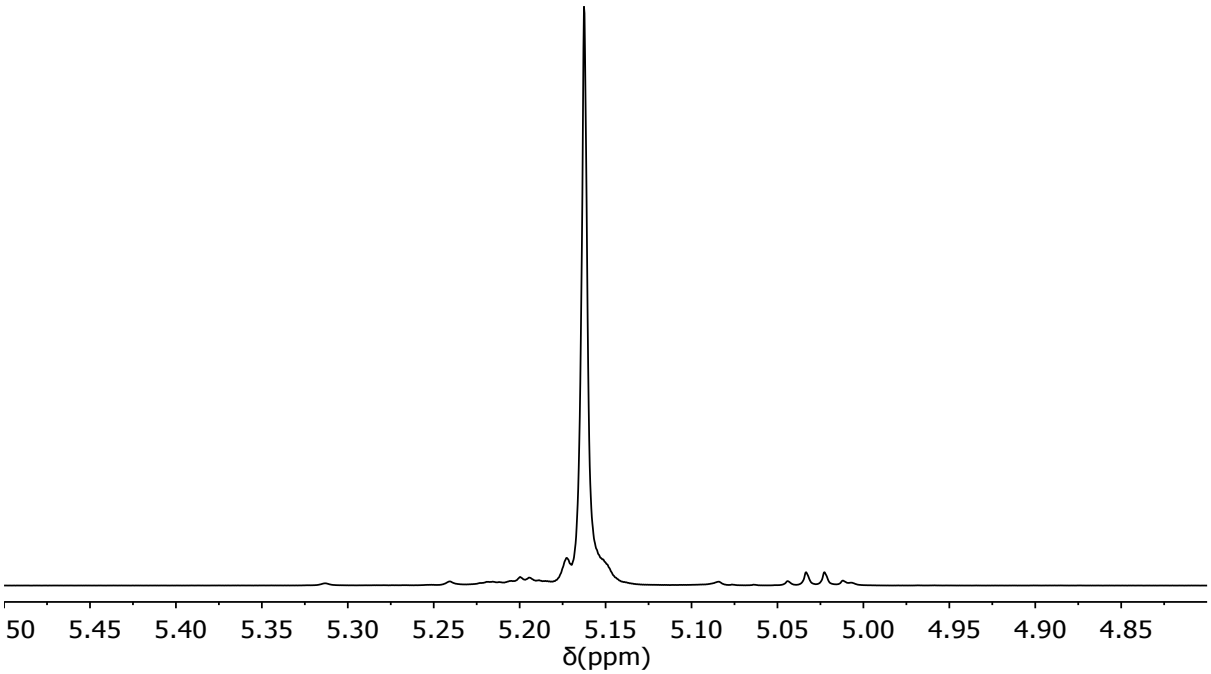

Figure S42: $^{1}H\{^{1}H\}$ NMR spectrum of poly-L-lactide synthesised using complex $[(^{Cy}CAAC)_3K][Sr(N\{SiMe_3\}_2)_3]$ (**6**) in chloroform-d_1 at 23 °C on a 500 MHz. Polymerisation conditions: benzene-d_6 at 23 °C with $[LA]_0/[M]_0 = 200$, $[LA]_0 = 0.5$ M. L-lactide at 5.03 ppm.

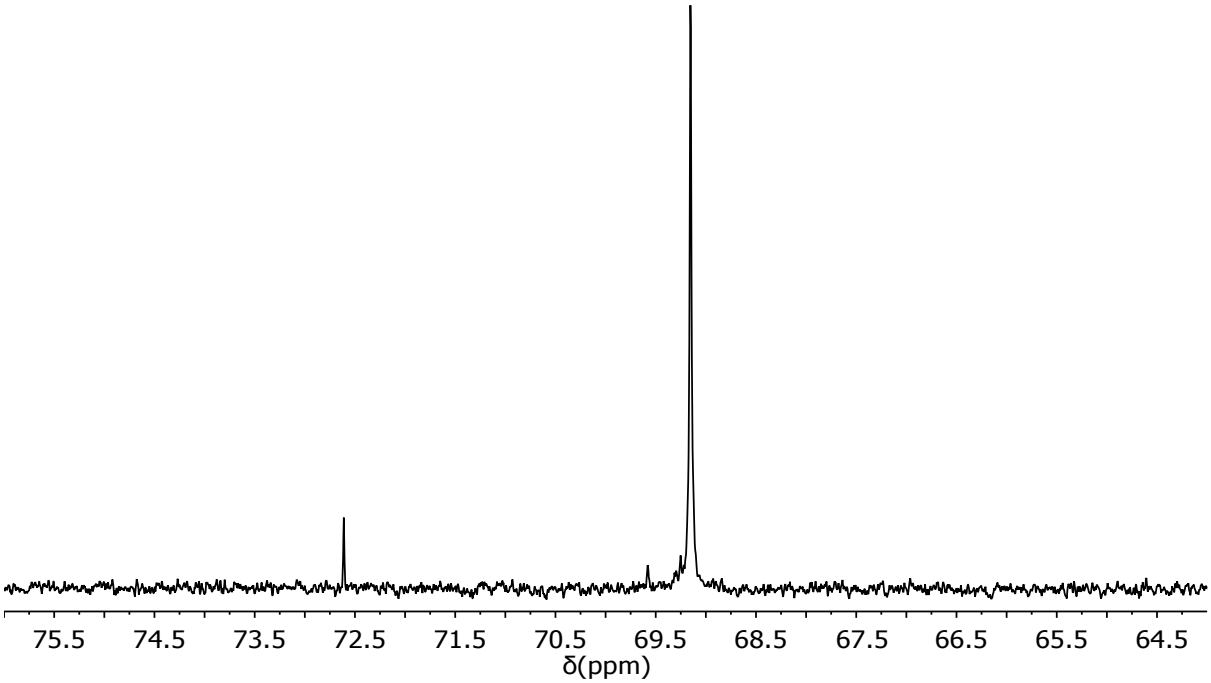

Figure S43: $^{13}C\{^{1}H\}$ NMR spectrum of poly-L-lactide synthesised using complex $[(^{Cy}CAAC)_3K][Sr(N\{SiMe_3\}_2)_3]$ (**6**) in chloroform-d_1 at 23 °C on a 500 MHz. Polymerisation conditions: benzene-d_6 at 23 °C with $[LA]_0/[M]_0 = 200$, $[LA]_0 = 0.5$ M. L-lactide at 72.60 ppm.

Table S16: *rac*-lactide polymerisation using [(^{Cy}CAAC)$_3$K][Sr(N{SiMe$_3$}$_2$)$_3$] (**6**). Polymerisation conditions: benzene-d_6, $[LA]_0/[M]_0 = 200$, [LA]0 = 0.5 M, 23 °C.

Time (h)	Conversion (%)
0.4	12.7
0.77	20.8
1.1	26.3
1.87	32.8
2.12	36.5
2.37	38.7
3.12	44.4
3.98	46.7
6.17	50.0
8.28	53.5
23.5	68.6

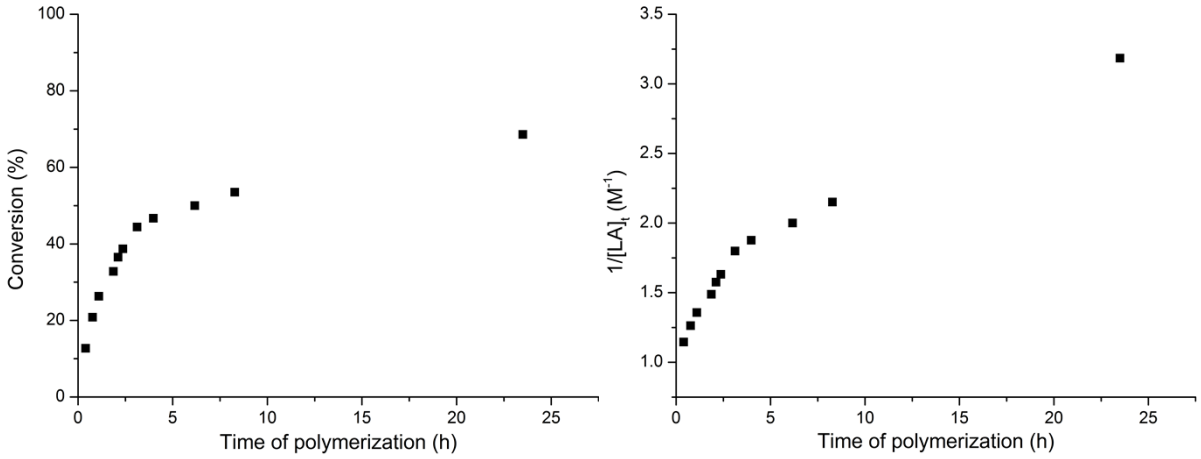

Figure S44: *rac*-lactide polymerisation using complex [(^{Cy}CAAC)$_3$K][Sr(N{SiMe$_3$}$_2$)$_3$] (**6**), conversion in function of time profile (left) and second-order rate plot (right). Polymerisation conditions: benzene-d_6 at 23 °C with $[LA]_0/[M]_0 = 200$, $[LA]_0 = 0.5$ M.

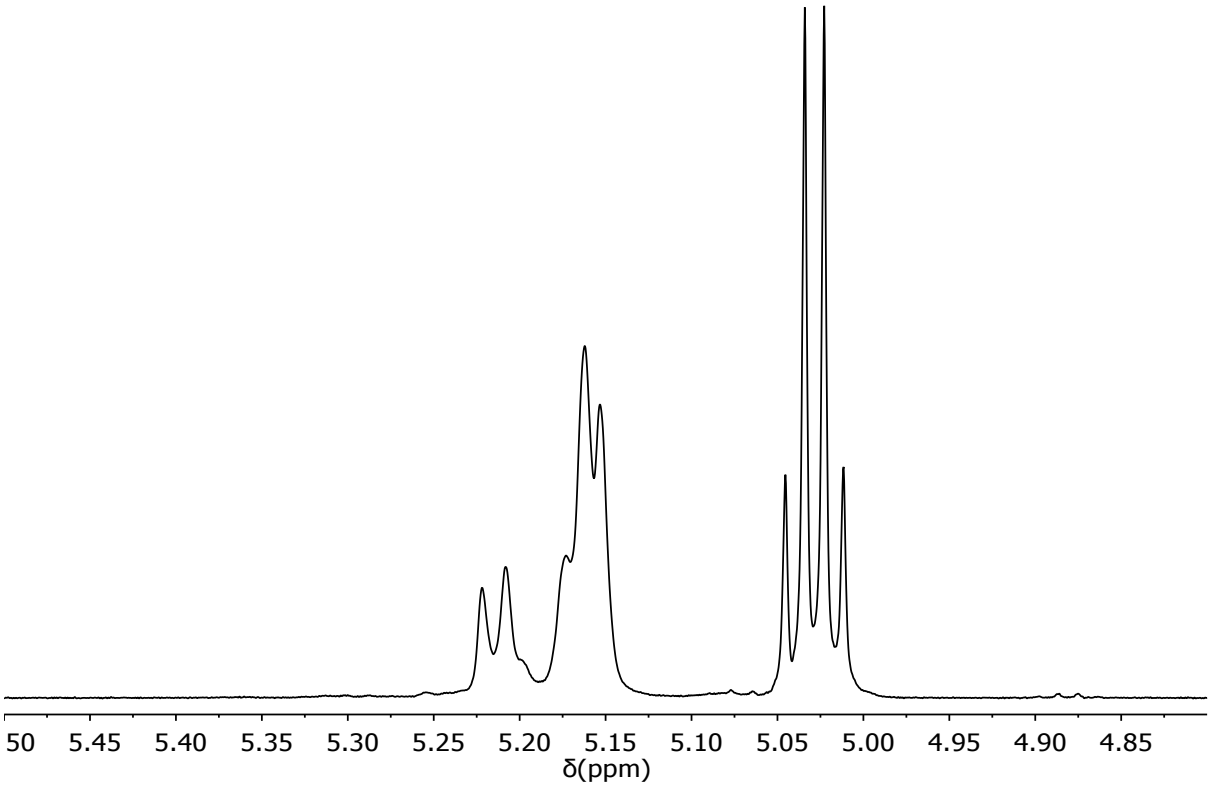

Figure S45: $^{1}H\{^{1}H\}$ NMR spectrum of poly-*rac*-lactide synthesised using complex $[(^{Cy}CAAC)_3K][Sr(N\{SiMe_3\}_2)_3]$ (**6**) in chloroform-d_1 at 23 °C on a 500 MHz. Polymerisation conditions: benzene-d_6 at 23 °C with $[LA]_0/[M]_0 = 200$, $[LA]_0 = 0.5$ M. *rac*-lactide at 5.03 ppm.

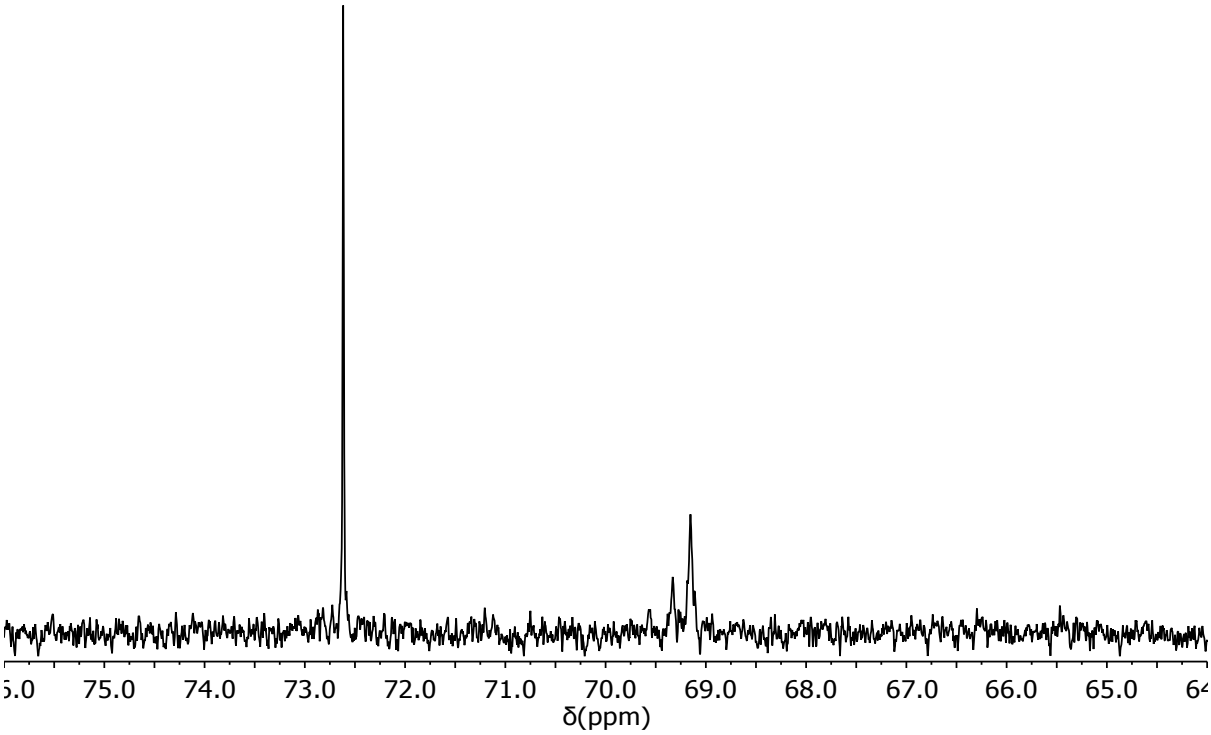

Figure S46: $^{13}C\{^{1}H\}$ NMR spectrum of poly-*rac*-lactide synthesised using complex $[(^{Cy}CAAC)_3K][Sr(N\{SiMe_3\}_2)_3]$ (**6**) in chloroform-d_1 at 23 °C on a 500 MHz. Polymerisation conditions: benzene-d_6 at 23 °C with $[LA]_0/[M]_0 = 200$, $[LA]_0 = 0.5$ M. *rac*-lactide at 72.60 ppm.

Using $[Mg(N\{SiMe_3\}_2)_2]_2$

Table S17: L-lactide polymerisation using $[Mg(N\{SiMe_3\}_2)_2]_2$. Polymerisation conditions: benzene-d_6, $[LA]_0/[M]_0 = 200$, [LA]0 = 0.5 M, 23 °C.

Time (h)	Conversion (%)
0.4	4.80
0.68	4.83
1.83	5.00
5.53	5.40
7.18	5.50
10.27	5.60
23.5	6.70
32	7.10

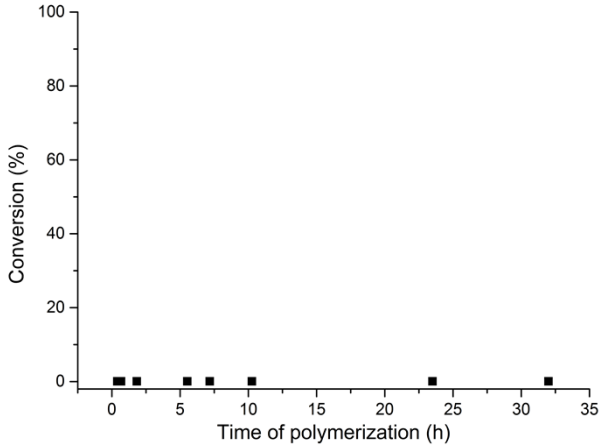

Figure S47: L-lactide polymerisation using complex $[Mg(N\{SiMe_3\}_2)_2]_2$, conversion in function of time profile. Polymerisation conditions: benzene-d_6 at 23 °C with $[LA]_0/[M]_0 = 200$, $[LA]_0 = 0.5$ M.

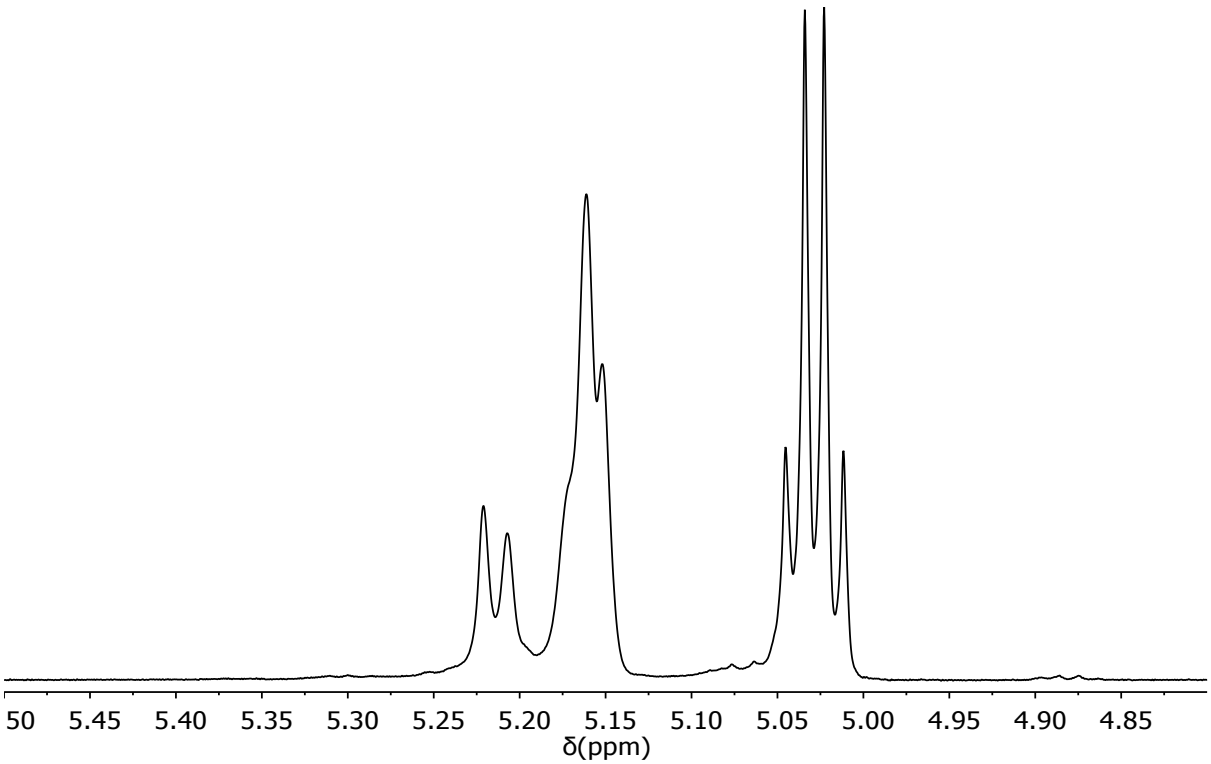

Figure S48: $^{1}H\{^{1}H\}$ NMR spectrum of poly-*rac*-lactide synthesised using complex $[Mg(N\{SiMe_3\}_2)_2]_2$ in chloroform-d_1 at 23 °C on a 500 MHz. Polymerisation conditions: benzene-d_6 at 23 °C with $[LA]_0/[M]_0 = 200$, $[LA]_0 = 0.5$ M. *rac*-lactide at 5.03 ppm.

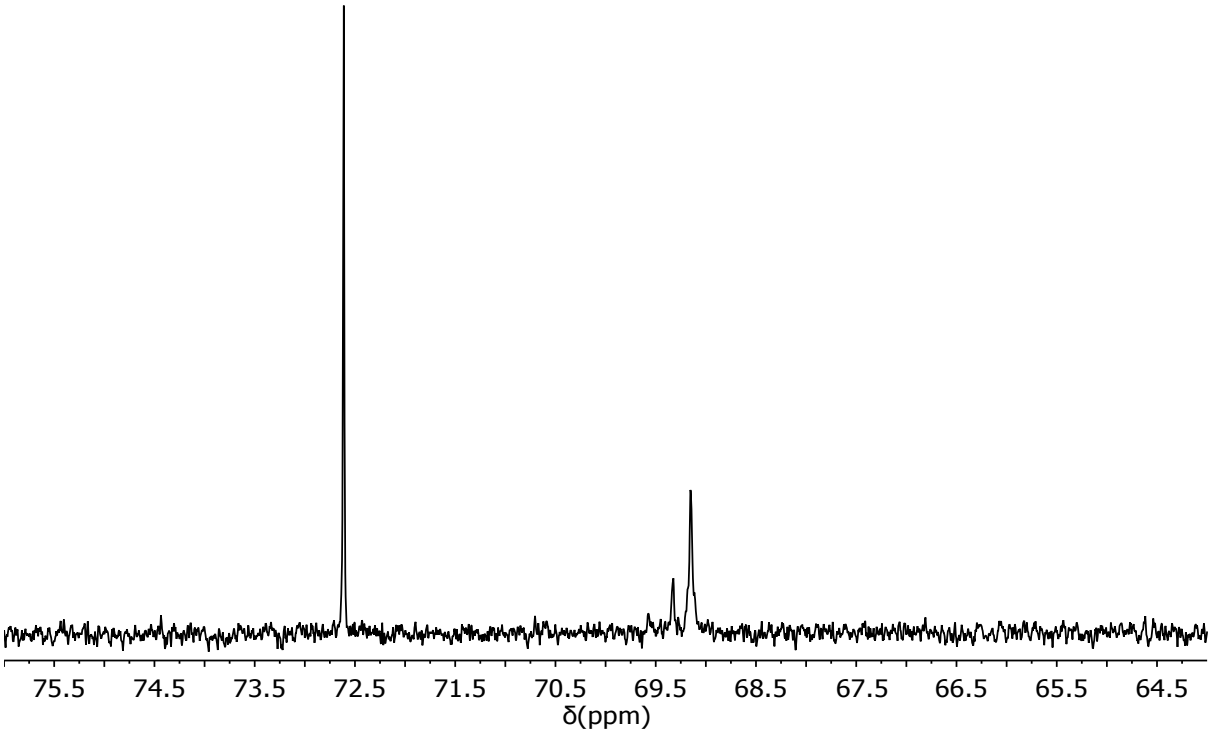

Figure S49: $^{13}C\{^{1}H\}$ NMR spectrum of poly-*rac*-lactide synthesised using complex $[Mg(N\{SiMe_3\}_2)_2]_2$ in chloroform-d_1 at 23 °C on a 500 MHz. Polymerisation conditions: benzene-d_6 at 23 °C with $[LA]_0/[M]_0 = 200$, $[LA]_0 = 0.5$ M. *rac*-lactide at 72.60 ppm.

Using $[Sr(N\{SiMe_3\}_2)_2]_2$

Table S18: L-lactide polymerisation using $[Sr(N\{SiMe_3\}_2)_2]_2$. Polymerisation conditions: benzene-d_6, $[LA]_0/[M]_0 = 200$, [LA]0 = 0.5 M, 23 °C.

Time (h)	Conversion (%)
0.47	2.10
0.75	3.20
1.37	5.20
1.9	13.1
5.6	25.4
7.25	31.4
10.5	40.8
23.5	60.3
32	63.6

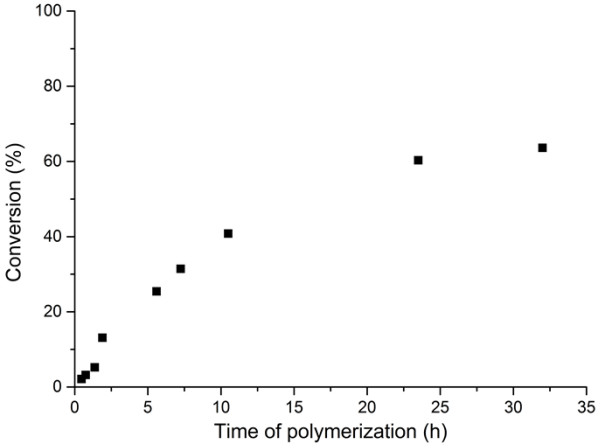

Figure S50: L-lactide polymerisation using complex $[Sr(N\{SiMe_3\}_2)_2]_2$, conversion in function of time profile. Polymerisation conditions: benzene-d_6 at 23 °C with $[LA]_0/[M]_0 = 200$, $[LA]_0 = 0.5$ M.

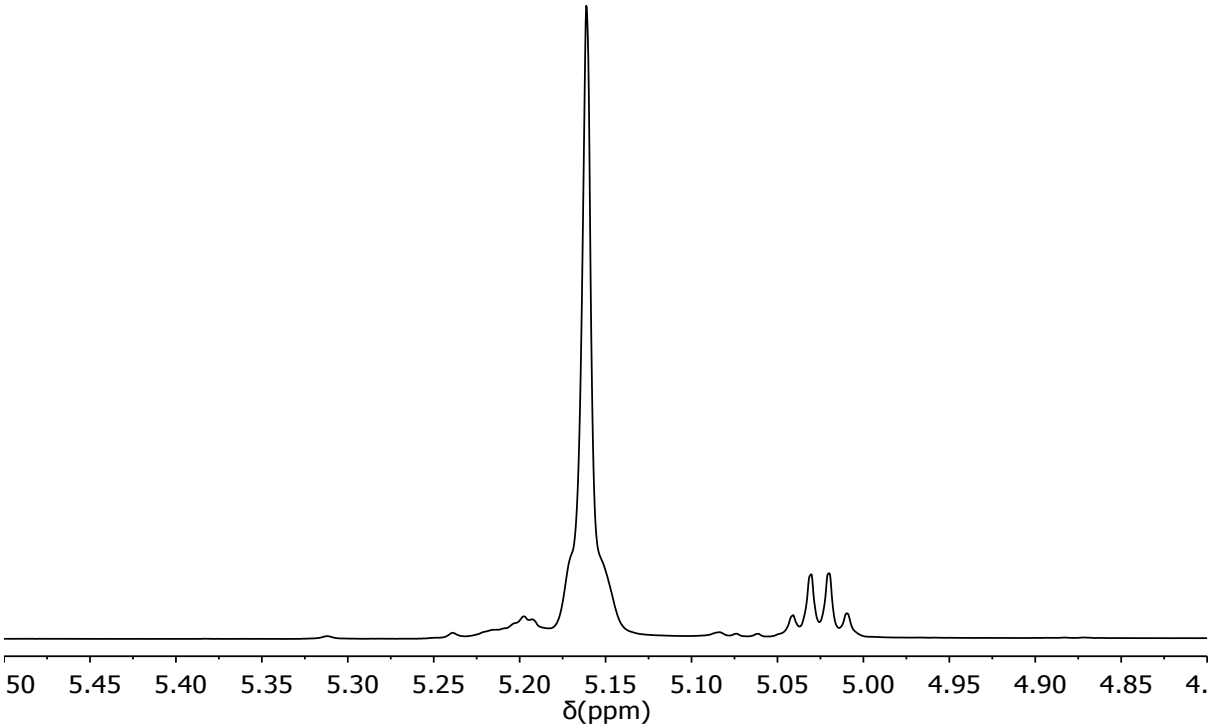

Figure S51: $^{1}H\{^{1}H\}$ NMR spectrum of poly-L-lactide synthesised using complex $[Sr(N\{SiMe_3\}_2)_2]_2$ in chloroform-d_1 at 23 °C on a 500 MHz. Polymerisation conditions: benzene-d_6 at 23 °C with $[LA]_0/[M]_0 = 200$, $[LA]_0 = 0.5$ M. L-lactide at 5.03 ppm.

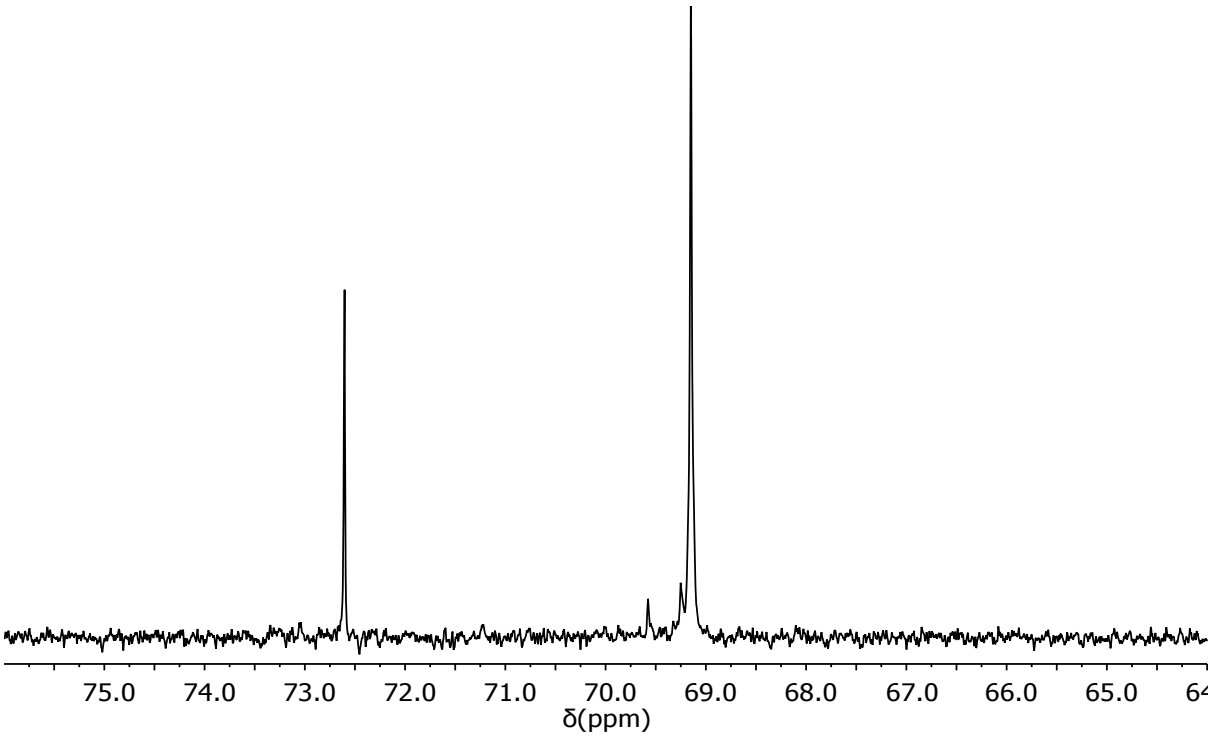

Figure S52: $^{13}C\{^{1}H\}$ NMR spectrum of poly-L-lactide synthesised using complex $[Sr(N\{SiMe_3\}_2)_2]_2$ in chloroform-d_1 at 23 °C on a 500 MHz. Polymerisation conditions: benzene-d_6 at 23 °C with $[LA]_0/[M]_0 = 200$, $[LA]_0 = 0.5$ M. L-lactide at 72.60 ppm.

Table S19: *rac*-lactide polymerisation using $[Sr(N\{SiMe_3\}_2)_2]_2$. Polymerisation conditions: benzene-d_6, $[LA]_0/[M]_0 = 200$, [LA]0 = 0.5 M, 23 °C.

Time (h)	Conversion (%)
0.52	2.3
0.82	3.8
1.42	4.6
1.95	5.5
7.3	11.7
10.62	16.1
23.5	29.2
32	31.3

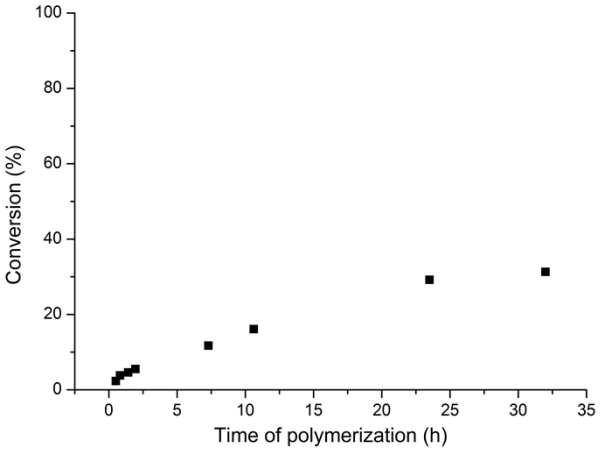

Figure S53: *rac* -lactide polymerisation using complex $[Sr(N\{SiMe_3\}_2)_2]_2$, conversion in function of time profile. Polymerisation conditions: benzene-d_6 at 23 °C with $[LA]_0/[M]_0 = 200$, $[LA]_0 = 0.5$ M.

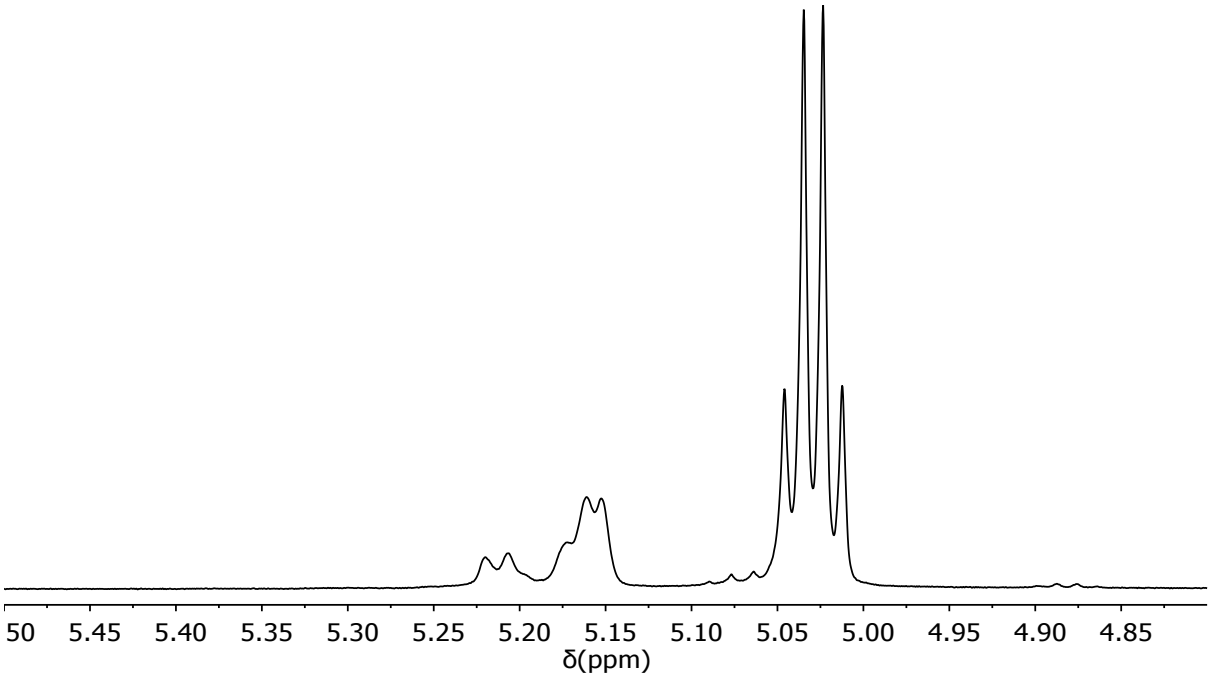

Figure S54: $^1H\{^1H\}$ NMR spectrum of poly-*rac*-lactide synthesised using complex $[Sr(N\{SiMe_3\}_2)_2]_2$ in chloroform-d_1 at 23 °C on a 500 MHz. Polymerisation conditions: benzene-d_6 at 23 °C with $[LA]_0/[M]_0 = 200$, $[LA]_0 = 0.5$ M. *rac*-lactide at 5.03 ppm.

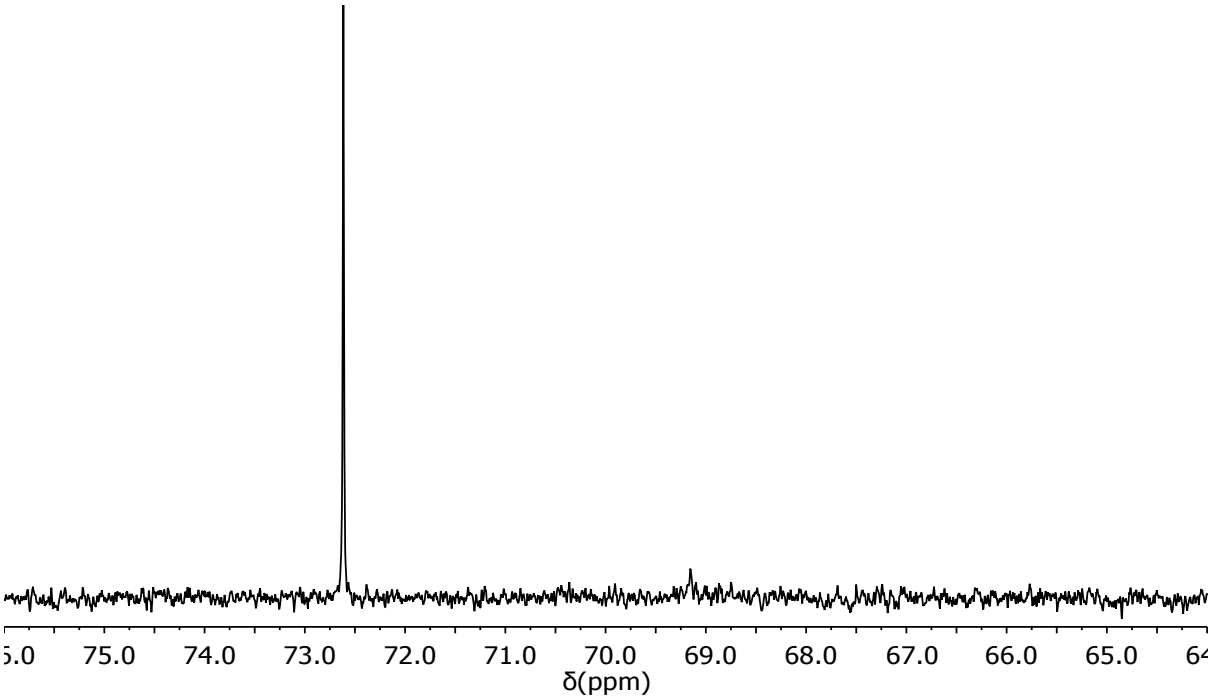

Figure S55: $^{13}C\{^{1}H\}$ NMR spectrum of poly-L-lactide synthesised using complex $[Sr(N\{SiMe_3\}_2)_2]_2$ in chloroform-d_1 at 23 °C on a 500 MHz. Polymerisation conditions: benzene-d_6 at 23 °C with $[LA]_0/[M]_0 = 200$, $[LA]_0 = 0.5$ M. *rac*-lactide at 72.60 ppm.

Using $Ba(N\{SiMe_3\}_2)_2(thf)_{1.6}$

Table S20: L-lactide polymerisation using $Ba(N\{SiMe_3\}_2)_2(thf)_{1.6}$. Polymerisation conditions: benzene-d_6, $[LA]_0/[M]_0 = 200$, [LA]0 = 0.5 M, 23 °C.

Time (h)	Conversion (%)
0.37	0.7
0.73	1.0
1.15	1.2
2.3	2.1
3.82	2.8
8.67	4.2

Table S21: *rac*-lactide polymerisation using $Ba(N\{SiMe_3\}_2)_2(thf)_{1.6}$. Polymerisation conditions: benzene-d_6, $[LA]_0/[M]_0 = 200$, [LA]0 = 0.5 M, 23 °C.

Time (h)	Conversion (%)
0.43	1.1
0.8	1.9
1.22	2.8
2.35	4.9
3.88	7.9
8.72	15.4

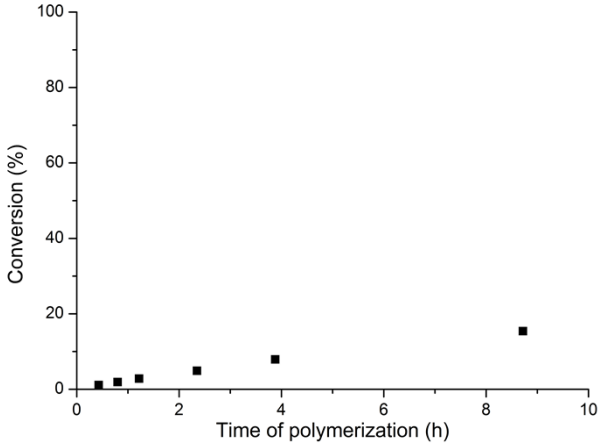

Figure S56: *rac*-lactide polymerisation using complex $Ba(N\{SiMe_3\}_2)_2(thf)_{1.6}$, conversion in function of time profile. Polymerisation conditions: benzene-d_6 at 23 °C with $[LA]_0/[M]_0 = 200$, $[LA]_0 = 0.5$ M.

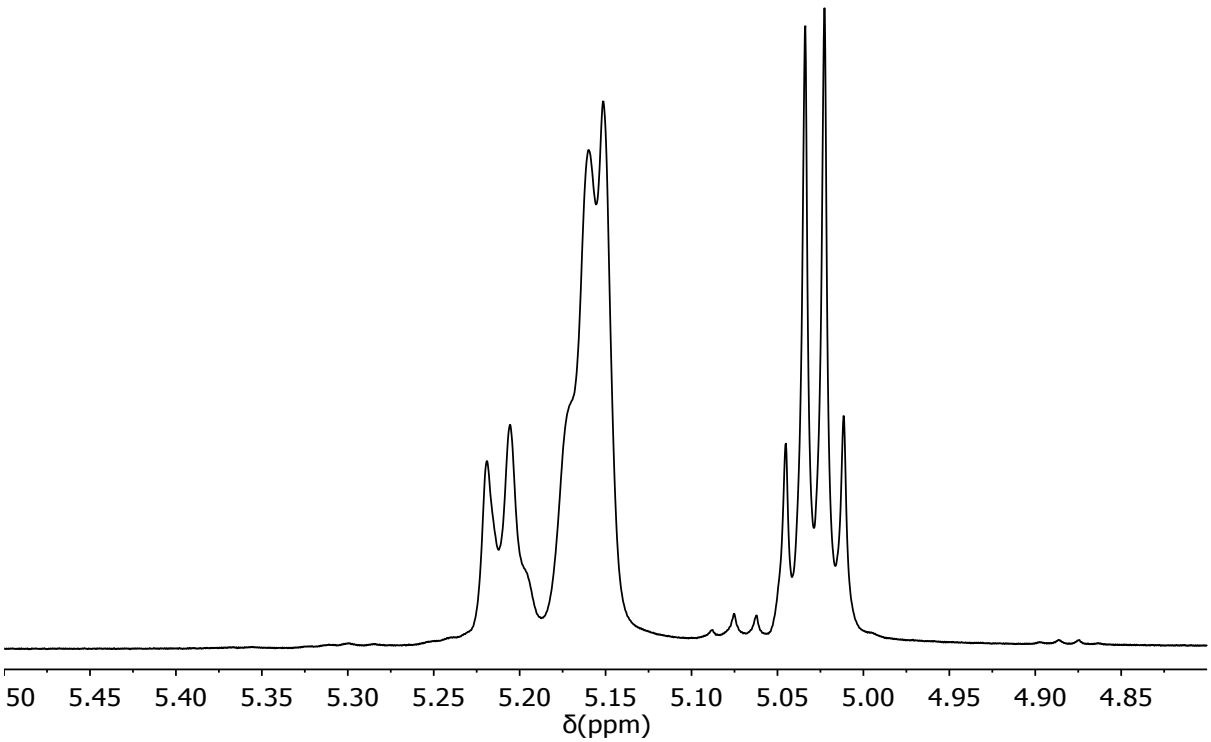

Figure S57: $^{1}H\{^{1}H\}$ NMR spectrum of poly-*rac*-lactide synthesised using complex $Ba(N\{SiMe_3\}_2)_2(thf)_{1.6}$ in chloroform-d_1 at 23 °C on a 500 MHz. Polymerisation conditions: benzene-d_6 at 23 °C with $[LA]_0/[M]_0 = 200$, $[LA]_0 = 0.5$ M. *rac*-lactide at 5.03 ppm.

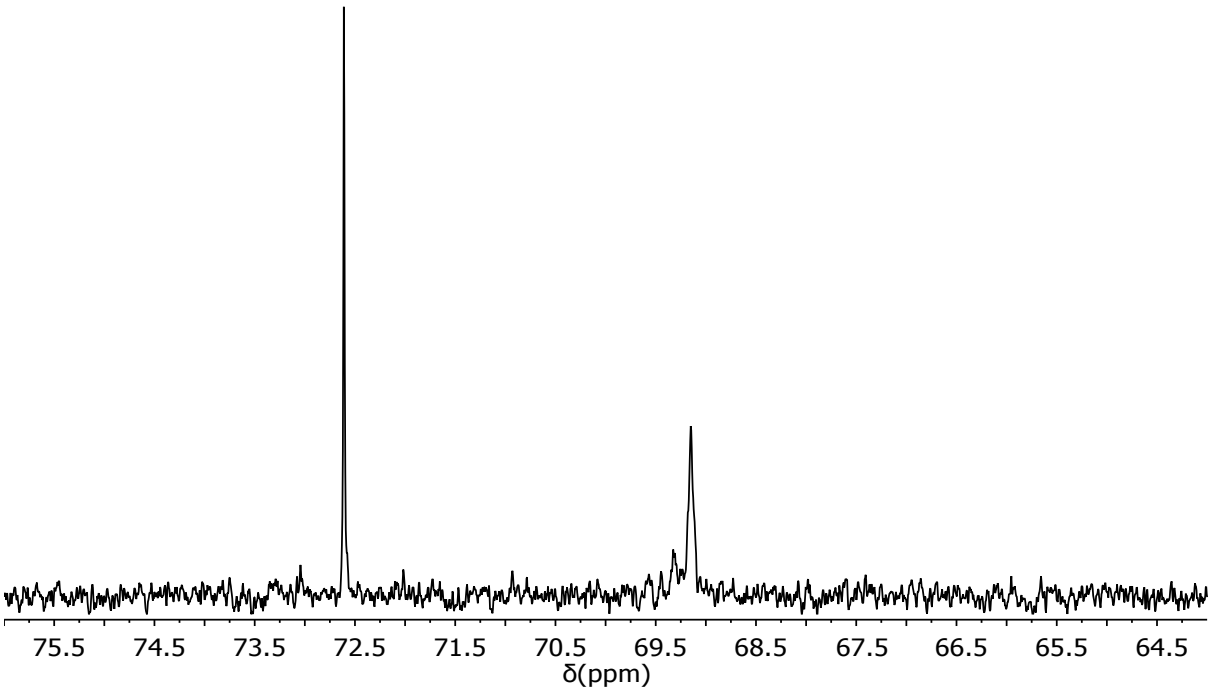

Figure S58: $^{13}C\{^{1}H\}$ NMR spectrum of poly-*rac*-lactide synthesised using complex $Ba(N\{SiMe_3\}_2)_2(thf)_{1.6}$ in chloroform-d_1 at 23 °C on a 500 MHz. Polymerisation conditions: benzene-d_6 at 23 °C with $[LA]_0/[M]_0 = 200$, $[LA]_0 = 0.5$ M. *rac*-lactide at 72.60 ppm.

Using ^{Me2}CAAC

Table S22: L-lactide polymerisation using ^{Me2}CAAC. Polymerisation conditions: benzene-d_6, $[LA]_0/[M]_0 = 200$, [LA]0 = 0.5 M, 23 °C.

Time (h)	Conversion (%)
0.18	~0
1.42	~0
2.52	~0
4.02	~0
28	~0
72	~0

Table S23: *rac*-lactide polymerisation using ^{Me2}CAAC. Polymerisation conditions: benzene-d_6, $[LA]_0/[M]_0 = 200$, [LA]0 = 0.5 M, 23 °C.

Time (h)	Conversion (%)
0.33	~0
0.92	~0
1.50	~0
2.57	~0
4.10	~0
28	~0
72	1.1

End of chain experiments

Table S24: L-lactide polymerisation using (^{Me2}CAAC)Ba(N{SiMe$_3$}$_2$)$_2$ (**4**). Polymerisation conditions: benzene-d_6, $[LA]_0/[M]_0 = 20$, $[LA]0 = 0.5$ M, 23 °C.

Time (h)	Conversion (%)
0.17	27.7
0.32	55.3
1.83	91.7
3.72	96.6

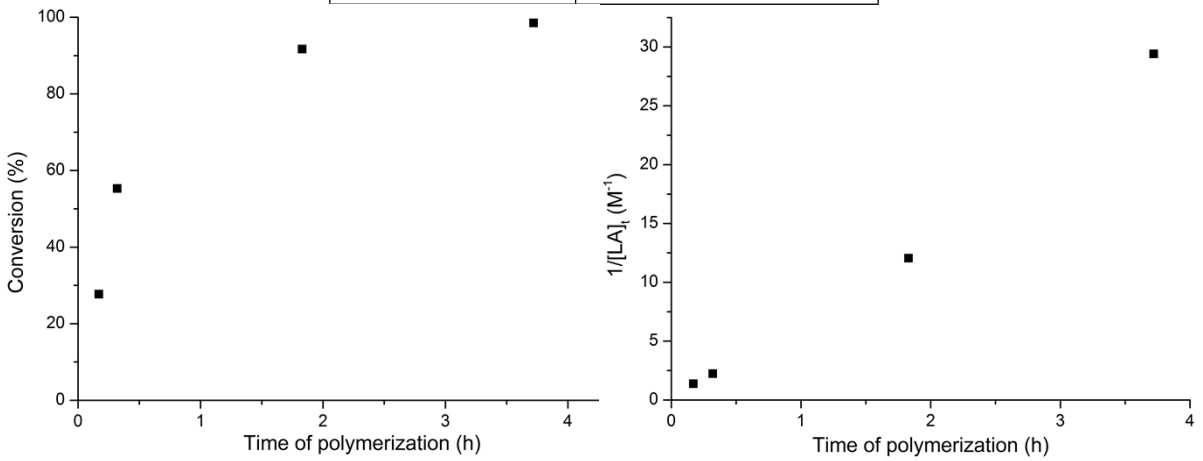

Figure S59: L-lactide polymerisation using complex (^{Me2}CAAC)Ba(N{SiMe$_3$}$_2$)$_2$ (**4**), conversion in function of time profile (left) and second-order rate plot (right). Polymerisation conditions: benzene-d_6 at 23 °C with $[LA]_0/[M]_0 = 20$, $[LA]_0 = 0.5$ M.

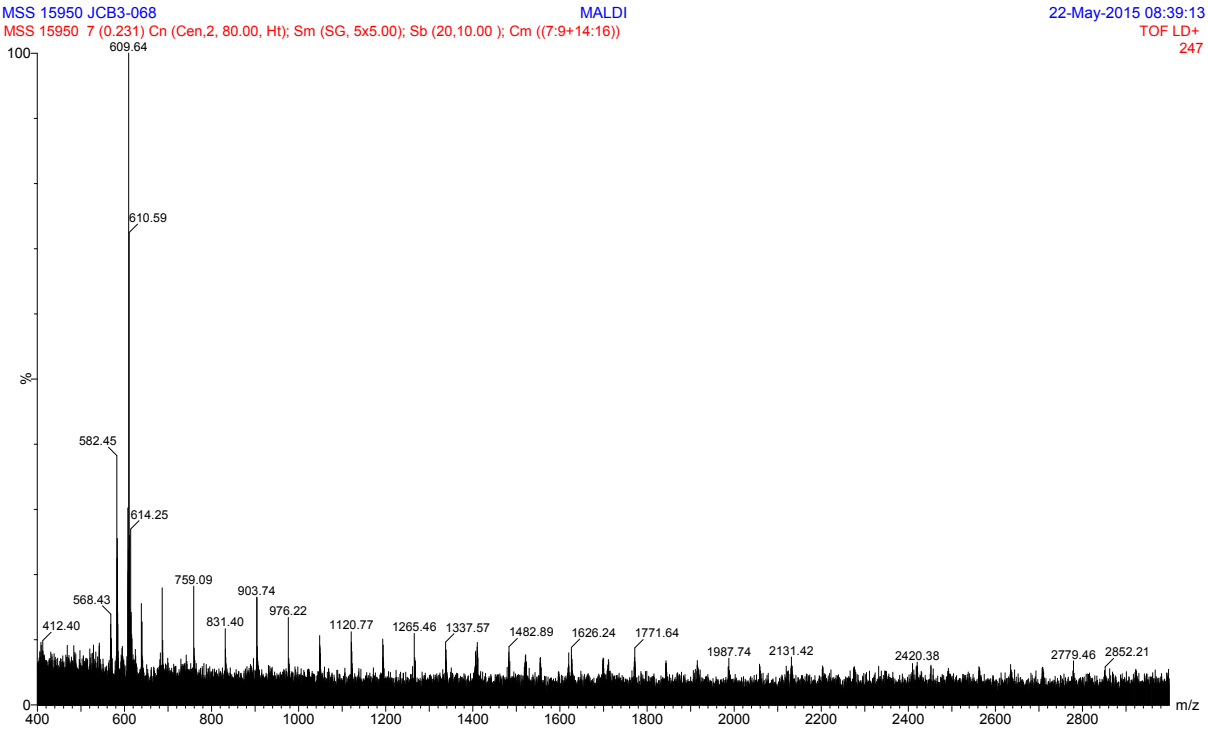

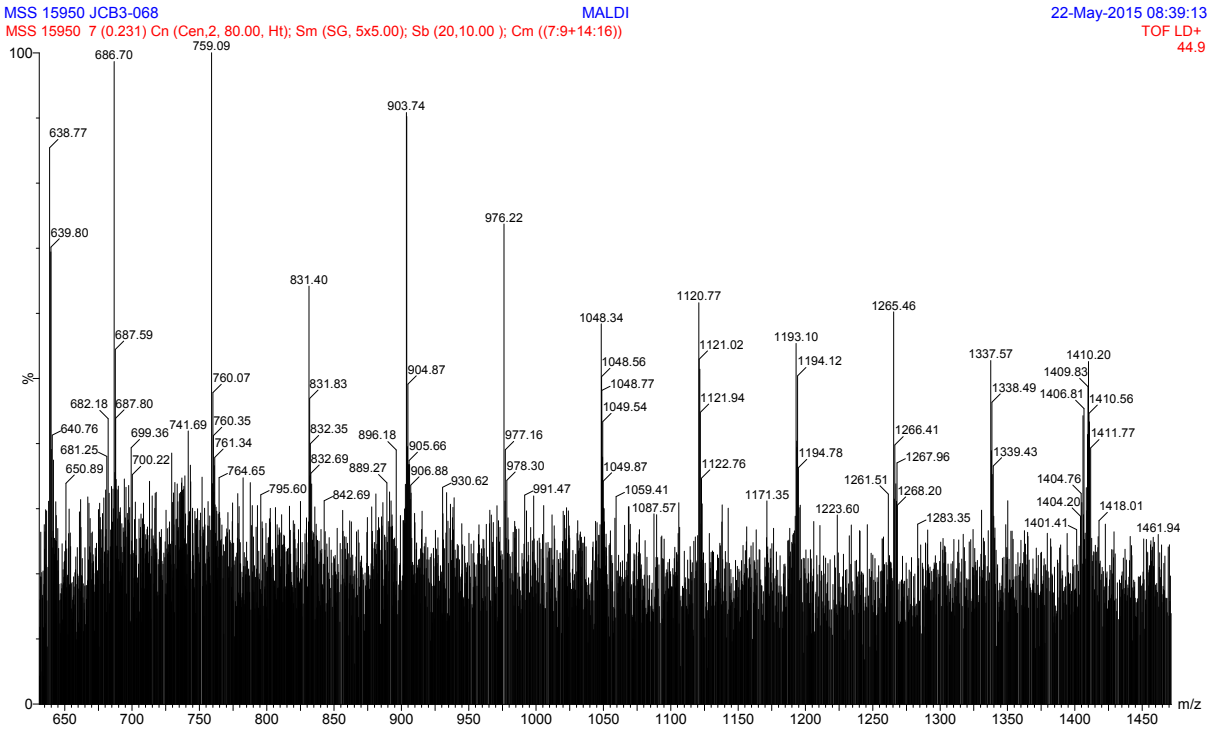

Figure S60: MALDI-TOF spectra of poly-L-lactide synthesised using complex (^{Me2}CAAC)Ba(N{SiMe$_3$}$_2$)$_2$ (**4**). Polymerisation conditions: benzene-d_6 at 23 °C with $[LA]_0/[M]_0$ = 20, $[LA]_0$ = 0.5 M.

Table S25: *rac*-lactide polymerisation using (^{Me2}CAAC)Ba(N{SiMe$_3$}$_2$)$_2$ (**4**). Polymerisation conditions: benzene-d_6, $[LA]_0/[M]_0$ = 20, [LA]0 = 0.5 M, 23 °C.

Time (h)	Conversion (%)
0.23	25.5
0.38	56.3
1.88	93.1
3.78	97.4

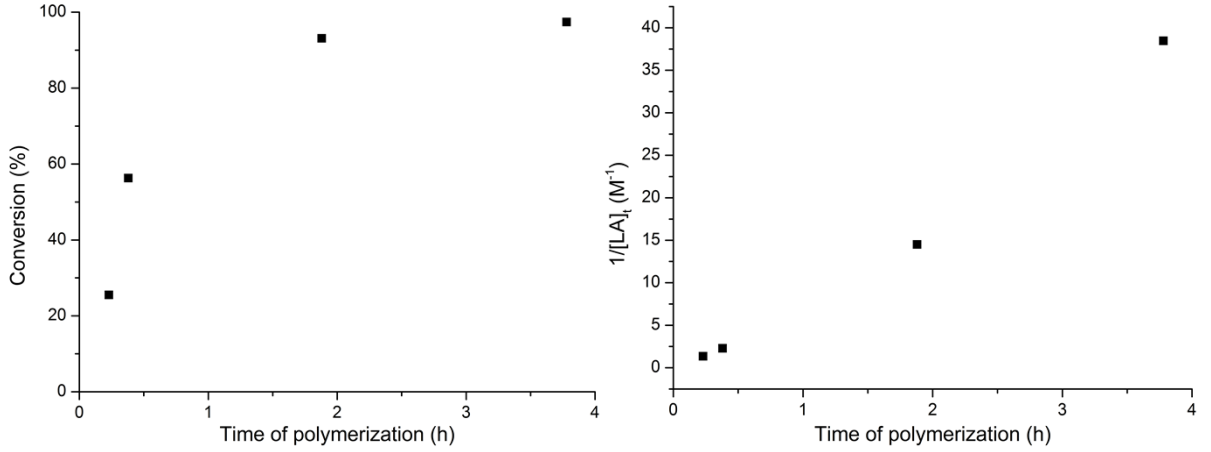

Figure S61: *rac*-lactide polymerisation using complex (^{Me2}CAAC)Ba(N{SiMe$_3$}$_2$)$_2$ (**4**), conversion in function of time profile (left) and second-order rate plot (right). Polymerisation conditions: benzene-d_6 at 23 °C with $[LA]_0/[M]_0$ = 20, $[LA]_0$ = 0.5 M.

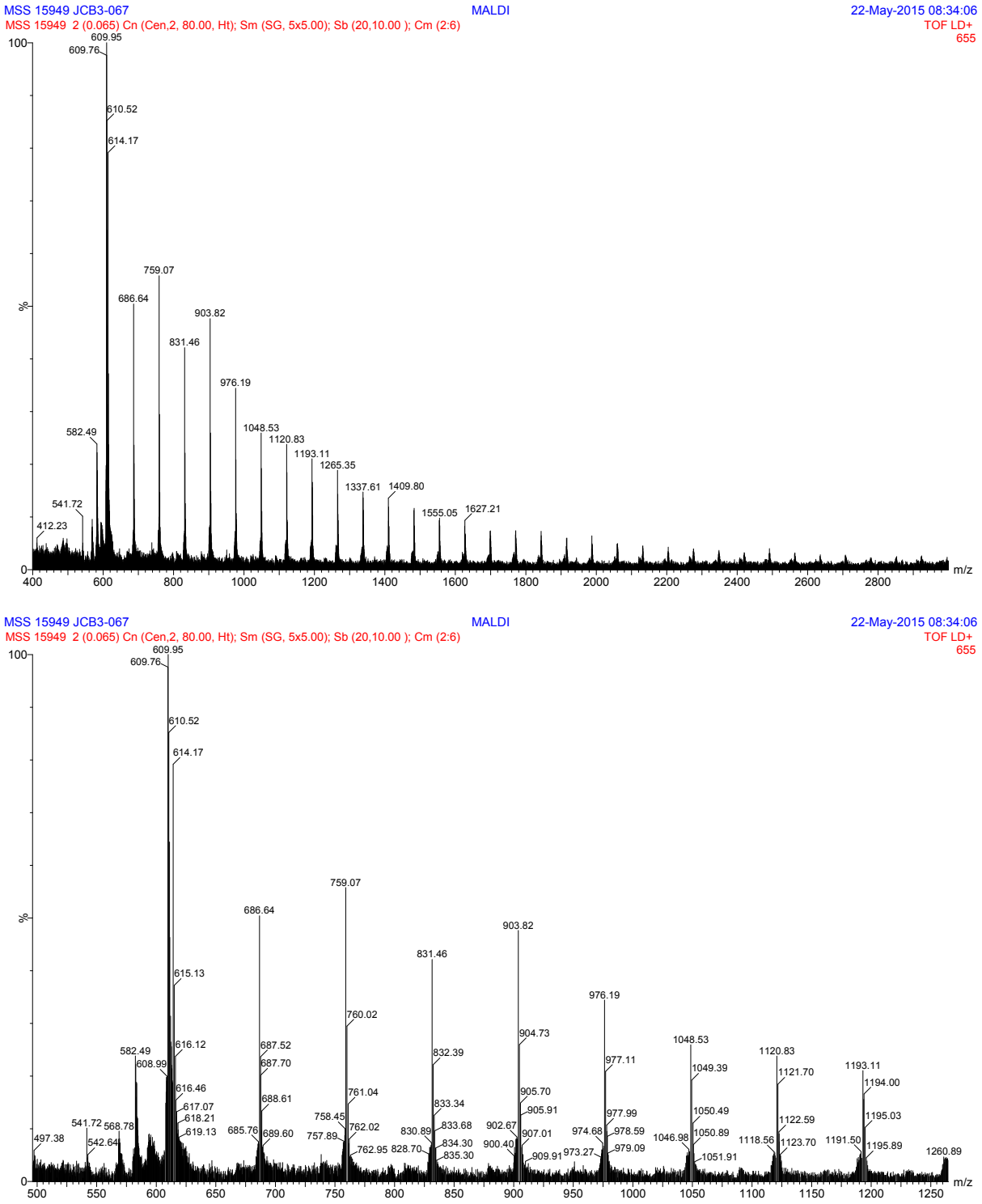

Figure S62: MALDI-TOF spectra of poly-*rac*-lactide synthesised using complex (^{Me2}CAAC)Ba(N{SiMe$_3$}$_2$)$_2$ (**4**). Polymerisation conditions: benzene-d_6 at 23 °C with $[LA]_0/[M]_0$ = 20, $[LA]_0$ = 0.5 M.

Summary of the kinetics of polymerisation

Table S26: lactide polymerisation using complexes **1**, **3**, **4** and **6**. Polymerisation conditions: benzene-d_6, $[LA]_0/[M]_0 = 200$, [LA]0 = 0.5 M, 23 °C.

Complex	LA	k_{app}[a] (M^{-1} h^{-1})	R^2 [a]
1	L-	0.024(2)	0.989
3	L	0.556(40)	0.990
3	*rac*-	0.134(5)	0.996
4	L-	0.839(25)	0.997
4	*rac*-	0.171(3)	0.999
4[b]	L-	1.478(32)	0.999[5]
4[c]	L-	5.720(354)	0.994

[a]apparent second order constant ($k_{app} = k_p[MN"]_0[CAAC]_0$) for consumption of lactide with standard error and R2 determined by linear regression analysis. [b]$[LA]_0/[M]_0 = 150$. [c]$[LA]_0/[M]_0 = 100$.

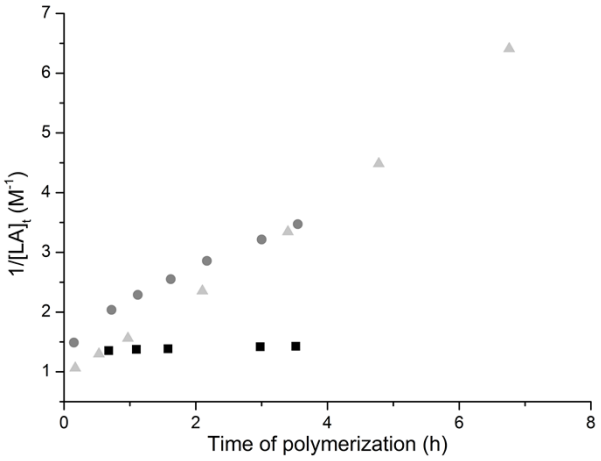

Figure S63: Second-order rate plot of the polymerisation of L-lactide using (^{Me2}CAAC)Mg(N{SiMe$_3$}$_2$)$_2$ (**1**, black square), (^{Me2}CAAC)Sr(N{SiMe$_3$}$_2$)$_2$ (**3**, dark grey circle) and (^{Me2}CAAC)Ba(N{SiMe$_3$}$_2$)$_2$ (**4**, light grey triangle). Polymerisation conditions: benzene-d_6 at 23 °C with $[LA]_0/[M]_0 = 200$, $[LA]_0 = 0.5$ M.

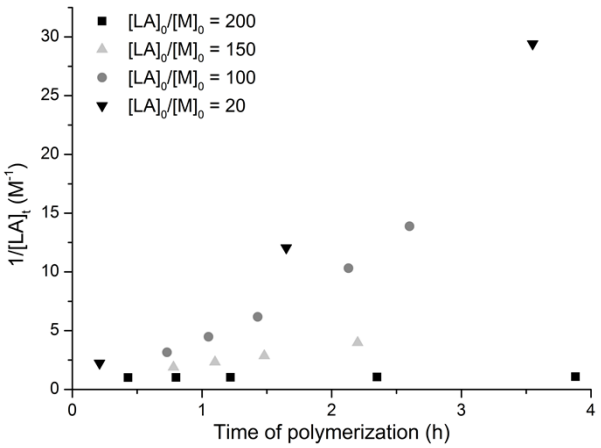

Figure S64: Second-order rate plot of the polymerisation of L-lactide using (^{Me2}CAAC)Ba(N{SiMe$_3$}$_2$)$_2$ (**4**): $[LA]_0/[M]_0 = 200$ (black square), $[LA]_0/[M]_0 = 150$ (light grey

triangle) and $[LA]_0/[M]_0$ = 100 (dark grey circle) and $[LA]_0/[M]_0$ = 20 (black inverted triangle). Polymerisation conditions: benzene-d_6 at 23 °C with $[LA]_0$ = 0.5 M.

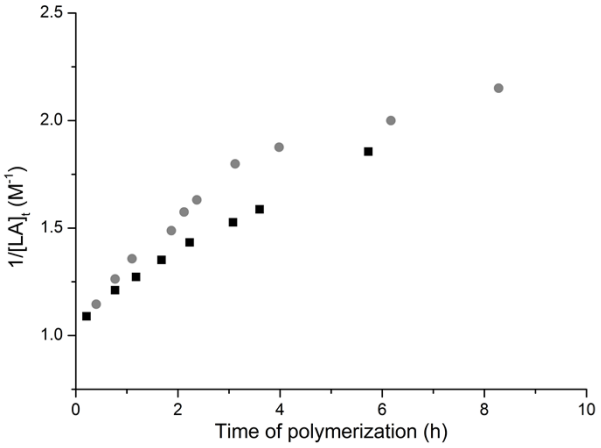

Figure S65: Second-order rate plot of the polymerisation of *rac*-lactide using (^{Me2}CAAC)Sr(N{SiMe$_3$}$_2$)$_2$ (**3**, black square) and [(^{Cy}CAAC)$_3$K][Sr(N{SiMe$_3$}$_2$)$_3$] (**6**, dark grey circle). Polymerisation conditions: benzene-d_6 at 23 °C with $[LA]_0/[M]_0$ = 200, $[LA]_0$ = 0.5 M.

GPC characterisation

Table S27: lactide polymerisation using complexes **1**, **3**, **4** and **6**. Polymerisation conditions: benzene-d_6, $[LA]_0/[M]_0$ = 200, [LA]0 = 0.5 M, 23 °C.

Complex	LA	Time of isolation (h)	Conversion[a]	M_n (calculated)[b] (g/mol)	*M*n (GPC)[c] (g/mol)	M_w/M_n[c]
1	L-	9.3	70	20178	12879	3.26
3	L-	9.2	97	27961	28199	1.35
3	*rac*-	28.0	74	21331	21742	1.67
4	L-	8.5	95	27385	25006	1.99
4[d]	L-	2.7	94	20322	23417	2.19
4[e]	L-	2.6	98	14124	20580	2.11
4[f]	L-	0.7	67	19313	4797	2.07
6	L-	32.5	95	27384	14714	1.54
6	*rac*-	23.1	50	14413	8426	1.66

[a]Reactions monitored by ^{1}H NMR spectroscopy in chlorform-d_1, all quoted conversion refer to the last point where M_n (GPC) was determined. [b]M_n(Calculated) = Conv × $[LA]_0/[M]_0$ × M_{LA}. [c]Measured by GPC against polystyrene standards with appropriate Mark-Houwink corrections for PLA in thf at 30 °C. [d]$[LA]_0/[M]_0$ = 150. [e]$[LA]_0/[M]_0$ = 100. [f]tetrahydrofuran-d_8.

VII. References

1. Y. Sarazin, D. Roşca, V. Poirier, T. Roisnel, A. Silvestru, L. Maron and J.-F. Carpentier, *Organometallics*, 2010, **29**, 6569.
2. Y. Sarazin, R. H. Howard, D. L. Hughes, S. M. Humphrey and M. Bochmann, *Dalton Trans.*, 2006, DOI: 10.1039/B511851D, 340.
3. T. M. Cameron, C. Xu, A. G. Dipasquale and A. L. Rheingold, *Organometallics*, 2008, **27**, 1596.
4. R. Jazzar, R. D. Dewhurst, J.-B. Bourg, B. Donnadieu, Y. Canac and G. Bertrand, *Angew. Chem., Int. Ed.*, 2007, **46**, 2899.
5. J. Cosier and A. M. Glazer, *J. Appl. Crystallogr.*, 1986, **19**, 105.
6. *Journal*, CrysAlisPRO, Oxford Diffraction /Agilent Technologies UK Ltd, Yarnton, England.
7. A. Altomare, G. Cascarano, C. Giacovazzo and A. Guagliardi, *J. Appl. Crystallogr.*, 1993, **26**, 343.
8. L. Palatinus and G. Chapuis, *J. Appl. Crystallogr.*, 2007, **40**, 786.
9. A. J. Arduengo, F. Davidson, R. Krafczyk, W. J. Marshall and M. Tamm, *Organometallics*, 1998, **17**, 3375.
10. A. G. M. Barrett, M. R. Crimmin, M. S. Hill, G. Kociok-Köhn, D. J. MacDougall, M. F. Mahon and P. A. Procopiou, *Organometallics*, 2008, **27**, 3939.
11. F. Neese, Orca − an ab initio, DFT and Semiempirical Electronic Structure Package, Version2.8, Revision 2360; Institut für Physikalische und Theoretische Chemie, Universität Bonn, Bonn (Germany)).
12. A. D. Becke, *J. Chem. Phys.*, 1986, **84**, 4524.
13. J. P. Perdew and W. Yue, *Phys. Rev. B: Condens. Matter Mater. Phys.*, 1986, **33**, 8800.
14. J. P. Perdew, *Phys. Rev. B: Condens. Matter Mater. Phys.*, 1986, **33**, 8822.
15. C. Lee, W. Yang and R. G. Parr, *Phys. Rev. B: Condens. Matter Mater. Phys.*, 1988, **37**, 785.
16. A. D. Becke, *J. Chem. Phys.*, 1993, **98**, 5648.
17. E. v. Lenthe, E. J. Baerends and J. G. Snijders, *J. Chem. Phys.*, 1993, **99**, 4597.
18. E. van Lenthe, E. J. Baerends and J. G. Snijders, *J. Chem. Phys.*, 1994, **101**, 9783.
19. E. van Lenthe, J. G. Snijders and E. J. Baerends, *J. Chem. Phys.*, 1996, **105**, 6505.
20. C. van Wüllen, *J. Chem. Phys.*, 1998, **109**, 392.
21. D. A. Pantazis, X.-Y. Chen, C. R. Landis and F. Neese, *J. Chem. Theory Comput.*, 2008, **4**, 908.
22. D. A. Pantazis and F. Neese, *J. Chem. Theory Comput.*, 2009, **5**, 2229.
23. A. Schäfer, C. Huber and R. Ahlrichs, *J. Chem. Phys.*, 1994, **100**, 5829.
24. F. Weigend and R. Ahlrichs, *PCCP*, 2005, **7**, 3297.
25. F. Weigend, *PCCP*, 2006, **8**, 1057.
26. K. Eichkorn, F. Weigend, O. Treutler and R. Ahlrichs, *Theor. Chem. Acc.*, 1997, **97**, 119.
27. K. Eichkorn, O. Treutler, H. Öhm, M. Häser and R. Ahlrichs, *Chem. Phys. Lett.*, 1995, **242**, 652.
28. K. Eichkorn, O. Treutler, H. Öhm, M. Häser and R. Ahlrichs, *Chem. Phys. Lett.*, 1995, **240**, 283.
29. E. F. Pettersen, T. D. Goddard, C. C. Huang, G. S. Couch, D. M. Greenblatt, E. C. Meng and T. E. Ferrin, *J. Comput. Chem.*, 2004, **25**, 1605.